TRANSCEND

Transformative Science and Engineering for Nuclear Decommissioning

# Development of an M-S-H cement mortar using corroded magnesium sludge simulant (CMgS)

Mercedes Baxter Chinery, Imperial College London

Supervised By:

Prof Hong Wong, Prof. Chris Cheeseman, Dr Mark Wenman

24th – 25th April 2023
London

Energy
For a Low Carbon Future

# Background

- Ponds at Sellafield contain magnesium hydroxide rich sludge
- Reduce waste volume by using as a raw material in cement
  - Determine if this is plausible
  - Understand behaviour

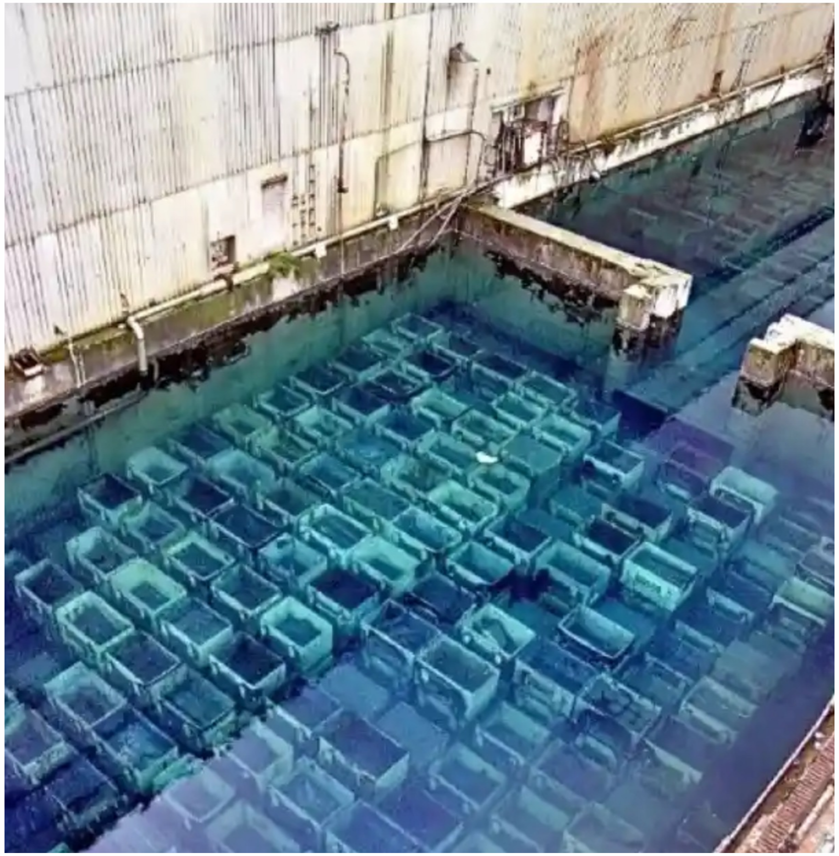

# Aims and Objectives

- Understand the durability of a magnesium-silicate-hydrate cement for application within nuclear encapsulation
  - Determine if CMgS can be used as a raw material in cement mortar in significant proportions
  - Understand and analyse the behaviour of the cement mortar to see if it achieves the requirements for encapsulation

# MgO-based M-S-H mortar

MgO-based M-S-H: 20 wt% MgO, 5 wt% $MgCO_3$, 25 wt% $SiO_2$, 50 wt% silica sand, w/s 0.35, 1 wt% NaHMP

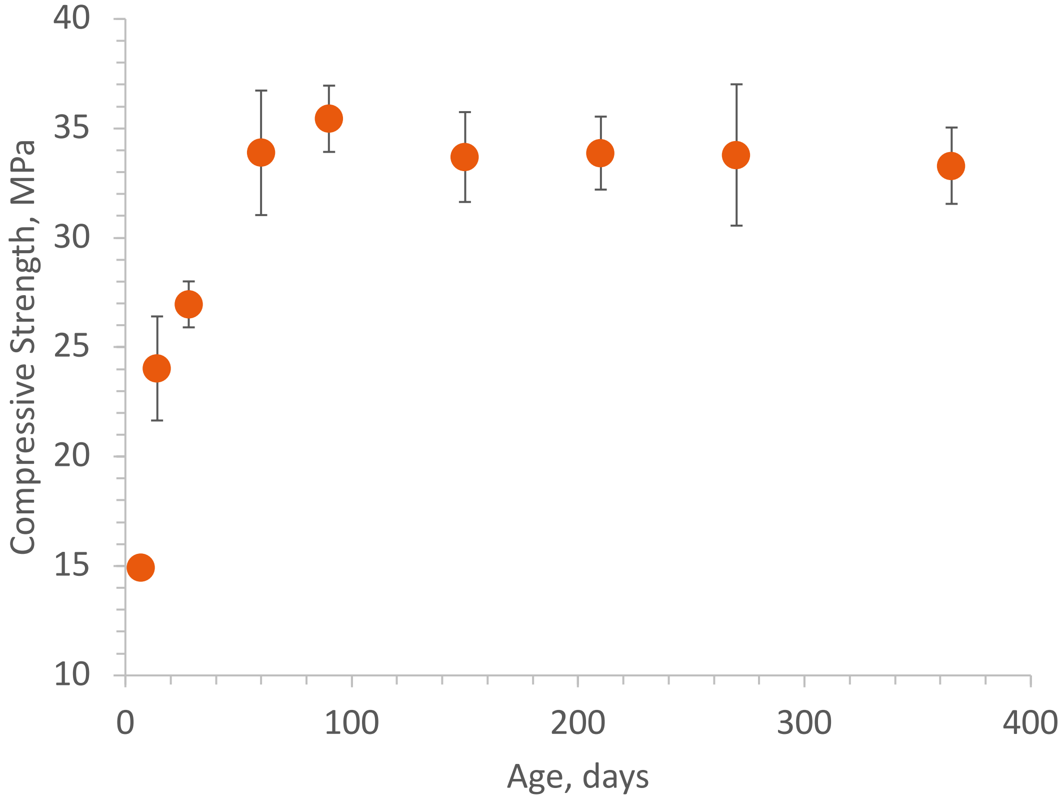


Figure 1: Compressive strength for the MgO based mortar at ages up to a year

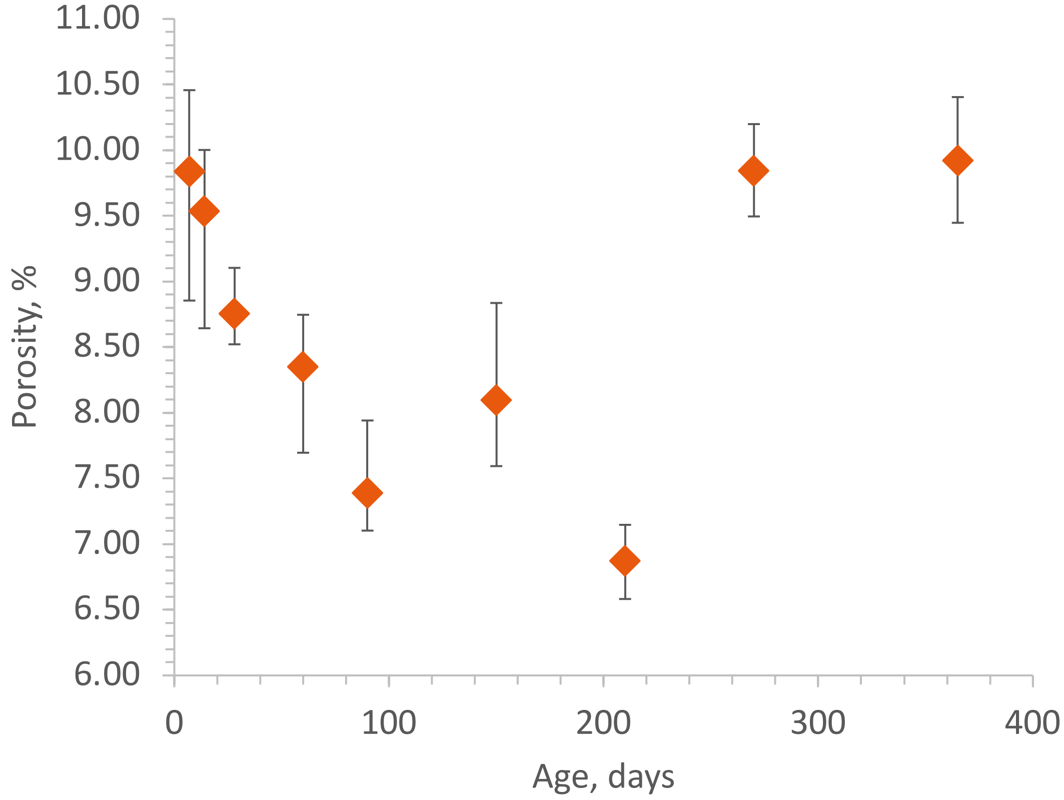


Figure 2: Porosity for the MgO based mortar at ages up to a year

# $Mg(OH)_2$-based M-S-H mortar

$Mg(OH)_2$-based M-S-H: 23.4 wt% $Mg(OH)_2$, 9.1 wt% MgO, 27.5 wt% $SiO_2$ and 40 wt% silica sand, w/s 0.35, 1 wt% NaHMP

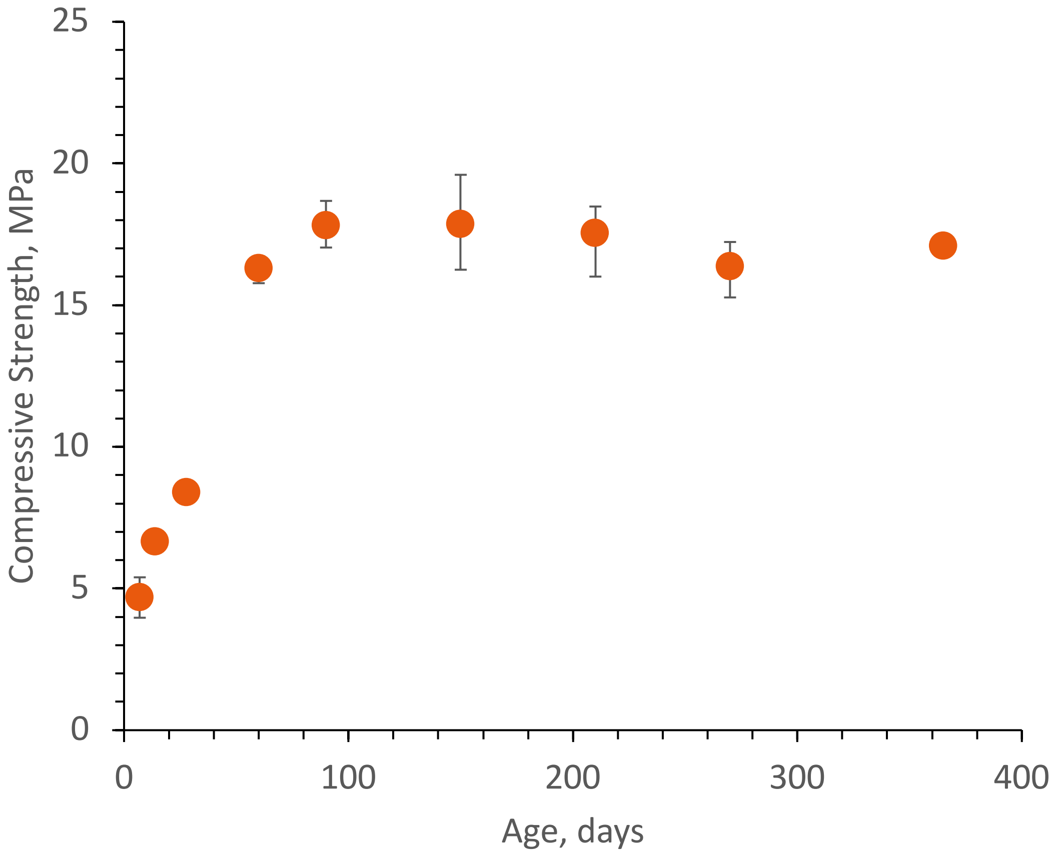


Figure 1: Compressive strength for the $Mg(OH)_2$ based mortar at ages up to a year

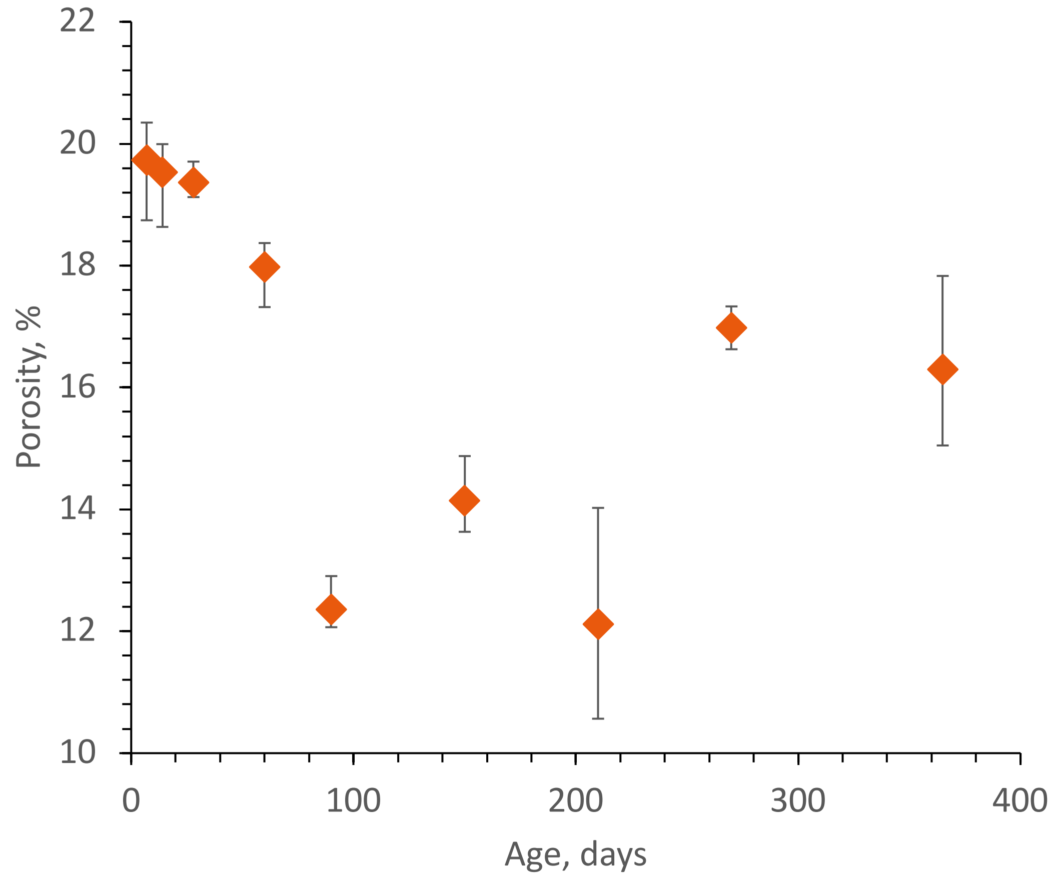


Figure 2: Porosity for the $Mg(OH)_2$ based mortar at ages up to a year

# Characterising the CMgS Sludge

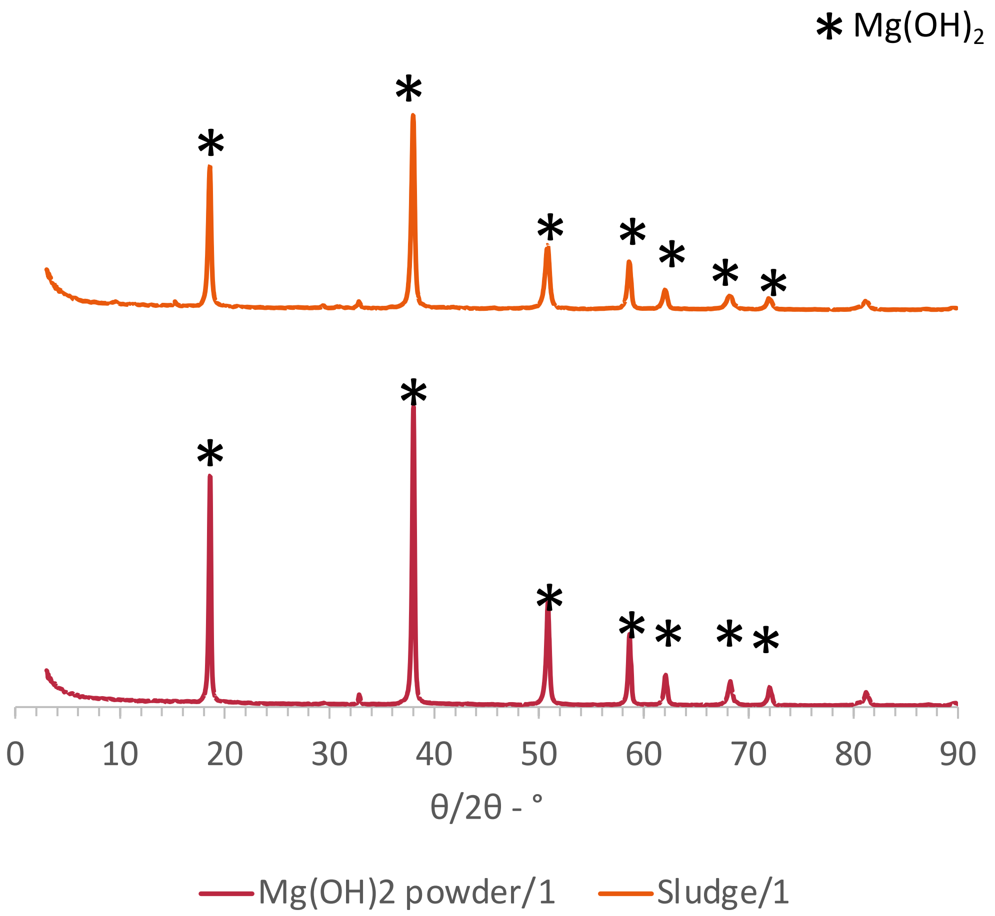


Figure 1: XRD patterns for the $Mg(OH)_2$ powder and the dehydrated sludge.
Sludge was placed in an oven at 105°C for 24 hours prior to testing.

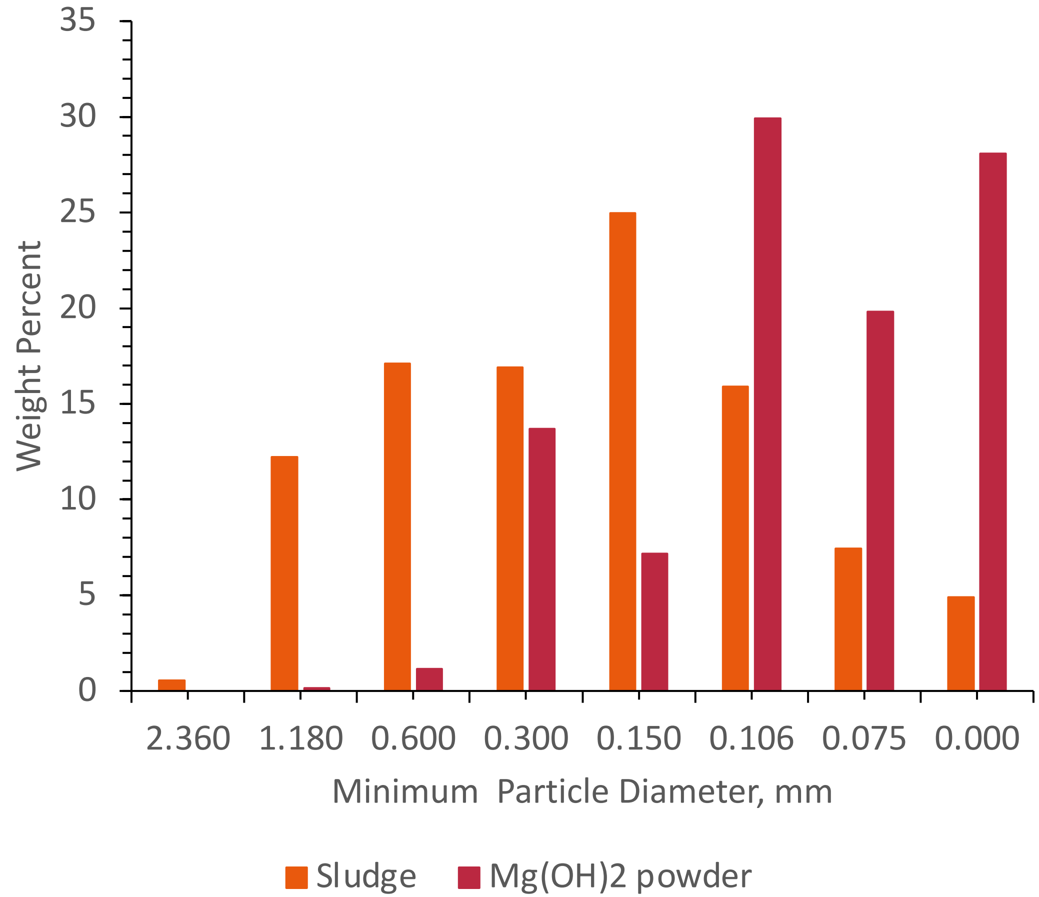


Figure 2: distribution of particle size for dehydrated sludge and magnesium hydroxide powder.
Sludge was placed in an oven at 105°C for 24 hours prior to testing.

Transformative Science and Engineering for Nuclear Decommissioning

# Reproduction of $Mg(OH)_2$-based M-S-H mortar

Mix proportions: 43.3 wt% CMgS, 6.7 wt% MgO, 20.4 wt% $SiO_2$, 29.6 wt% silica sand, 1 wt% NaHMP

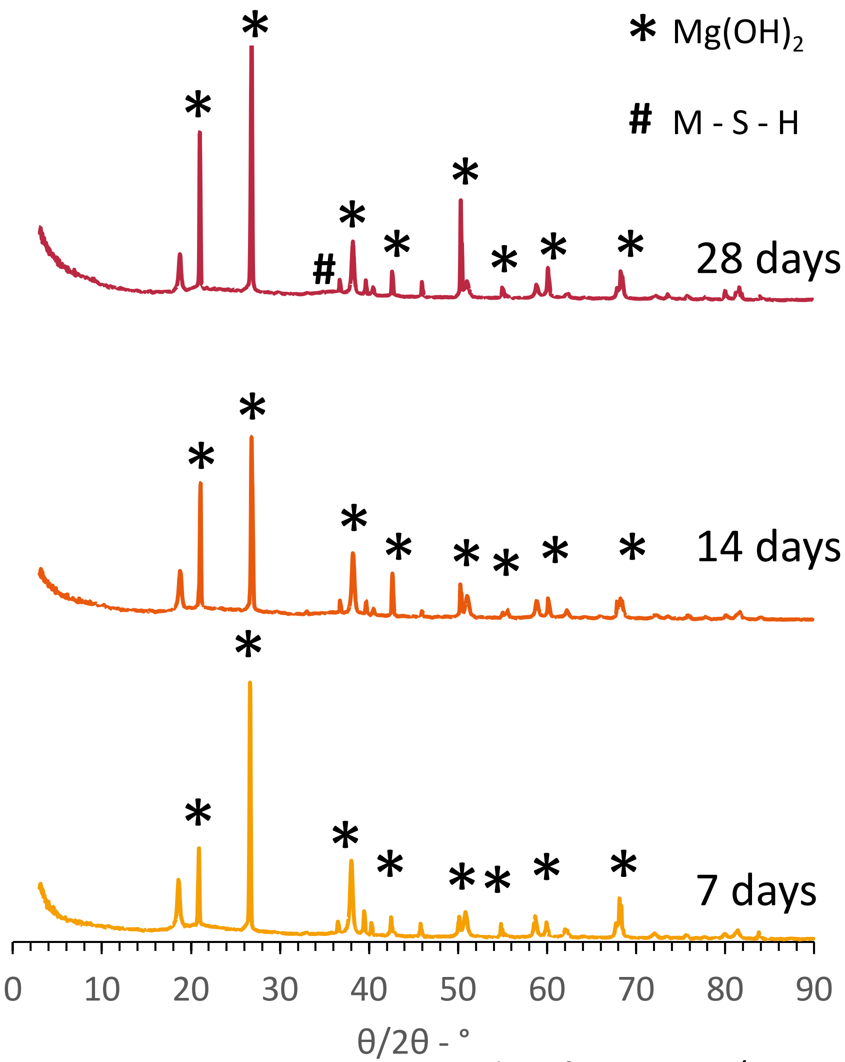


Figure 1: XRD pattern at 7, 14, 28 days for 0.375 w/s ratio cement mortar

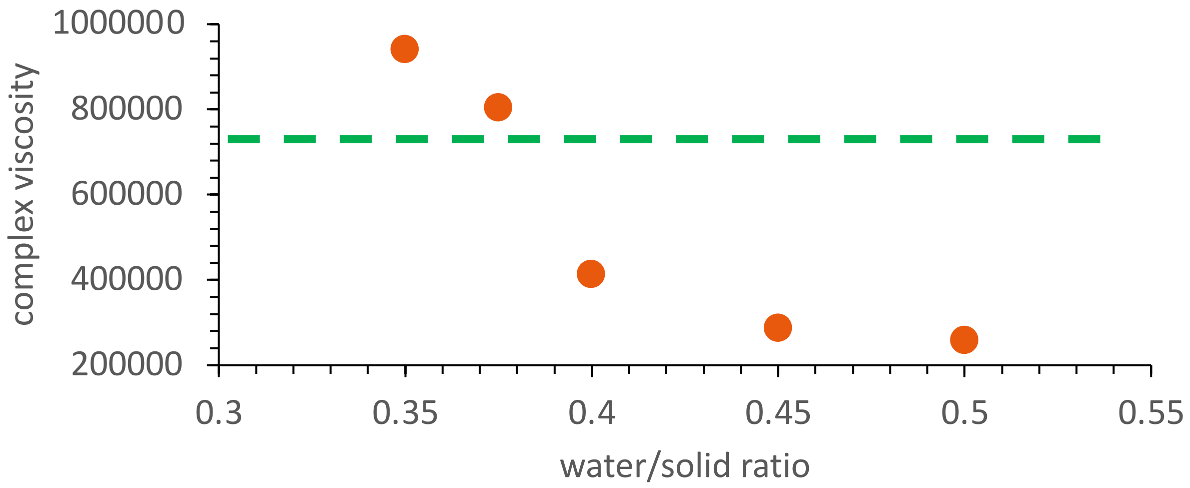


Figure 2: Decreasing viscosity with increasing water/solid ratio

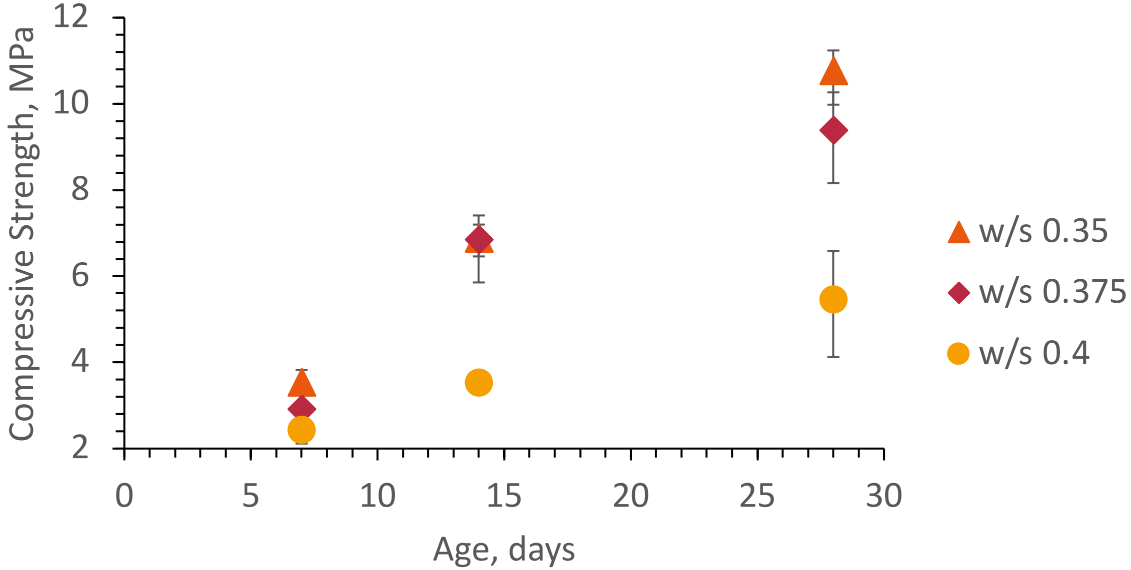


Figure 3: Decreasing strength with increasing water/solid ratio

# Improving M-S-H mortar properties

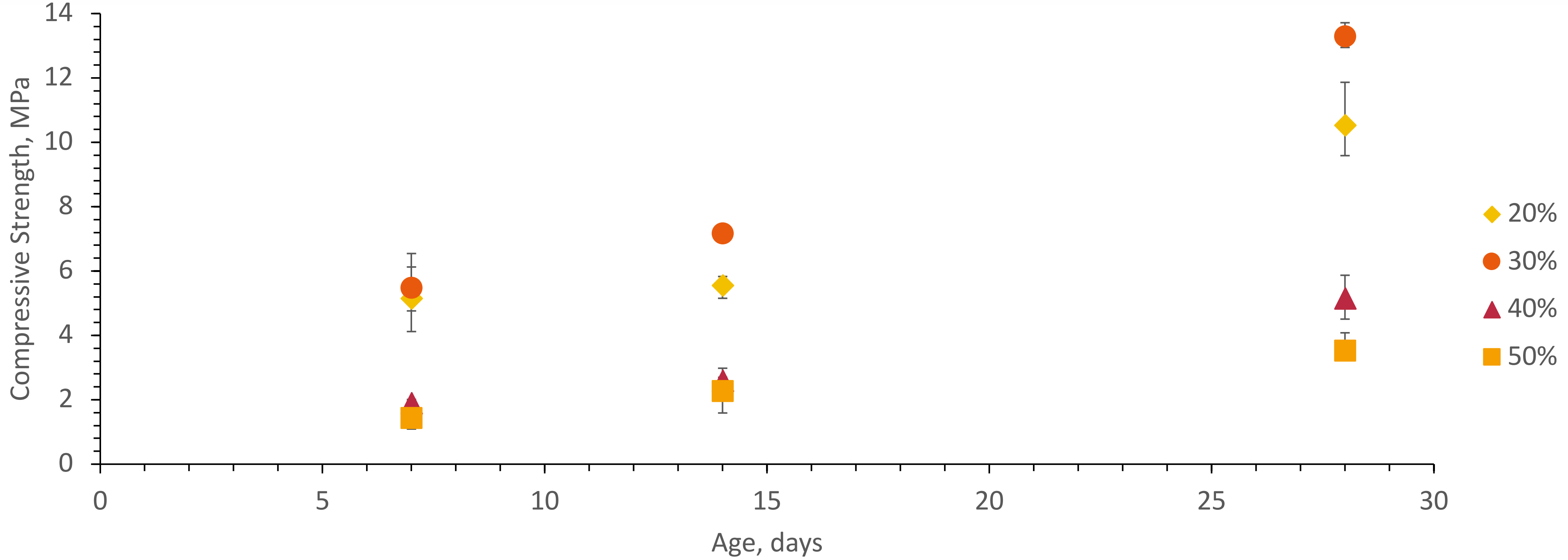


Figure 1: Compressive strength of sludge based M-S-H mortars with various proportions of silica sand filler substituted for the sludge

Table 1: Mix proportions of the sludge based mortars

| Mix (proportion of sludge substituted as filler) | CMgS wt% solids | MgO powder wt% solids | $SiO_2$ powder wt% solids | Silica sand wt% solids | Added water per 100g of mix | w/s ratio (including incorporated water) |
|---|---|---|---|---|---|---|
| **20%** | 40.0 | 8.7 | 21.0 | 30.4 | 10.8 | 0.375 |
| **30%** | 46.6 | 8.1 | 20.2 | 25.2 | 0 | 0.388 |
| **40%** | 52.8 | 7.66 | 19.1 | 20.4 | 0 | 0.463 |
| **50%** | 58.3 | 7.28 | 18.2 | 16.3 | 0 | 0.537 |

# Comparing M-S-H mortars

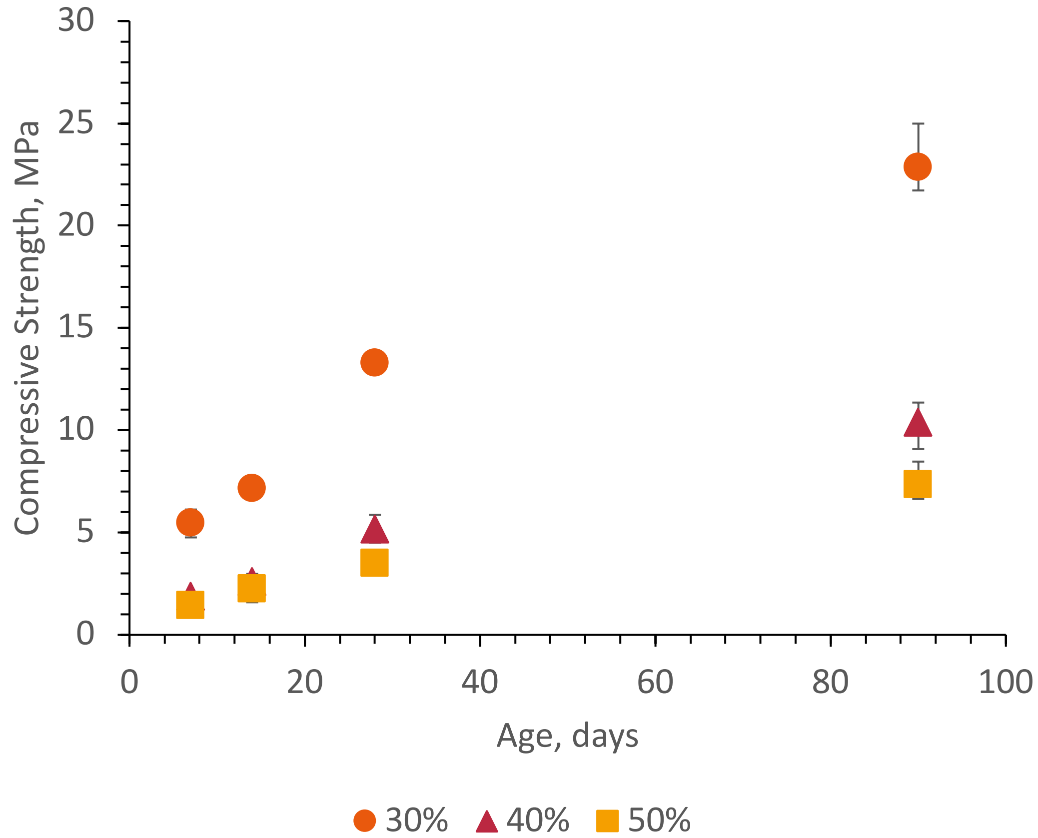


Figure 1: Compressive strength of sludge based M-S-H mortars studied for up to 90 days, for the 30%, 40% and 50% filler substitution mixes.

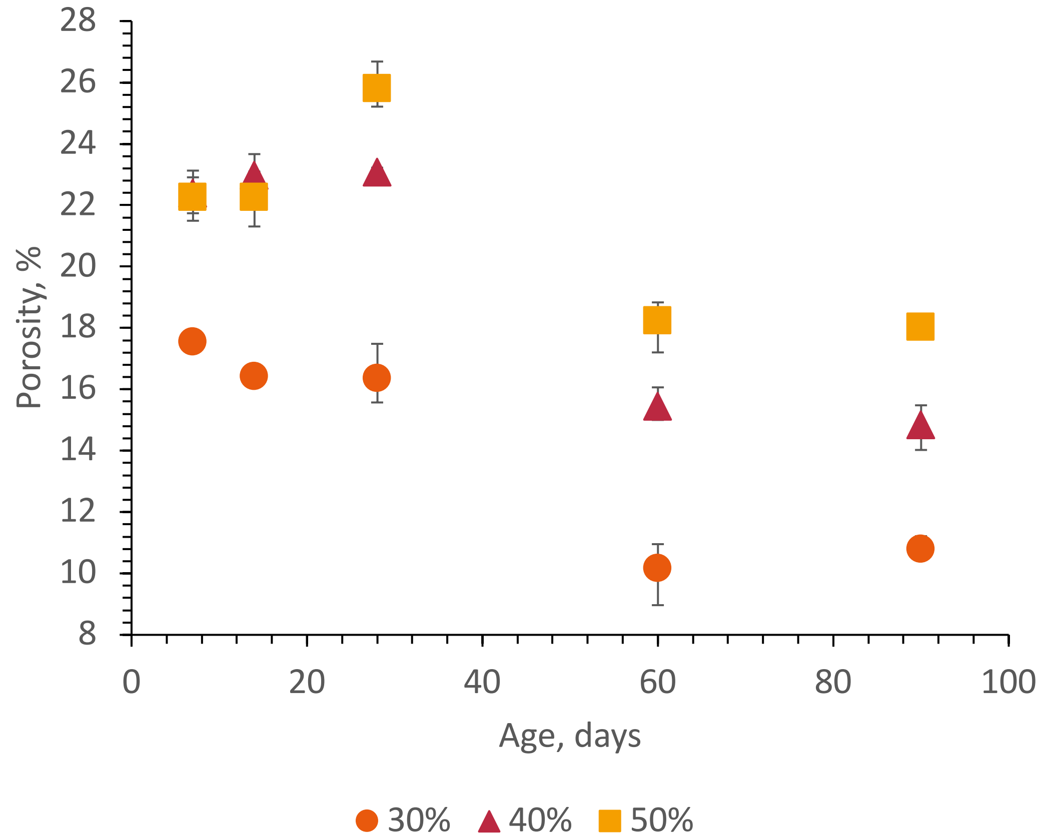


Figure 2: Porosity of sludge based M-S-H mortars studied for up to 90 days, for the 30%, 40% and 50% filler substitution mixes.

# Increasing CMgS proportions

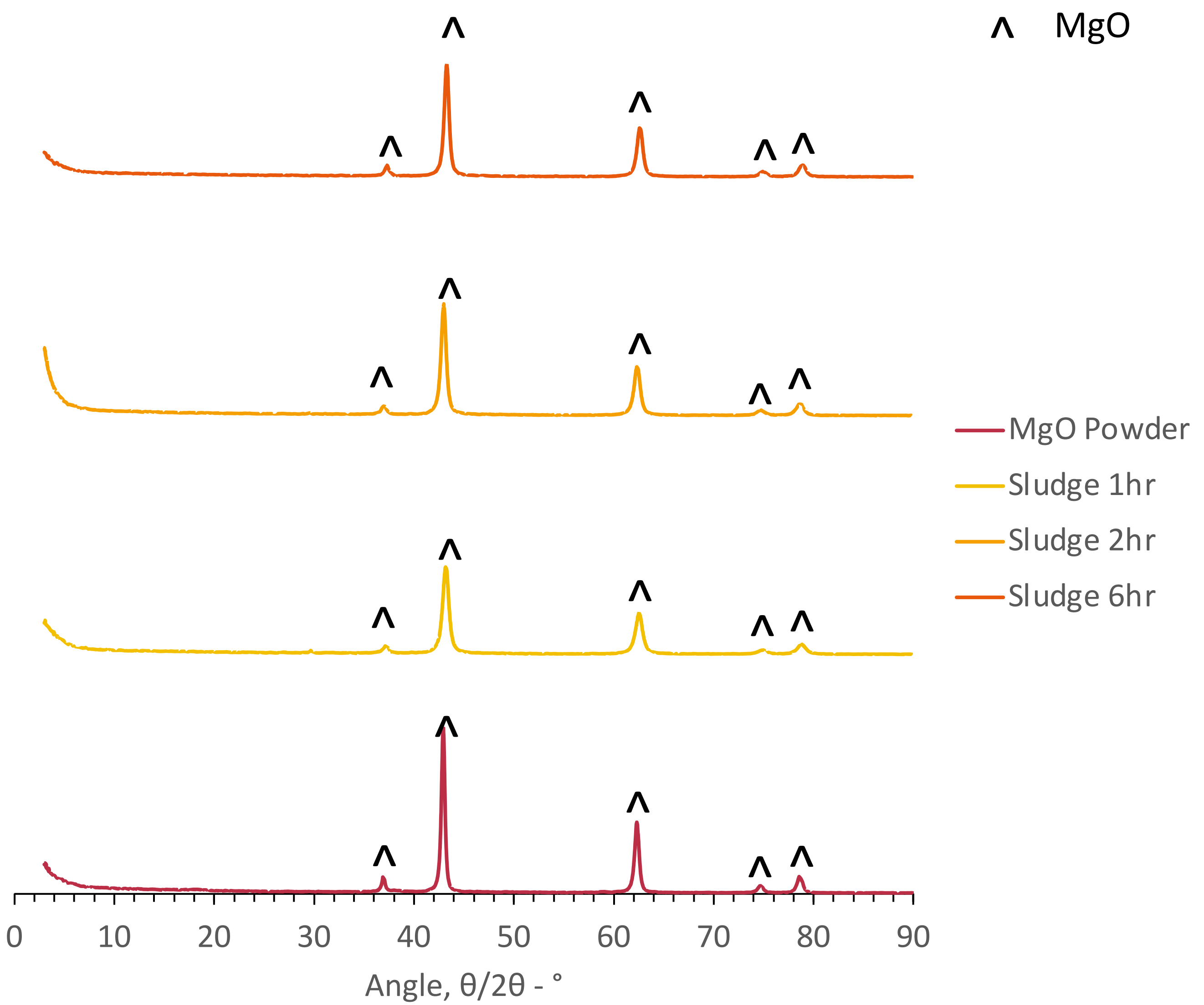


Figure 1: XRD pattern for MgO powder and brucite heated in a furnace at 600°C for various times

TRANSCEND

Transformative Science and Engineering for Nuclear Decommissioning

# Increasing CMgS proportions

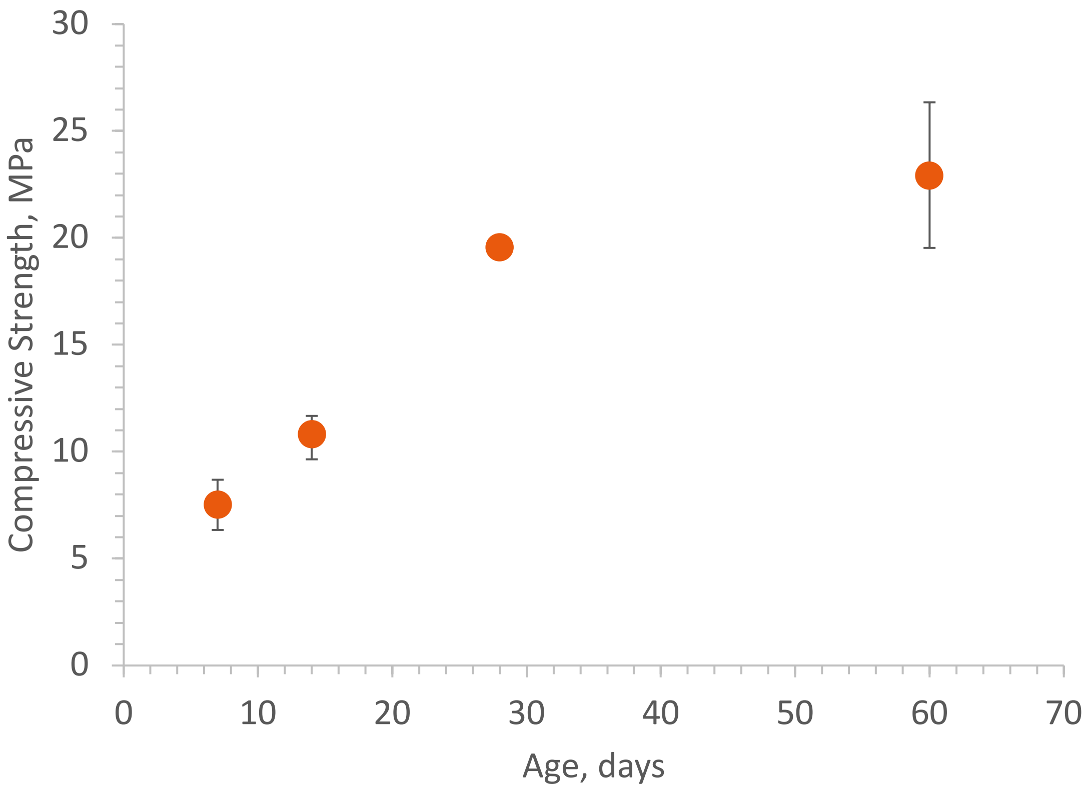


Figure 1: Compressive strength of a sludge based M-S-H mortar with sludge as the magnesium oxide component studied for up to 28 days

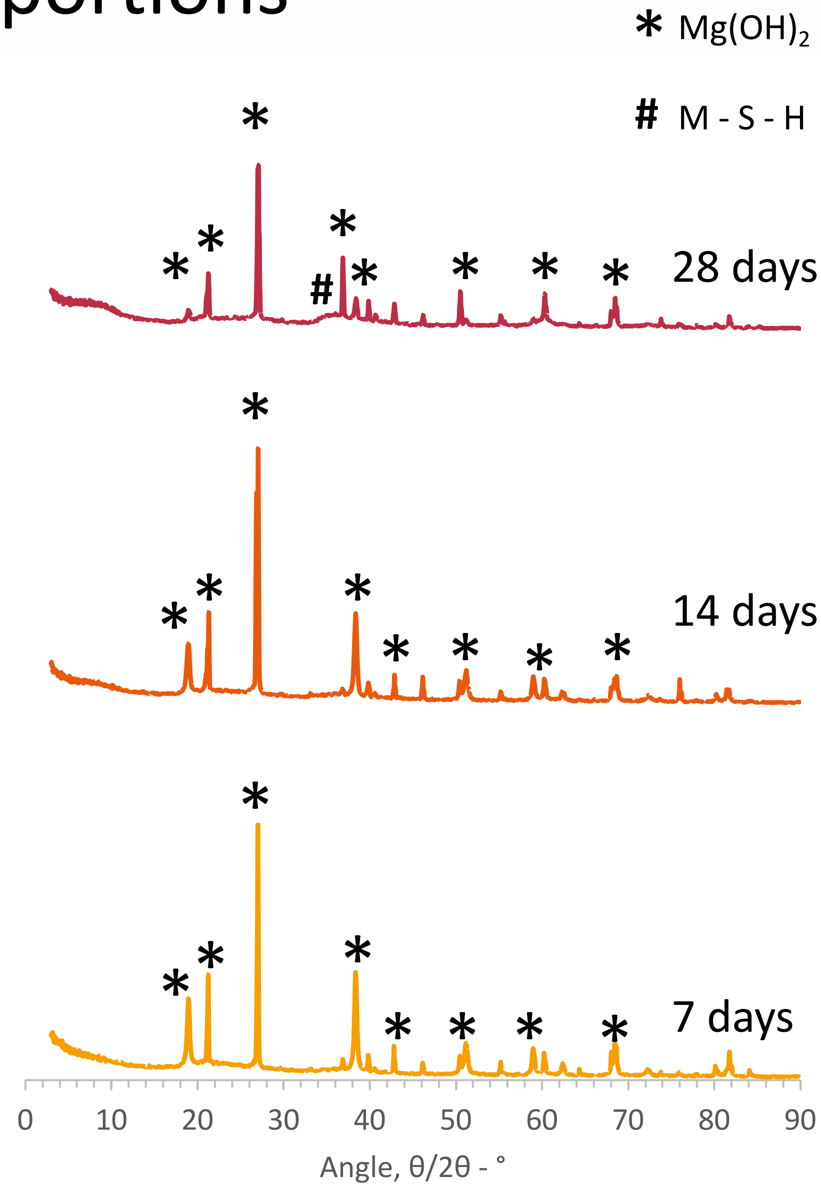


Figure 2: XRD pattern for the M-S-H mortar over 28 days

# Conclusions

- An M-S-H cement can be produced using CMgS as one of the raw materials
- Magnesium oxide powder is required to produce early strength characteristics
- A mortar has been developed which achieves strengths over 10 MPa and has a proportion of over 50 wt% CMgS
- M-S-H is formed within 28 days in this cement mortar
- Higher water/solid ratio is needed when using CMgS due to some of the water already being incorporated in the sludge

# Future Work

- Study properties of sludge-based M-S-H mortars for up to a year
- Determine effect of irradiation on MgO and $Mg(OH)_2$-based M-S-H mortars
- Understand early age properties
- Analyse behaviour of all three mortars in various environments

# Acknowledgements

NATIONAL NUCLEAR LABORATORY

Sellafield Ltd

MINERALS MARKETING

Nuclear Energy Futures
EPSRC Centre for Doctoral Training

TRANSCEND

IMPERIAL MATERIALS
Est. 1851

TRANSCEND

Transformative Science and Engineering for Nuclear Decommissioning

Thank you

Mercedes Baxter Chinery, mcb119@ic.ac.uk
Prof. Hong Wong, hong.wong@imperial.ac.uk

Transformative Science and Engineering for Nuclear Decommissioning

# Advanced Characterisation of Irradiated Probes

Joseph Hartley, University of Leeds

TRANSCEND Annual Meeting

24/04/23
Regents University London

Transformative Science and Engineering for Nuclear Decommissioning

# Research Challenge

ILW legacy sludge at Sellafield needs to be processed for disposal.

Characterisation data on the sludge is difficult to collect.

A remote online monitoring system is needed to determine concentration and particle size.

**Figure 13: Composition of ILW by waste group**

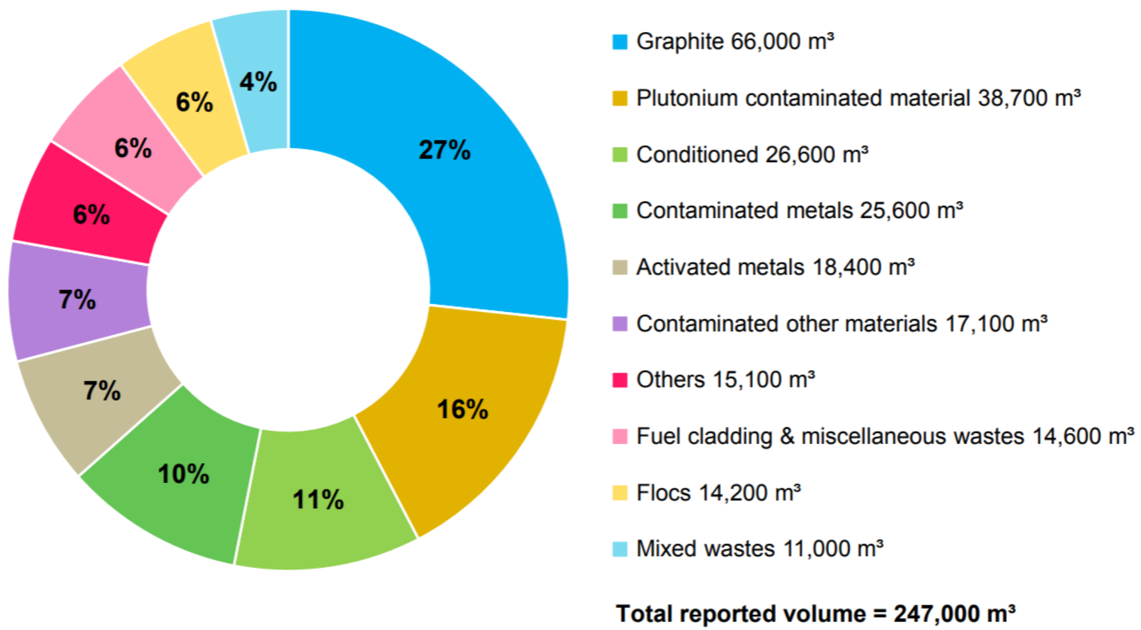



https://ukinventory.nda.gov.uk/wp-content/uploads/2020/01/2019-Waste-Report-Final.pdf https://www.youtube.com/watch?v=Yu7-D37SKOY&ab_channel=SellafieldLtd

# Acoustics

Acoustics has been used to characterise sediments in estuarine environments and recently in nuclear decommissioning processes.

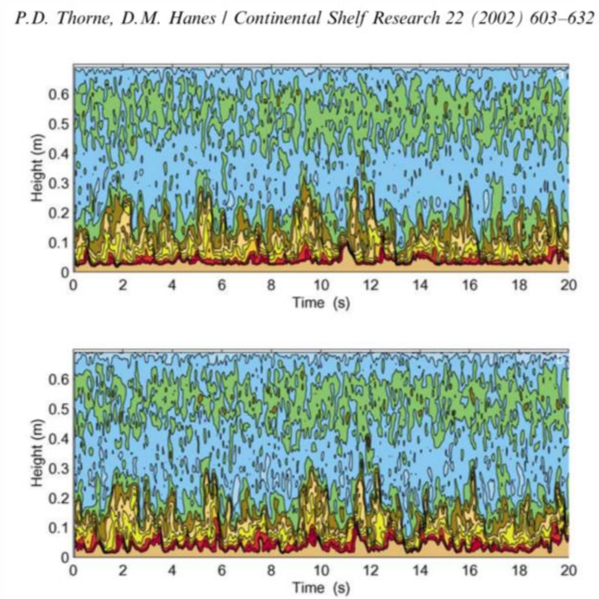


Thorne, Hanes; *A reveiw of acoustic measurement of small-scale sediment processes*

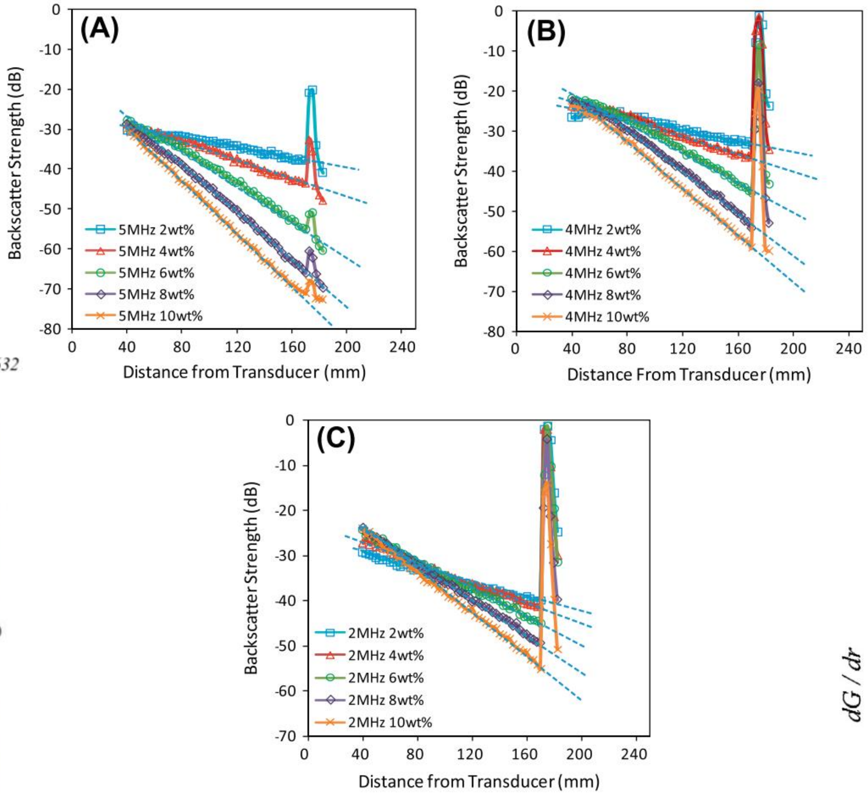


DOI:10.1016/j.mineng.2011.12.003

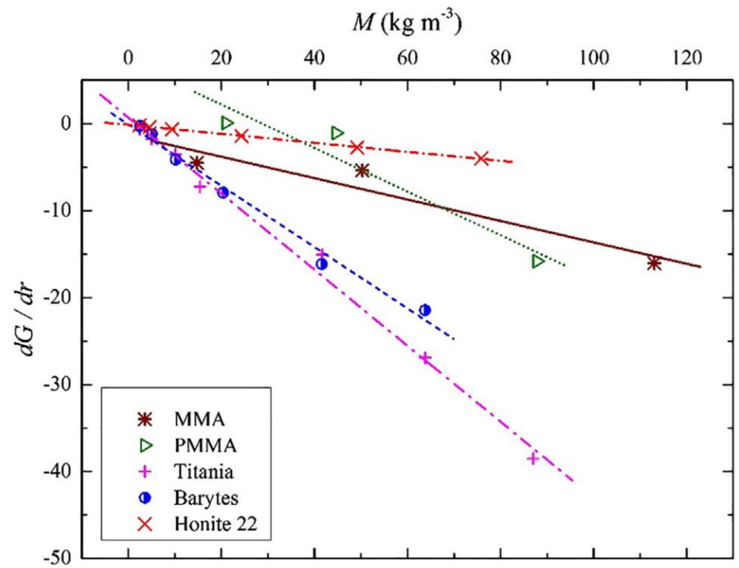


DOI: 10.1016/j.apacoust.2018.10.022

# Research Aims

- Size Characterisation of standard vs. sieved size fractions and bimodal size fraction mixtures of spherical glass particles.
- Development of Machine Learning code to characterise size and concentration of spherical glass particles.
- Application of aforementioned research to flocculated systems.
- Investigate the effects of radiation on ultrasonic transducer probes with advanced acoustic characterisation techniques.

# Methodology

The hydrophone beam plotting facility at the National Physical Laboratory, was used where the following tests were completed on two US transducer:

- ❑ Electrical impedance measurements.
- ❑ Axial beam-profiling.
- ❑ Detailed 2D raster scans, carried out at the last-axial maximum and close to the transducer face (< 3 mm).
- ❑ Reporting of the pulse-echo response of the transducer using a standard reflecting target.

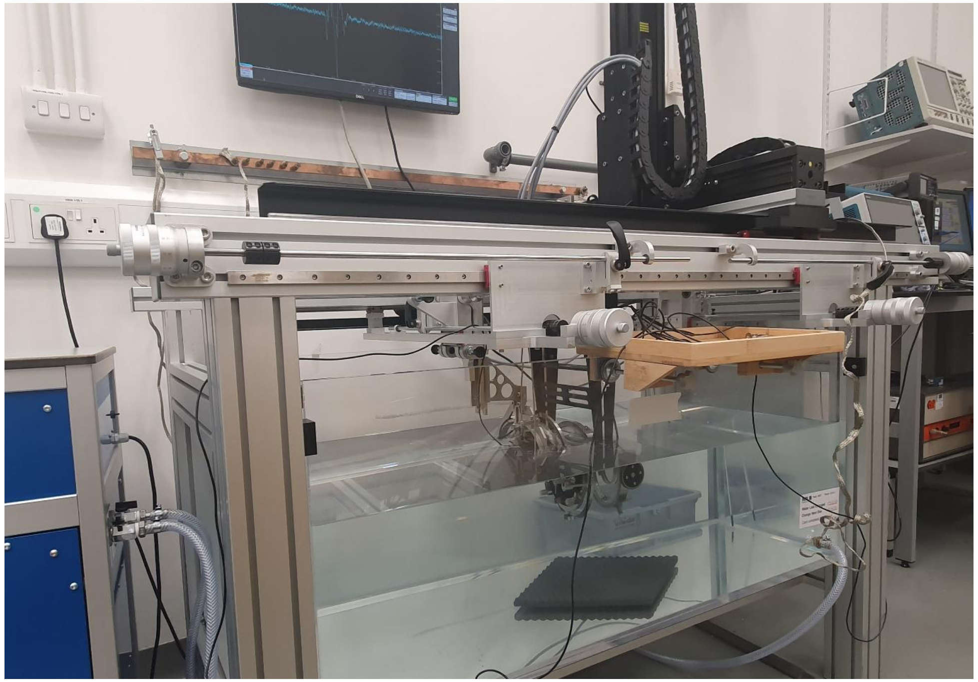

# Methodology

The probes were sent to the Dalton Cumbria Facility where they were irradiated with 1MGy of γ-radiation from a Cobalt-60 source.

Both probes were then retested using the same techniques to identify if the irradiation had caused any physical or performance degradation.

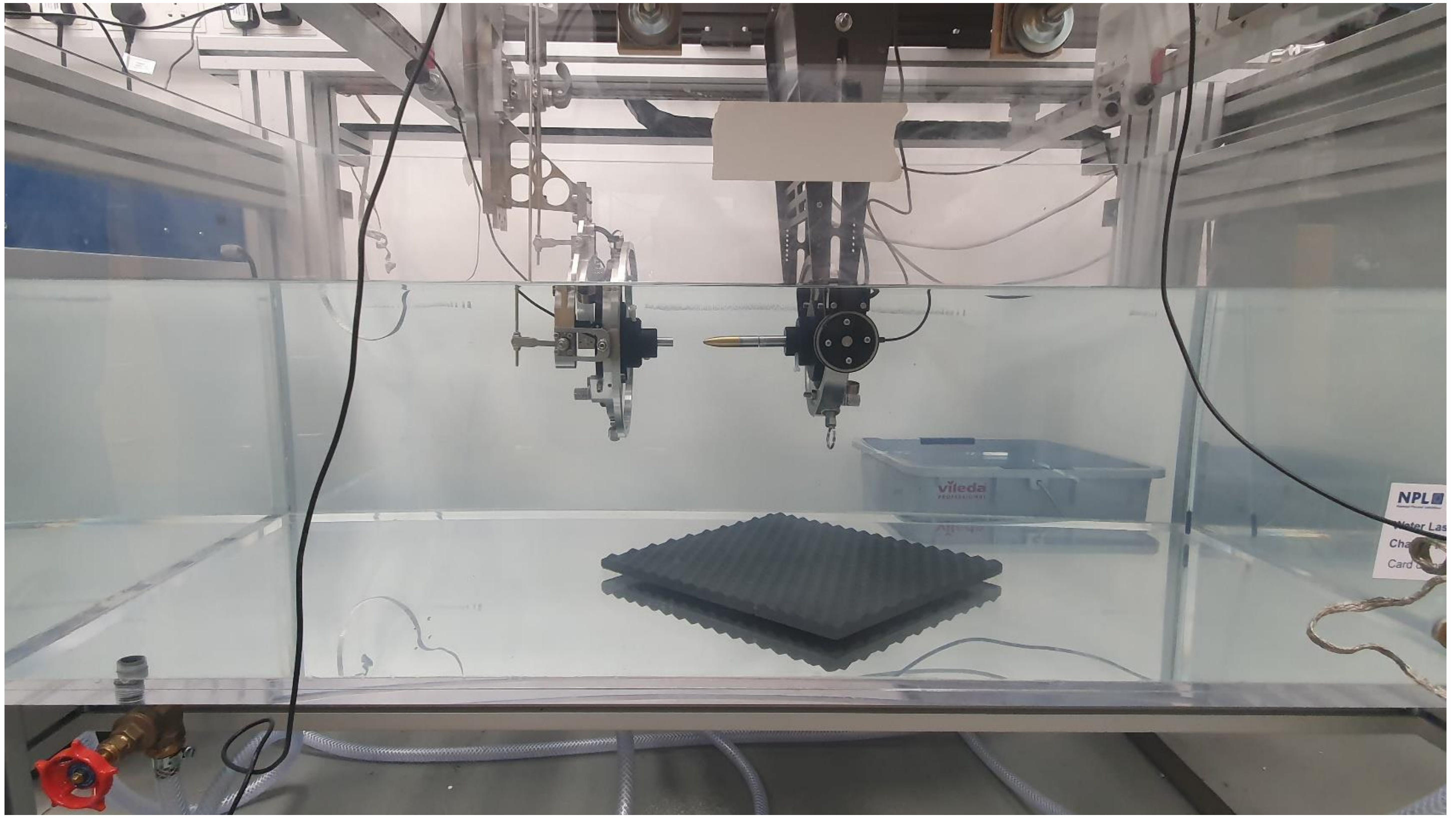

Transformative Science and Engineering for Nuclear Decommissioning

# Impedance measurements

Impedance measurements show any changes in the internal resistance and capacitance of the probes and signal driver.

Probe No. 8 shows no change – in agreement with 2D raster scan.

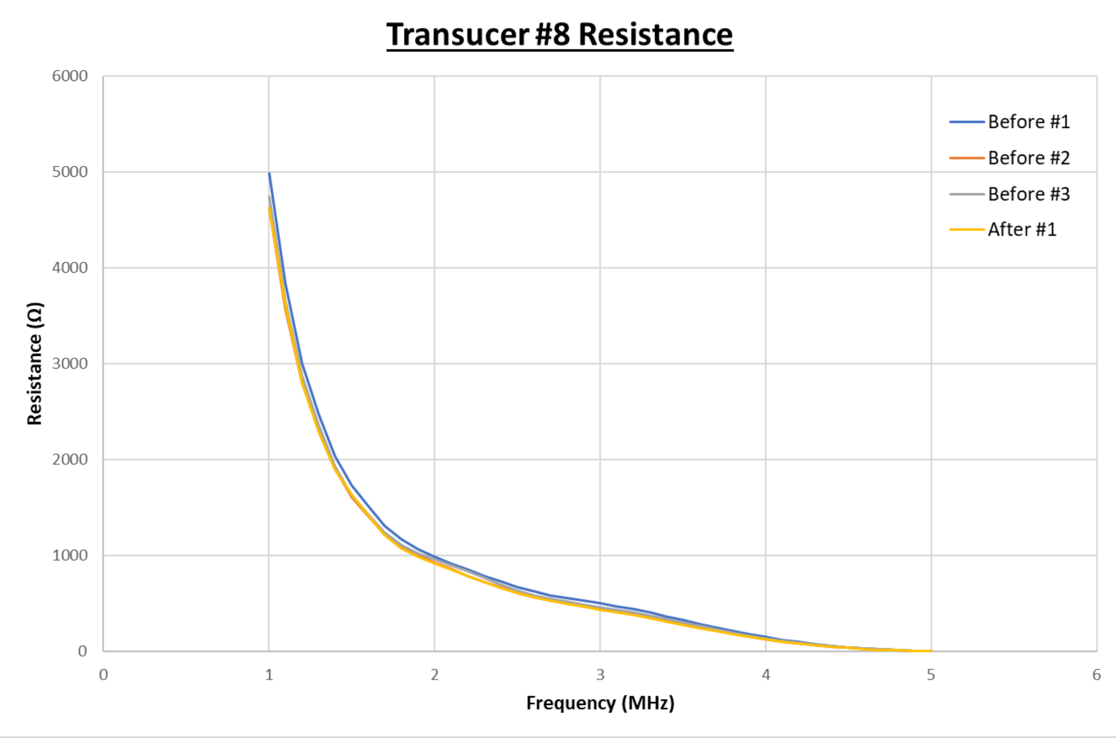


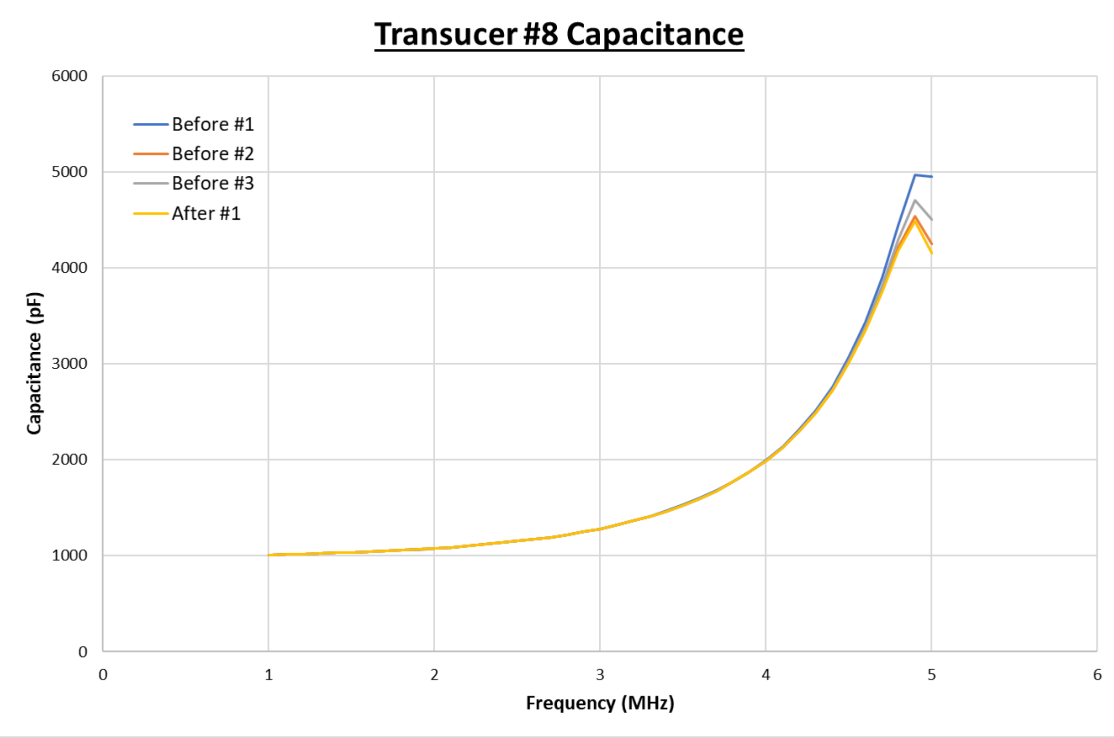

Transformative Science and Engineering for Nuclear Decommissioning

# Impedance measurements

Probe No. 9 shows significant changes in both resistance and capacitance.

Both plots mostly follow the same shape before and after irradiation.

Need to combine with 2D raster scan to determine where and how this changes the profile characteristics.

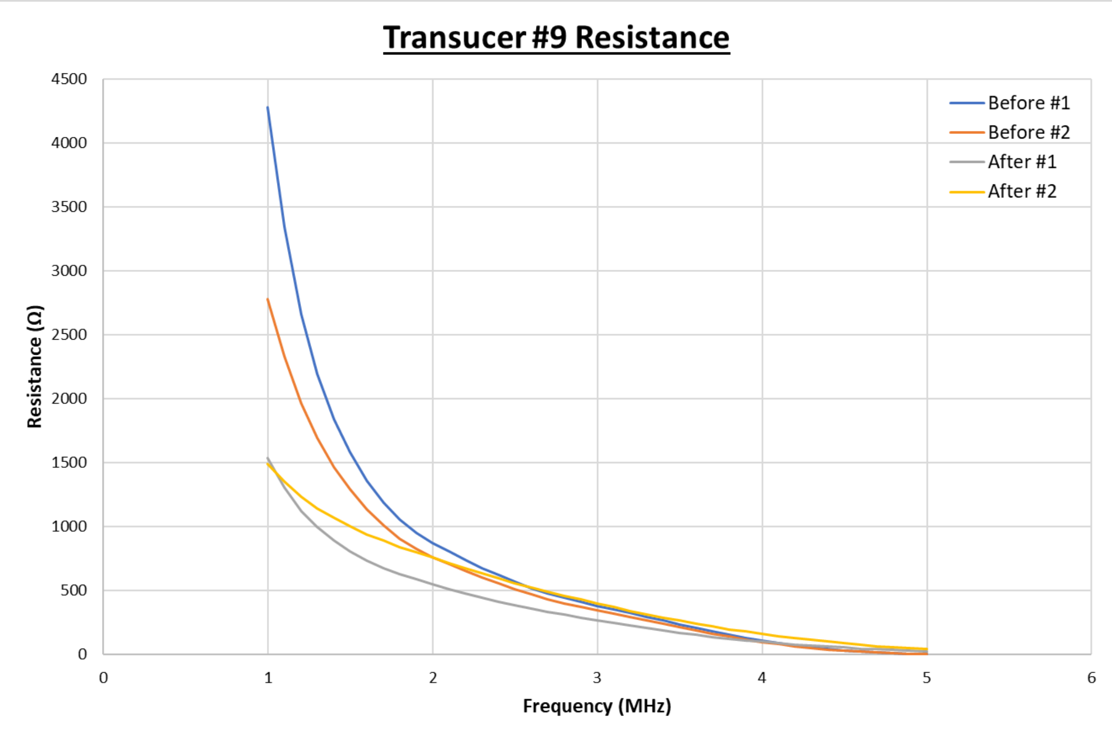


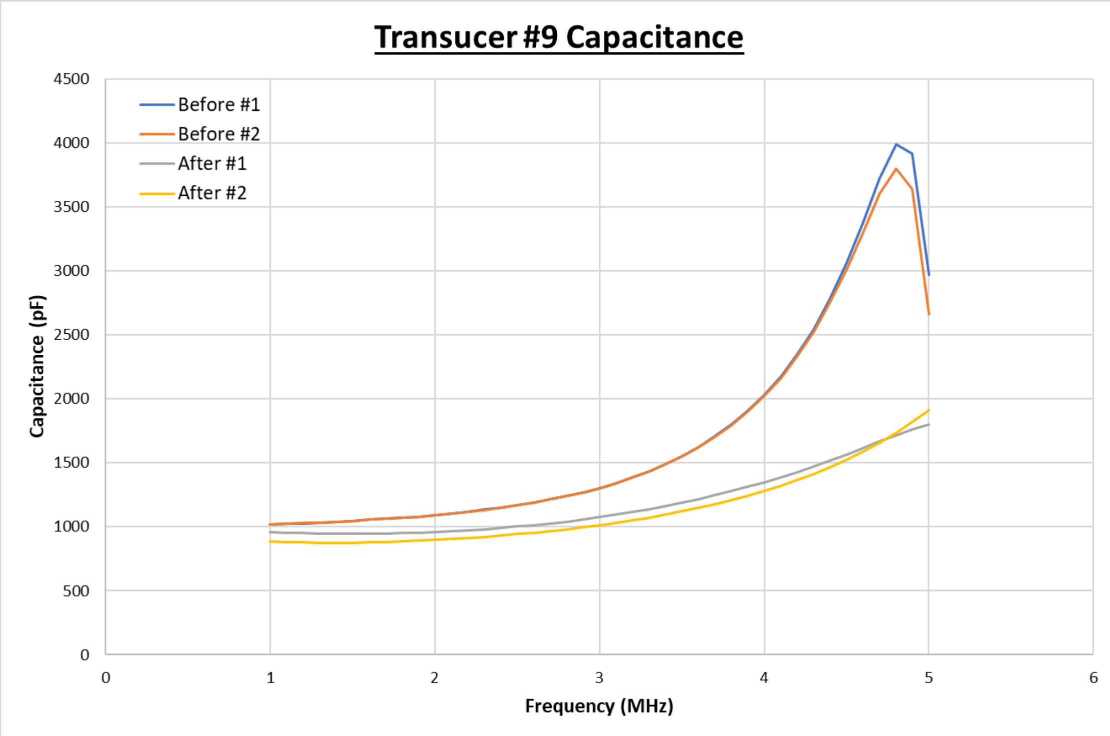

TRANSCEND

Transformative Science and Engineering for Nuclear Decommissioning

# Detailed 2D raster scans - Probe No. 8

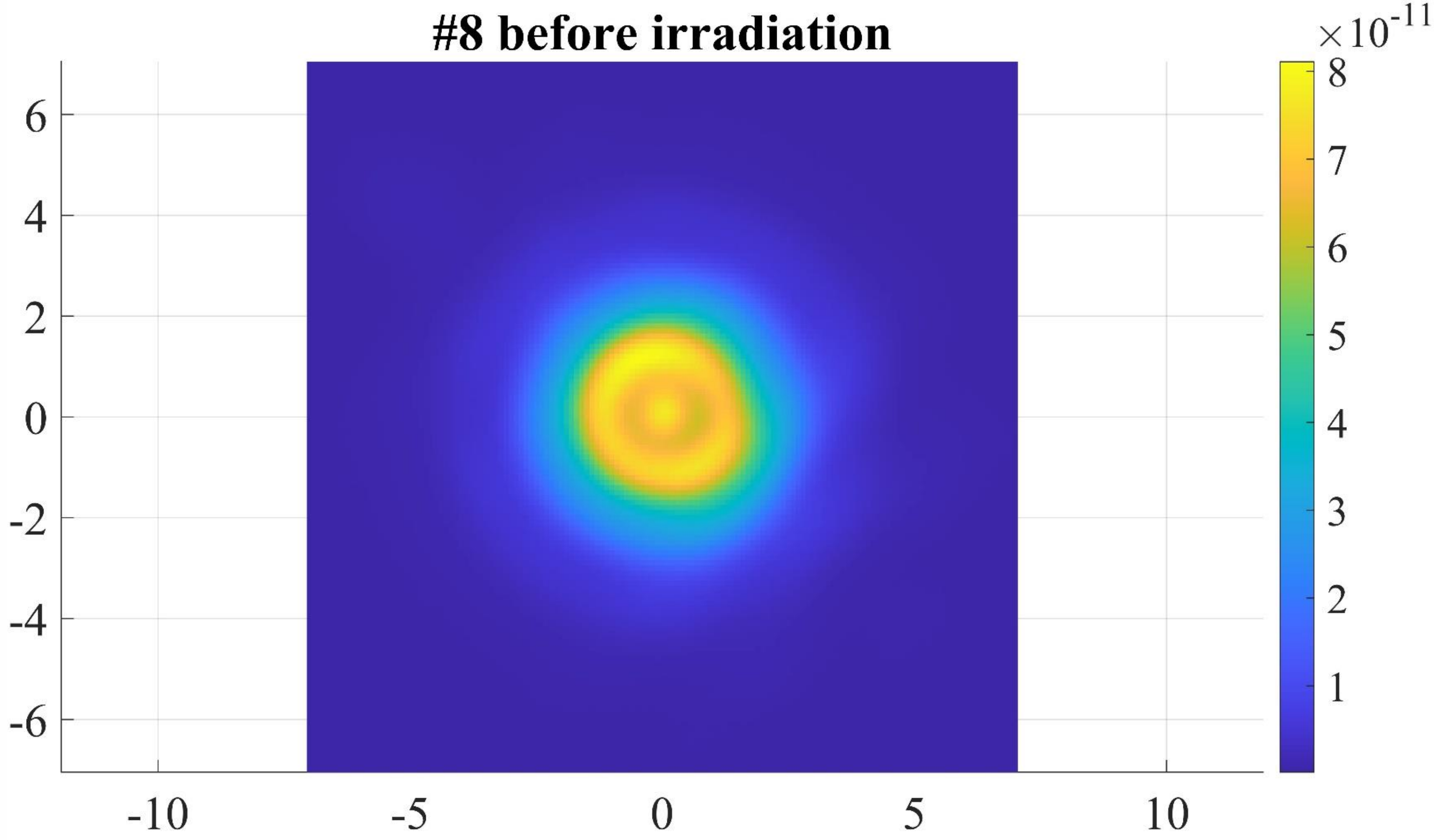

# Detailed 2D raster scans - Probe No. 8

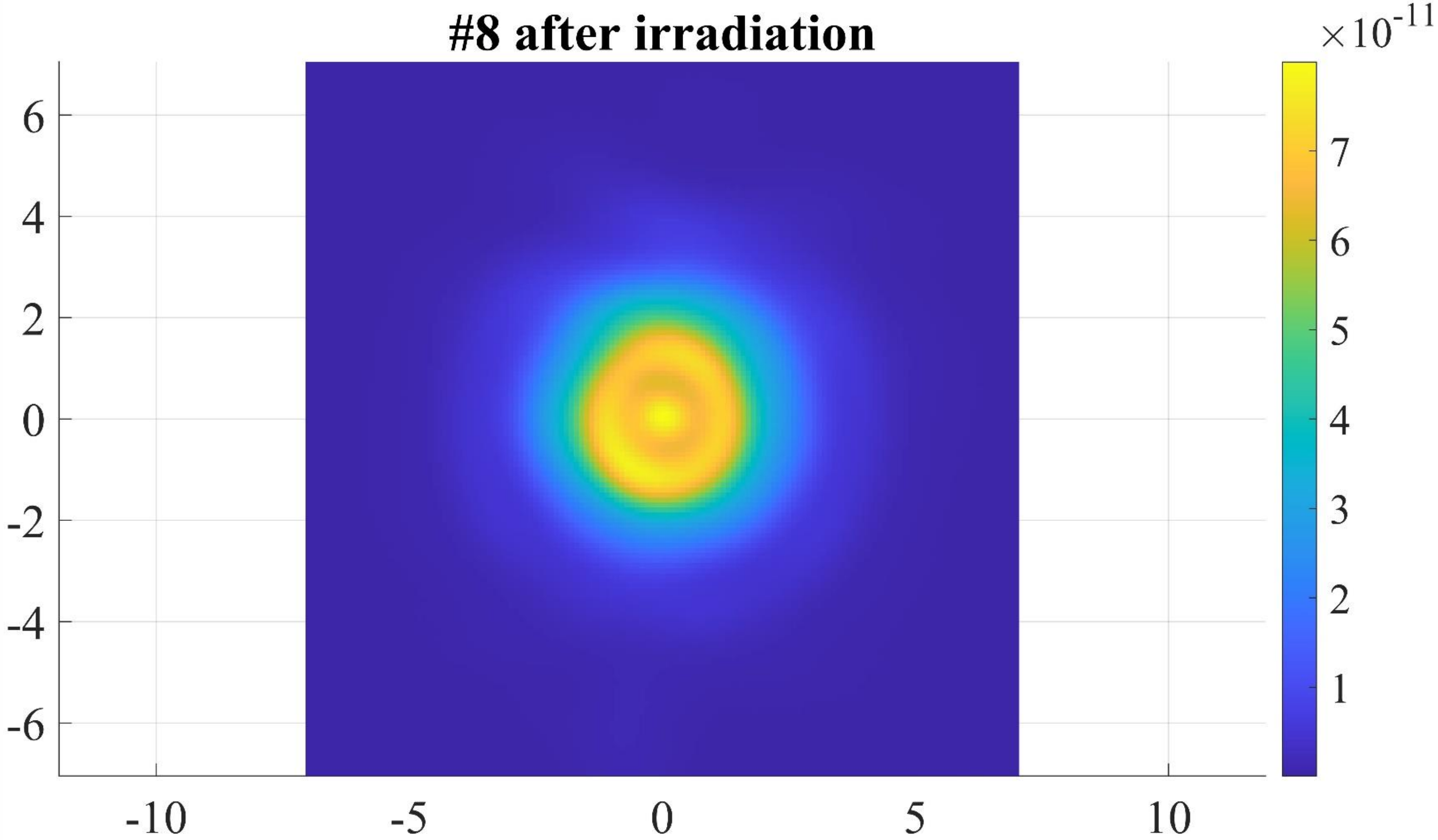

# Detailed 2D raster scans - Probe No. 9

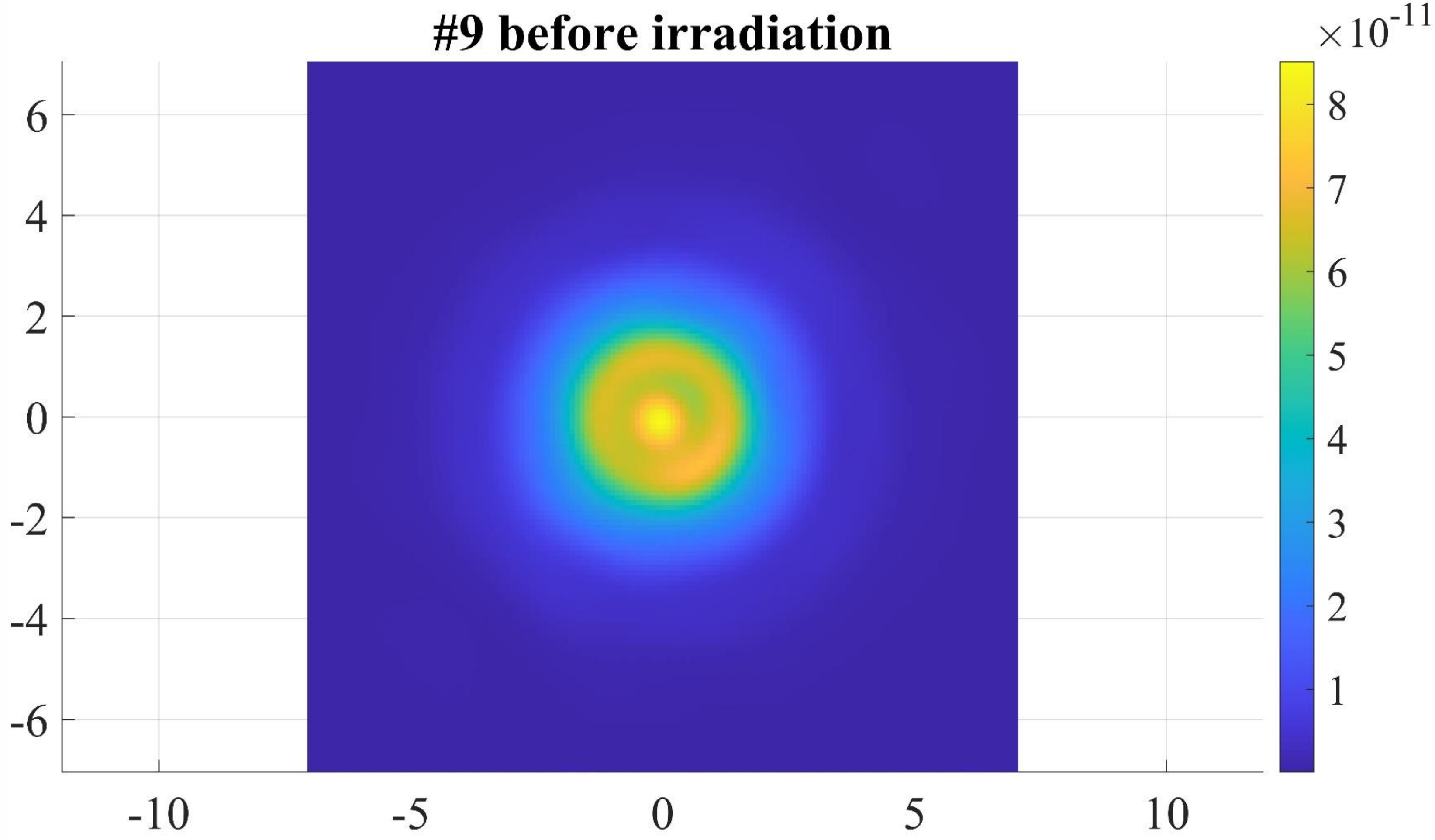

Transformative Science and Engineering for Nuclear Decommissioning

# Detailed 2D raster scans - Probe No. 9

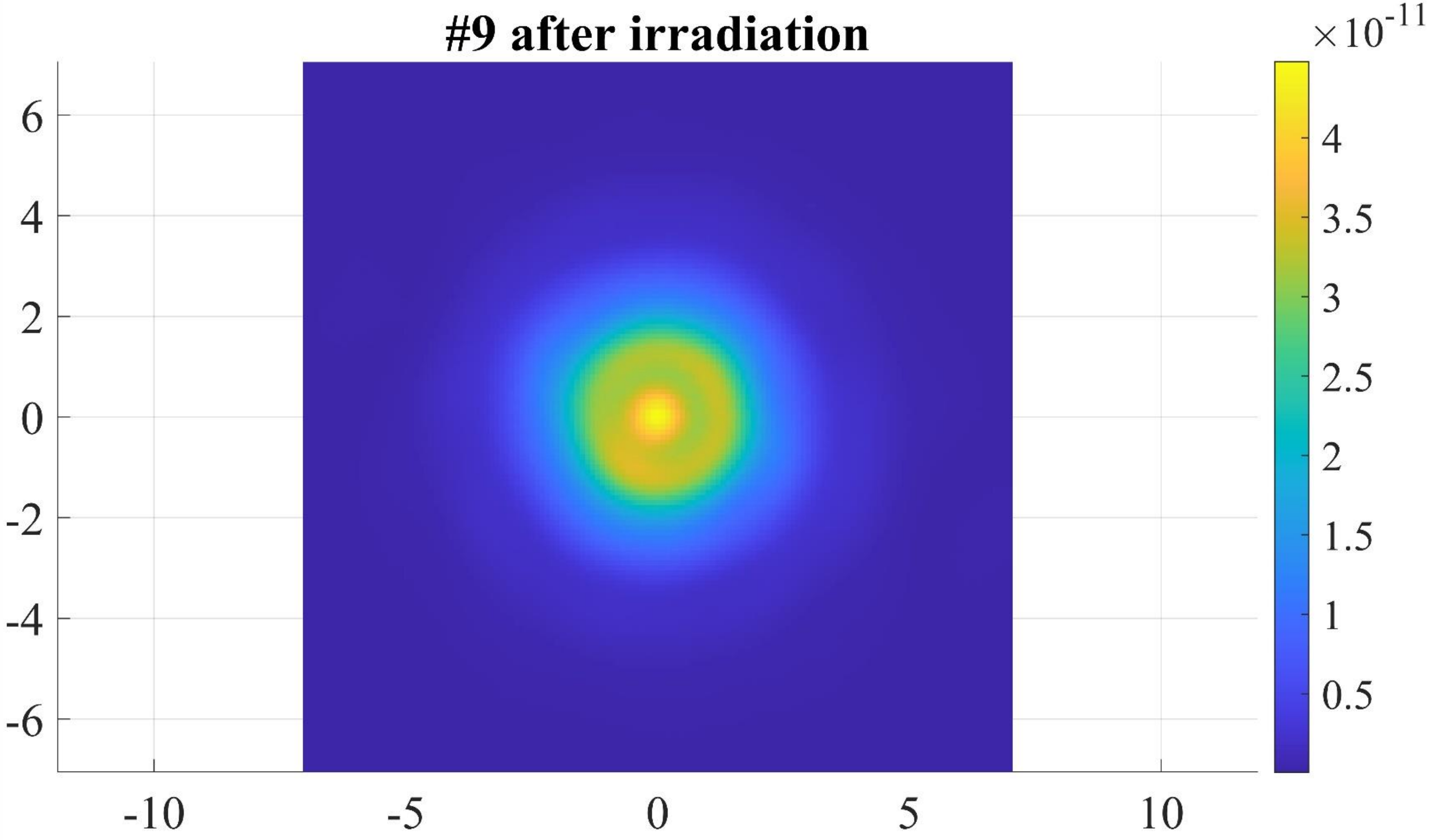

TRANSCEND

Transformative Science and Engineering for Nuclear Decommissioning

# Axial Hydrophone profile

Example of an axial scan completed with a hydrophone, with the Rayleigh distance (last axial maximum) highlighted where 2 further scans in the X and Y axes were completed.

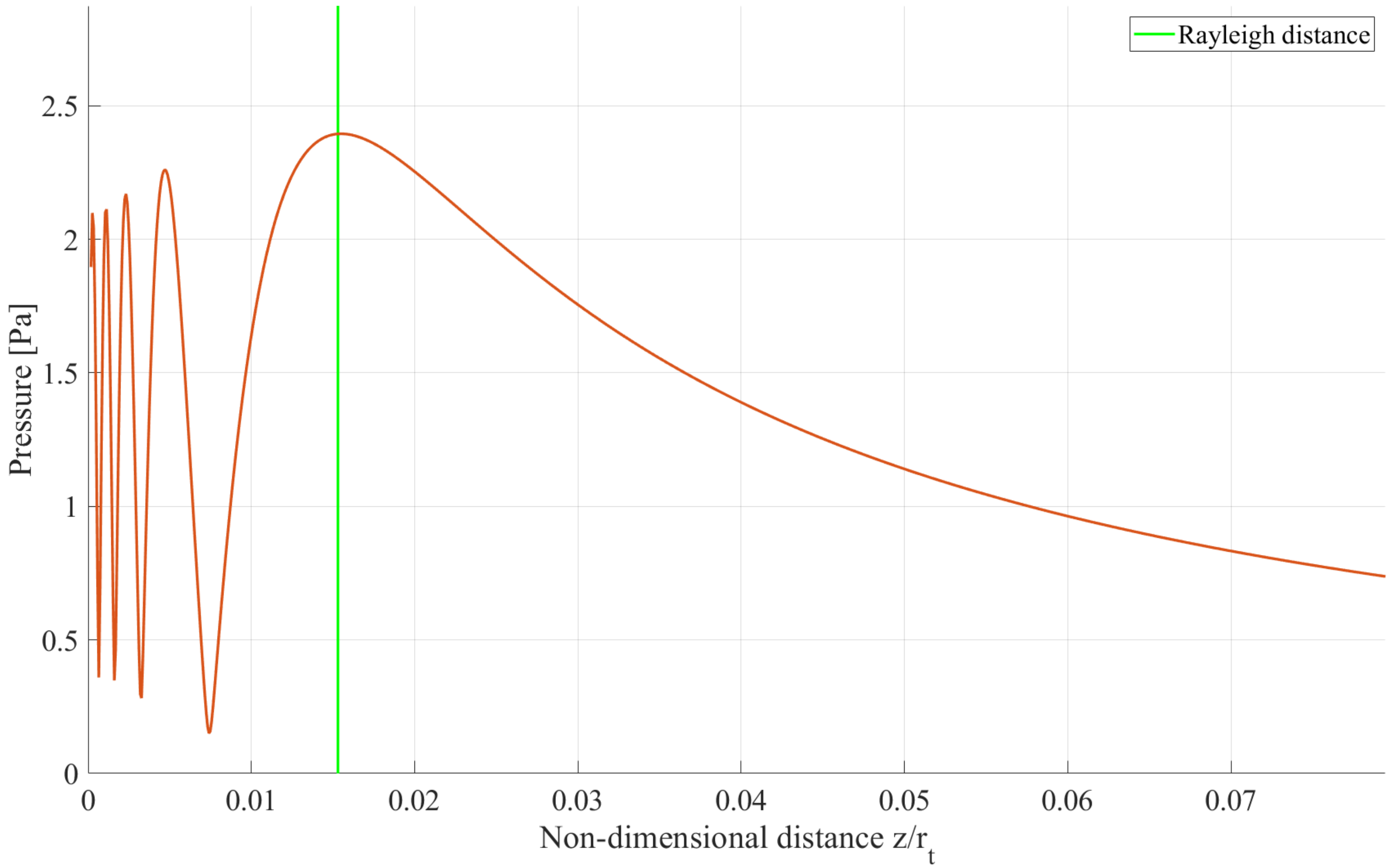

# Acoustic beam profile reconstruction

Combining the axial scans and 2D raster scan from each transducer, the complete acoustic beam profile can be reconstructed and comparisons between before and after irradiation identified.

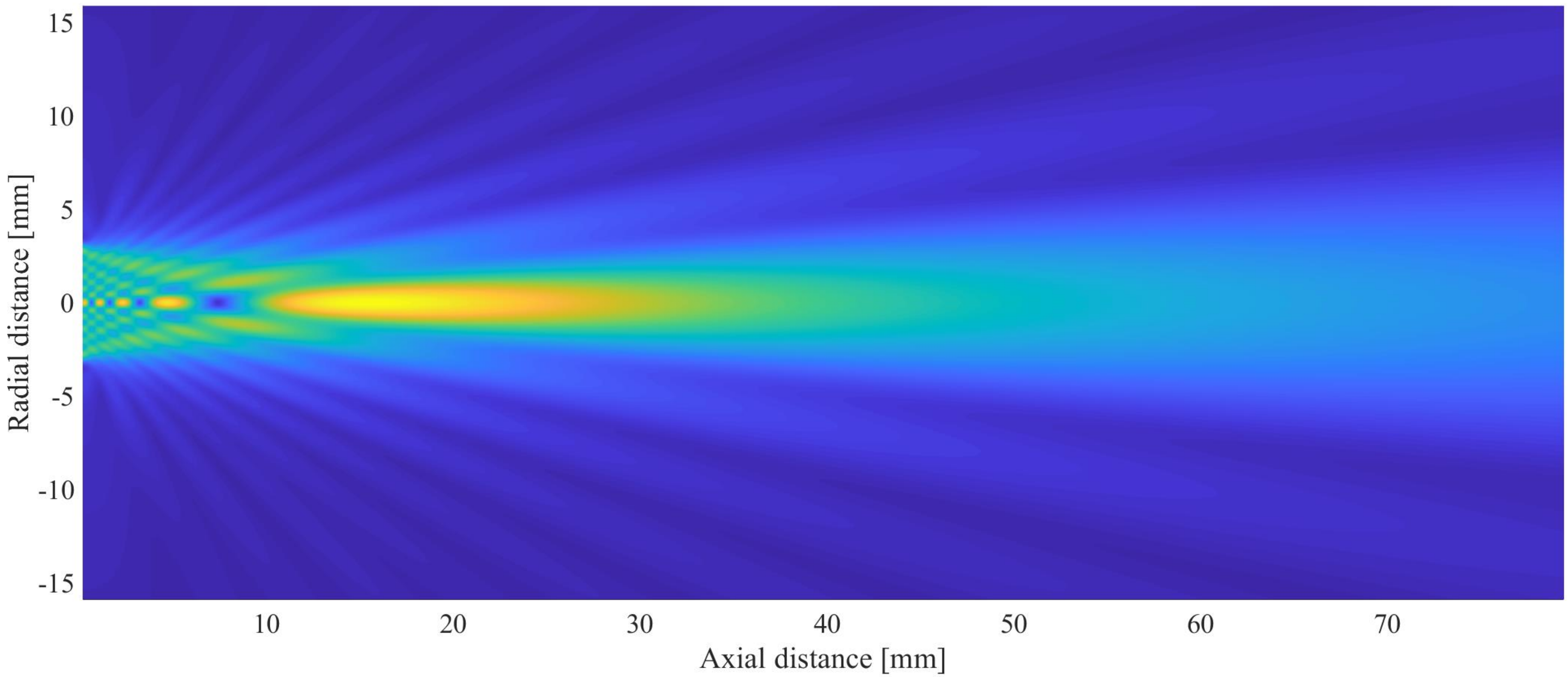

# Conclusions

- One transducer probe showed degradation from exposure to 1MGy of γ-radiation, this was identified by a decrease in intensity in 2D raster scans, as well as in the impedance measurements.
- The change is likely down to a change in the epoxy/glue within the probe, but the profile remained uniform and symmetrical, thus useable.
- Impedance measurements could be used as a check to determine whether probes in use are deteriorating from radiation.
- The other transducer showed little to no change in any measurements.

# Further work

- Quantify the changes in acoustic performance from the data gathered at NPL;
  - Impedance measurements
  - Pulse-echo response of the transducer using a standard reflecting target
  - Axial beam-profiling
  - Detailed 2D raster scans
  - Reconstruct full acoustic profiles
- Carry out US backscatter testing with the irradiated probes and compare performance and parameters to values before irradiation.
  - Sediment attenuation coefficient
  - Transducer backscatter coefficient
  - Sediment backscatter coefficient
- Collate all results and publish a paper

# Acknowledgements

Supervisors: Jeffrey Peakall, Richard Bourne, Jonathan Dodds, Timothy Hunter

NPL: Bajram Zeqiri, Piero Miloro, Andre Alvarenga

NPL

NUCLEAR ENGINEERING
University of Leeds

NATIONAL NUCLEAR LABORATORY

MANCHESTER 1824
The University of Manchester
Dalton Nuclear Institute

UKRI
Engineering and Physical Sciences Research Council

TRANSCEND

Transformative Science and Engineering for Nuclear Decommissioning

Thank you

Email: pmjha@leeds.ac.uk

# Electrokinetic remediation of difficult-to-measure radionuclides at nuclear sites

Shaun D. Hemming, Frances M. Burrell, Ian T. Burke, Richard I. Marsh, James Graham, Phil E. Warwick and Andy B. Cundy

S.D.Hemming@soton.ac.uk

National Oceanography Centre, Univ. Southampton, European Way, Southampton, UK SO14 3ZH

## What is Electrokinetic Remediation (EKR)?

- Clean-up of the UK's nuclear legacy is estimated at ~ £200 billion over 100 years
- There is an urgent need to reduce decommissioning costs - could new approaches to remediation help?
- Technique must work in different materials AND be site-scalable, cheap, energy efficient and sustainable

**EKR involves decontamination by electrocution, concentrating pollutants within cell or at electrodes. It is an adaptable and low-energy waste minimisation technique**

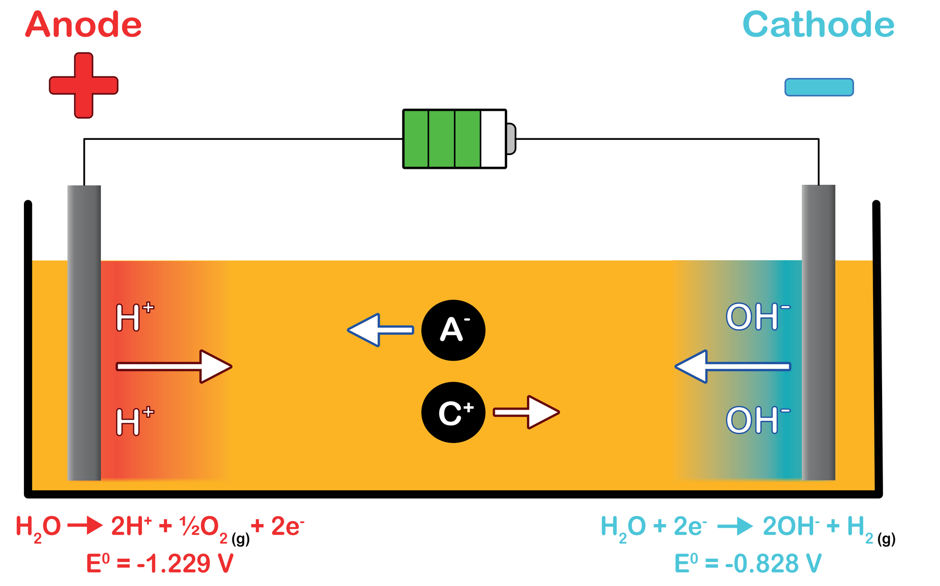


*Figure 1: A typical electrokinetic cell. $C^+$ are cations and $A^-$ are anions*

## Cements Work

- Collaborative work with University of Leeds and the NNUF-EXACT facility (Southampton) into whether EKR can remediate cement containing $^{236}$U, $^{137}$Cs, $^{129}$I, $^{90}$Sr and $^{3}$H
- Cement was chosen instead of concrete to simplify the system. Consequently, only cement and water were added, in a 2:1 ratio
- Cement cores were contaminated in 2 different ways:
  - Homogeneous Set - radionuclides were added as the cement and water were mixed (RNs are homogeneously distributed throughout core, simulating concrete biosheilding)
  - Soaking Set - cores were left to harden (known as curing) for 28 days and, afterwards, placed in a bath containing radionuclides (RNs are bound to the surface or near-surface, simulating storage pond concretes)
- Core treatment occurred for 41 days. Afterwards, the core was cut into sections for analysis (figure 2)

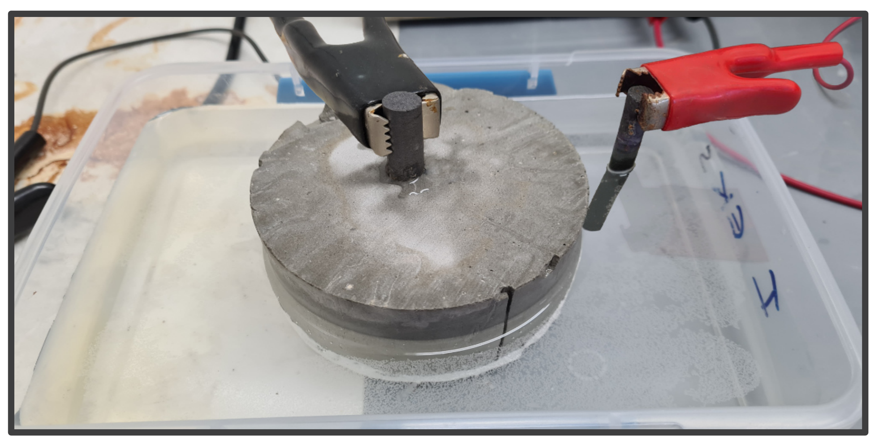

*Figure 2: **Left** - trial cement core undergoing electrokinetic treatment. **Right** - schematic showing how the core was cut, and the naming convention for each section*

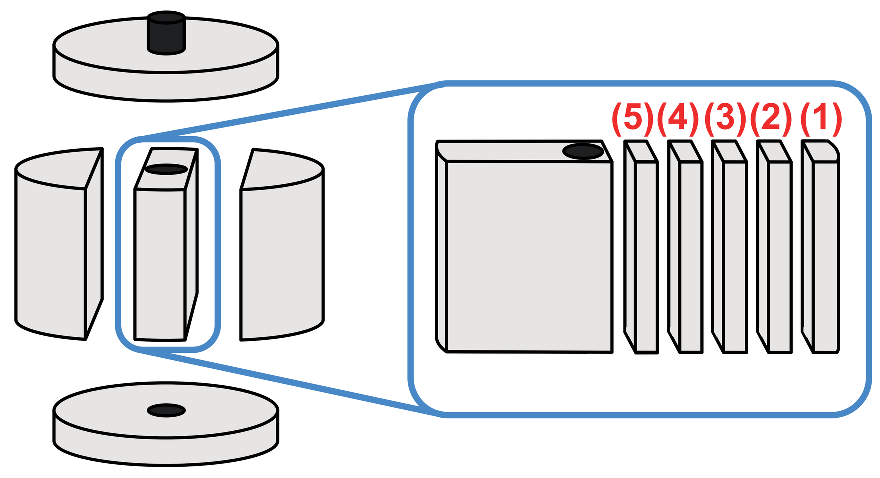


### Summary of Results

- **$^{137}$Cs shows high rates of mobility in the Homogeneous-Set when EKR is applied** (see below)
- **$^{236}$U, $^{129}$I and $^{90}$Sr all show little to no mobilisation in all cores** (See below for $^{129}$I). This is expected for $^{236}$U and $^{90}$Sr but surprising for $^{129}$I as it is commonly mobile in cementitious pore waters
- **$^{3}$H data are inconclusive due to notable loss of tritium in all cores**
- **For all radionuclides, a greater degrees of mobilisation is seen in the Soaking-Set compared to the Homogeneous-Set.** This is to be expected as the Soaking-Set has surface-adsorbed contamination whilst the Homogeneous-Set is likely to have contamination contained within cement mineral phases

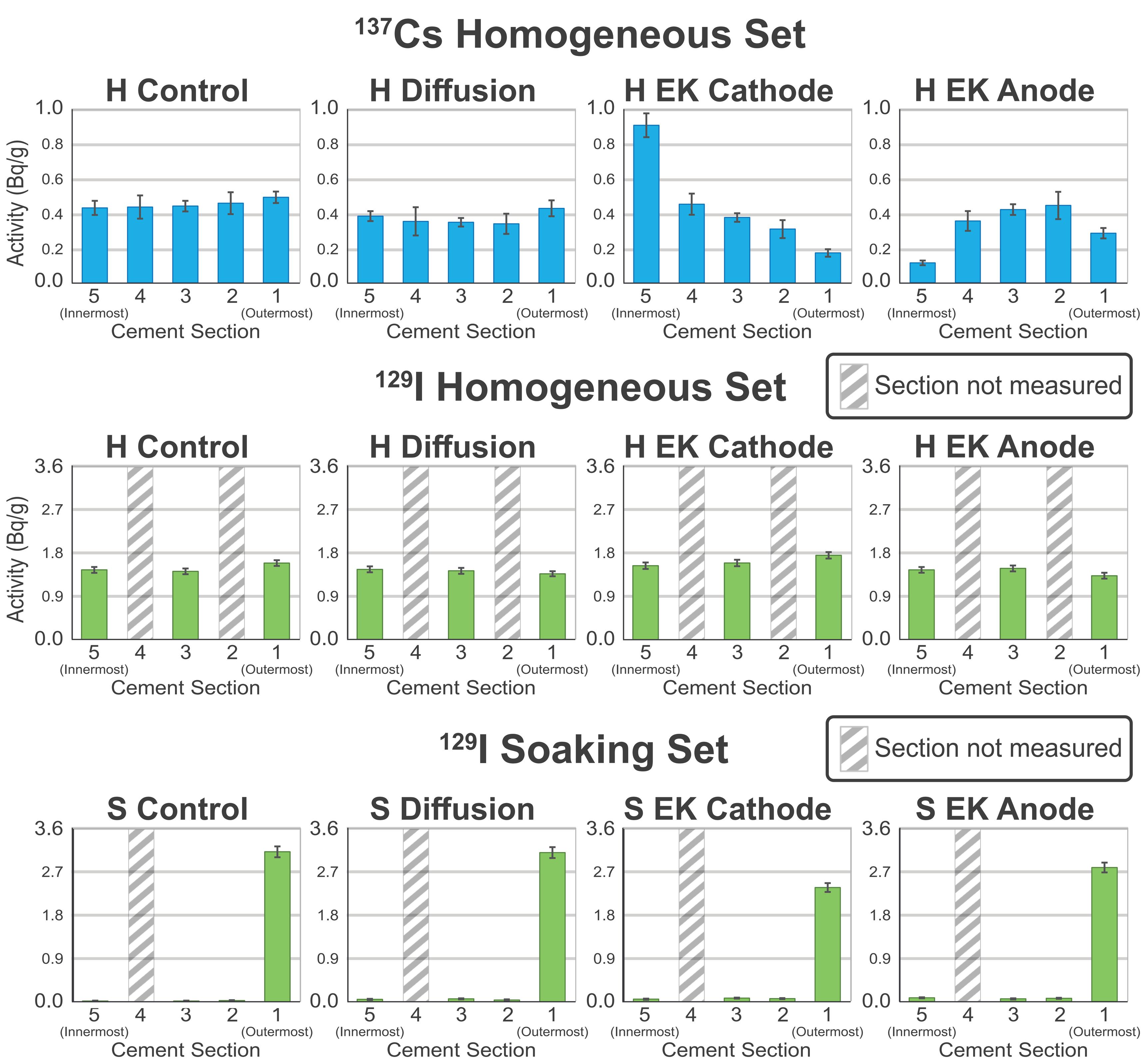


*Figure 3: **Left** - $^{137}$Cs data from Homogeneous-Set cores and $^{129}$I data from all cores. For schematic of where each section was positioned, see figure 2 (**right**)*

## Sediment Core - Commencing May 2023

- Evaluation of whether electrokinetics can migrate the radionuclides present in a 55 cm sediment core from the Ravenglass saltmarsh (~9 km south east of Sellafield)
- Sellafield discharges into the Irish Sea have accumulated in the saltmarsh
- Historical discharges are buried over time by new sediment, creating a discharge profile in the core
- Radionuclides may have been remobilised over time due to changes in conditions
- Itrax XRF scan shows stable element composition throughout the core. Key elements are:
  - S indicates whether the sulphidic zone of respiration has been reached
  - Mn and Fe mark sub-oxic zone of respiration
- Radionuclide analysis will follow soon

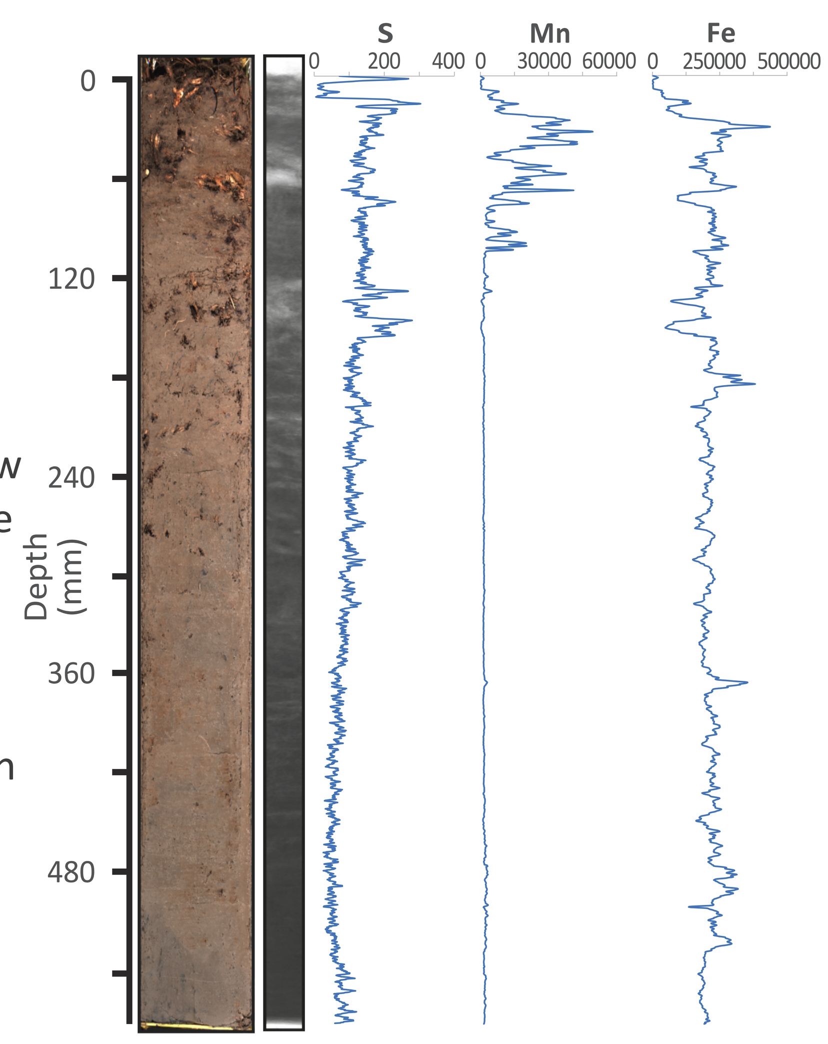


*Figure 4: Optical image, radiograph and Itrax XRF scan of key stable elements in the Ravenglass sediment core before EKR treatment*

**Acknowledgements:** GAU Radioanalytical; NERC, INSPIRE DTP and TRANSCEND consortium project (EPSRC grant number EP/S01019X/1) for funding; the British Ocean Sediment Core Research Facility (BOSCORF) for supporting XRF core scanning; the National Nuclear User Facility EXACT laboratory and team, via the UK EPSRC (grant EP/T011548/1), for support with cements work; the British Geological Survey for autoradiography data.

Transformative Science and Engineering for Nuclear Decommissioning

transcendconsortium.org

TRANSCEND

Transformative Science and Engineering for Nuclear Decommissioning

# Tomography of stress corrosion cracking from an in-situ tensile corrosion synchrotron experiment

Kuo Yuan, University of Bristol

Ronald Clark, National Nuclear Laboratory

Mahmoud Mostafavi, University of Bristol

Transcend Annual Meeting 2023

25th April 2023

Energy

For a Low Carbon Future

# Introduction

Aim: To develop a new small punch test (SPT) setup for spent AGR cladding with surrogate material (thermally sensitised 304 stainless steel) that can initiate SCC (stress corrosion cracking) of stainless steel in a short period time with DIC (Digital image correlation) observation.

Stress corrosion cracking is caused by a combination of susceptible material, corrosive environment and mechanical driving force.

An in-situ corrosion experiment was proposed to compare SCC propagation in 3D with surface propagation by using tomography from a synchrotron x-ray source.

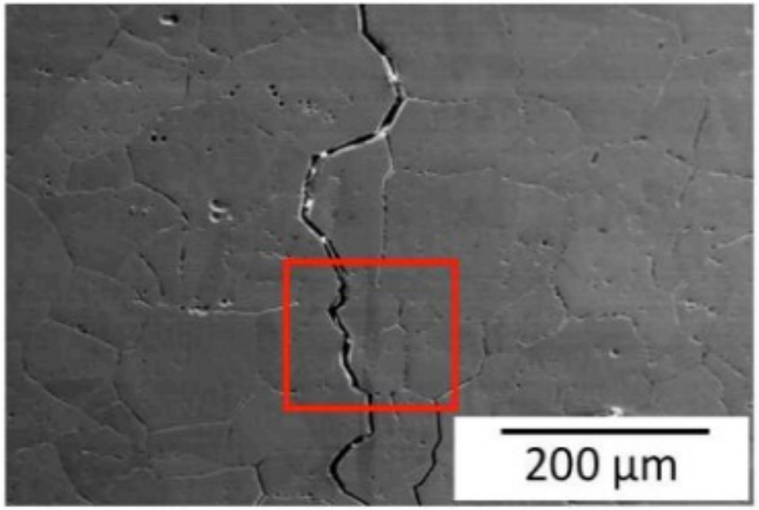


Fig. 1. Crack initiation of a stress corrosion crack [1]

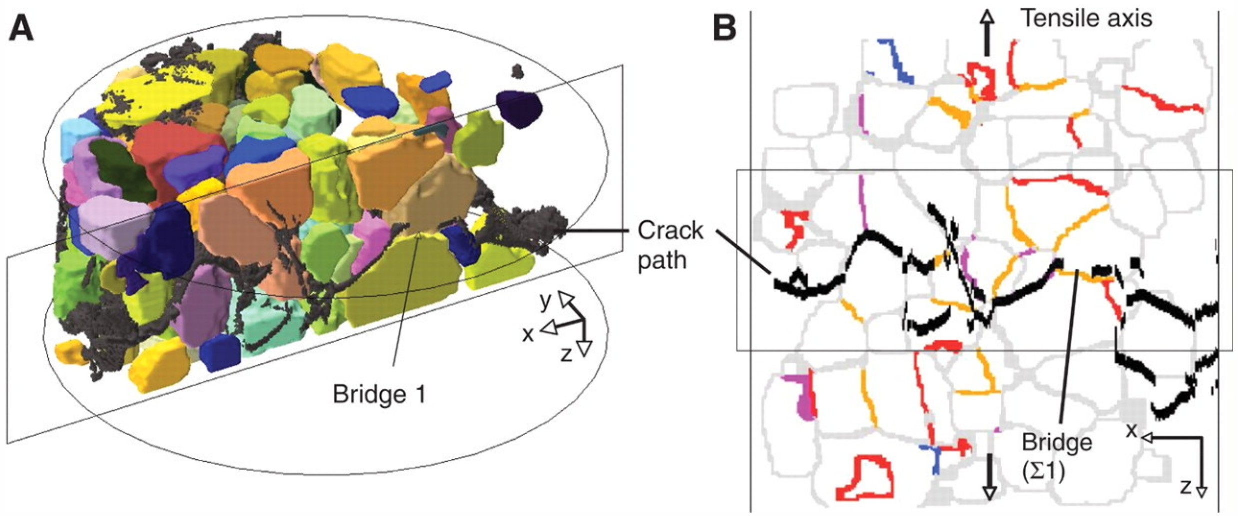


Fig. 2. DCT (diffraction contrast tomography) image showing the propagation of SCC in 3D [2]

[1] A. Stratulat, J. A. Duff, and T. J. Marrow, "Grain boundary structure and intergranular stress corrosion crack initiation in high temperature water of a thermally sensitised austenitic stainless steel, observed in situ," Corros. Sci., vol. 85, pp. 428–435, 2014, doi: 10.1016/j.corsci.2014.04.050.
[2] A. King, G. Johnson, D. Engelberg, W. Ludwig, and J. Marrow, "Observations of intergranular stress corrosion cracking in a grain-mapped polycrystal," 2008.

# Background

The synchrotron experiment was granted to carry out on 1st-4th March 2023 at DIAD (**D**ual **I**maging **A**nd **D**iffraction) beamline, Diamond Light Source, which allows imaging and diffraction (almost) at the same time with energy levels of 7-38 keV and a FOV of 1.4 mm x 1.2 mm.

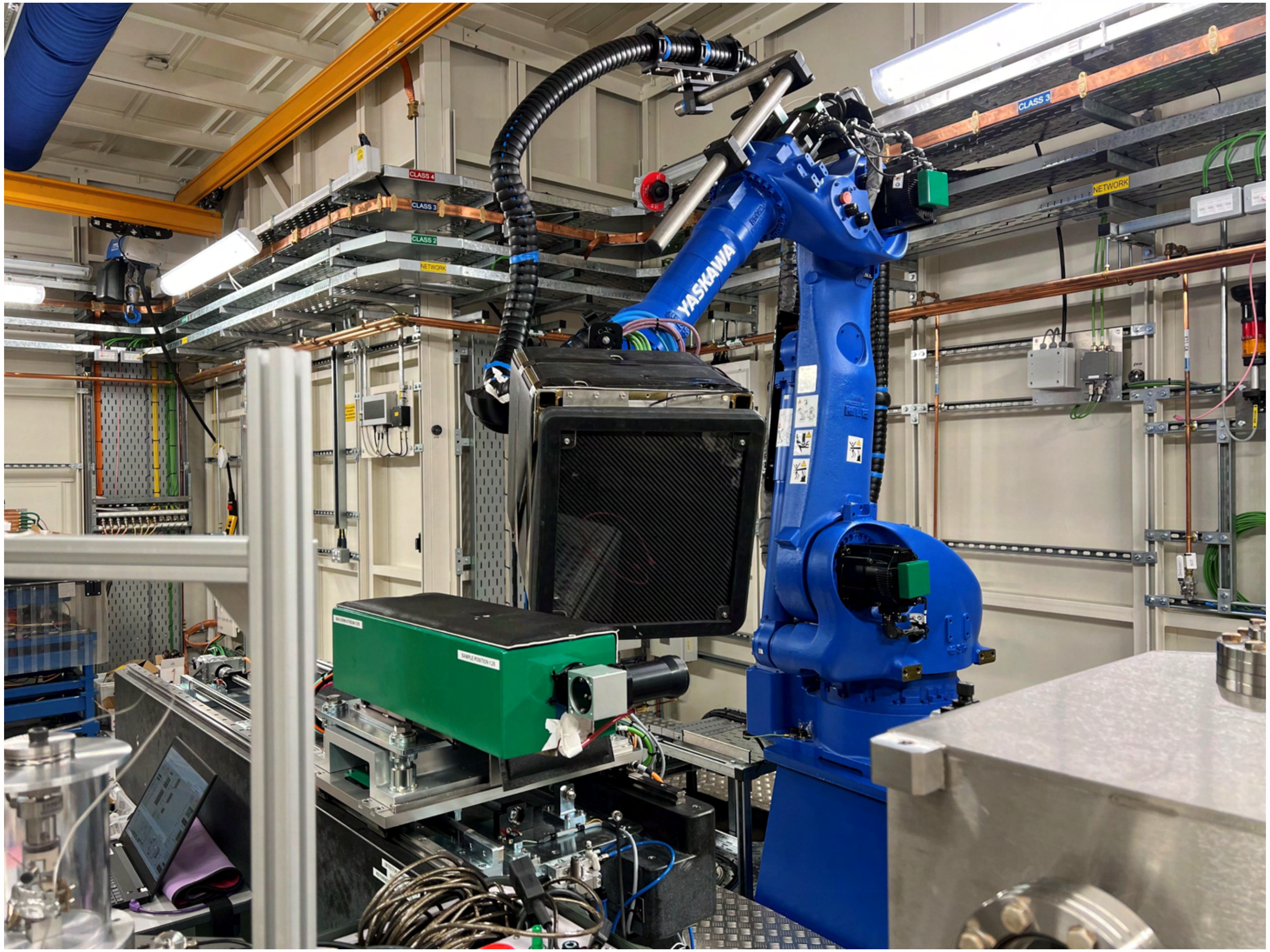


Fig. 3. Imaging camera and diffraction detector of DIAD

# Experimental plan

- An in-situ corrosion tensile experiment that can allow fast SCC initiation by holding a load and X-ray tomography imaging in real time.
- Test both the surrogate material (thermally sensitised 304 stainless steel) and AGR fuel cladding (thermally sensitised 20/25/Nb stainless steel.
- Diffraction between tomography scans to find the chemical composition near the cracks.
- FIB milling after the synchrotron experiment to study the relationship between the crack path and the grain boundary properties.

# Tensile rig

A tensile rig was designed and made:

- Two layers of polycarbonate tubes are X-ray transparent
- The tensile sample is placed in the inner tube
- A load can be applied by turning a bolt on top of the rig
- The load can be measured by the load cell
- A corrosive solution is filled in the inner tube through the nozzle
- The solution can be heated with a heating element and the temperature can be measured using the thermocouples
- The heater can keep the solution at 70°C when the target set at 85°C.

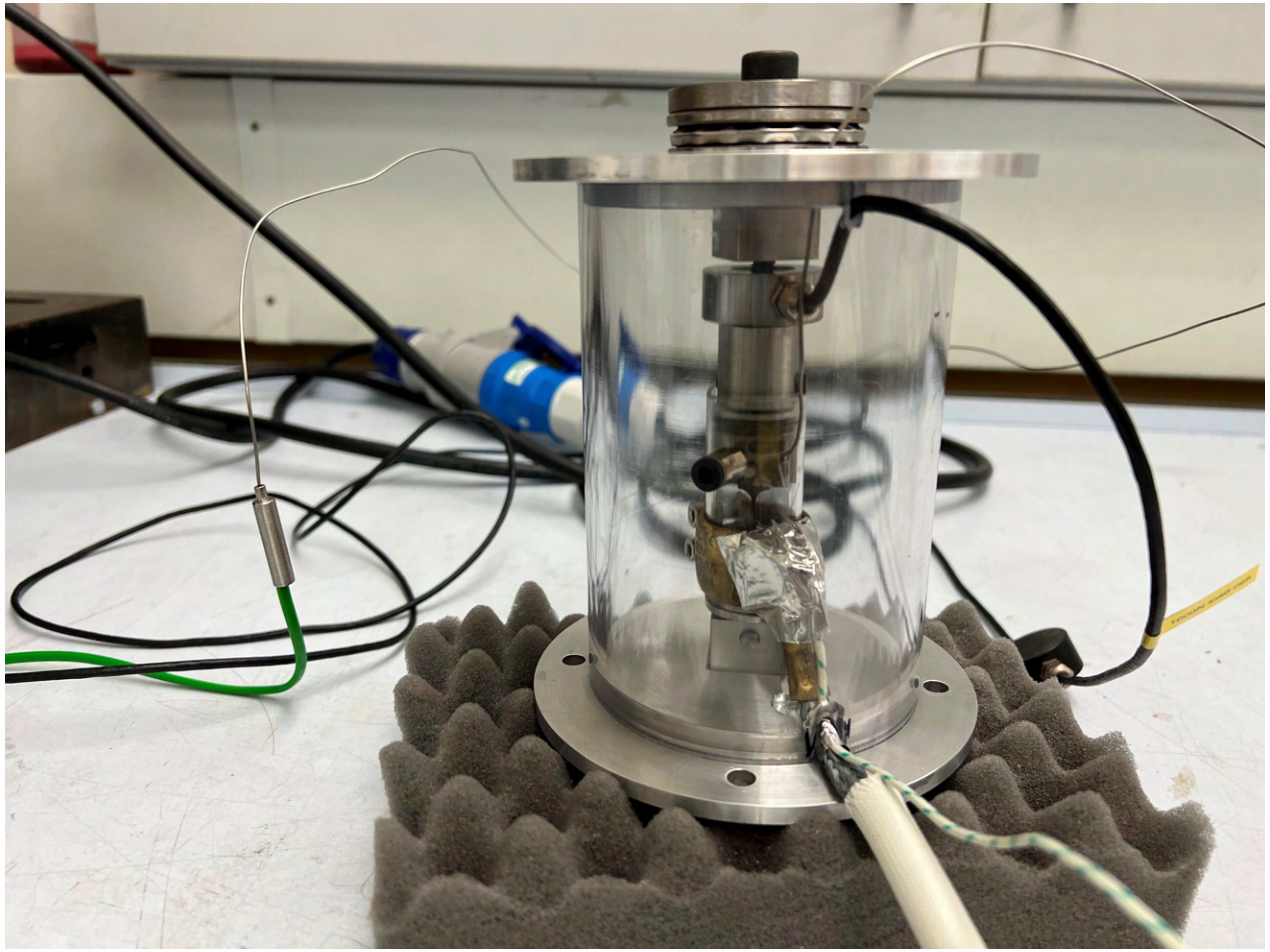

Fig. 4. Tensile rig for the in-situ synchrotron experiment

# Sample Preparation

Both 304 and 20/25/Nb stainless steel have been thermally sensitised:

- 304ss: aged at 600 °C for 50 hours and cooled in air;
- 20/25/Nb: annealed at 1050 °C in argon for 30 minutes and quenched in water then aged at 600 °C for 50 hours and cooled in air.

The dimensions of them are the same apart from the thickness: 20/25/Nb: 0.8mm, 304ss: 0.9mm.

Different combinations of surface finish were prepared to compare the relationship between SCC and the surface roughness:

- Rough sample: 600 grit for both the faces and the edges
- Fine sample: 1µm on the faces, 1200 grit on the edges
- Mixed samples with rough and fine surfaces

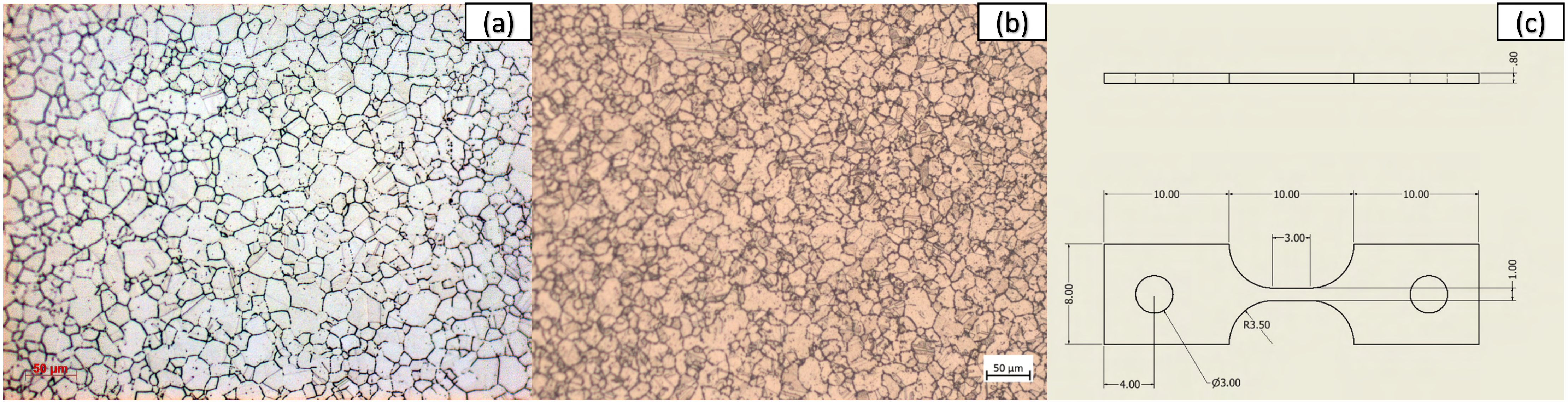


Fig. 5. Grains of etched (a) 304 stainless steel and 20/25/Nb stainless steel; (c) tensile sample design

# Load and environment

- Tensile tests using the Deben stage found the yield strength of two materials after the heat treatment: 304: 180 MPa; 20/25/Nb: 190 MPa. A load that can give 90% of yield stress will be applied to the samples accordingly.

- A corrosive solution with 1000ppm thiosulphate and 1440ppm $Cl^-$ heated to 80 °C was found to develop SCCs in 7 hours in a previous test.

- An inhibitor solution (1000ppm thiosulphate, 1440ppm $Cl^-$ and corresponding NaOH to increase pH to 11.4) will also be used to find out if it can reduce the rate of crack growth.

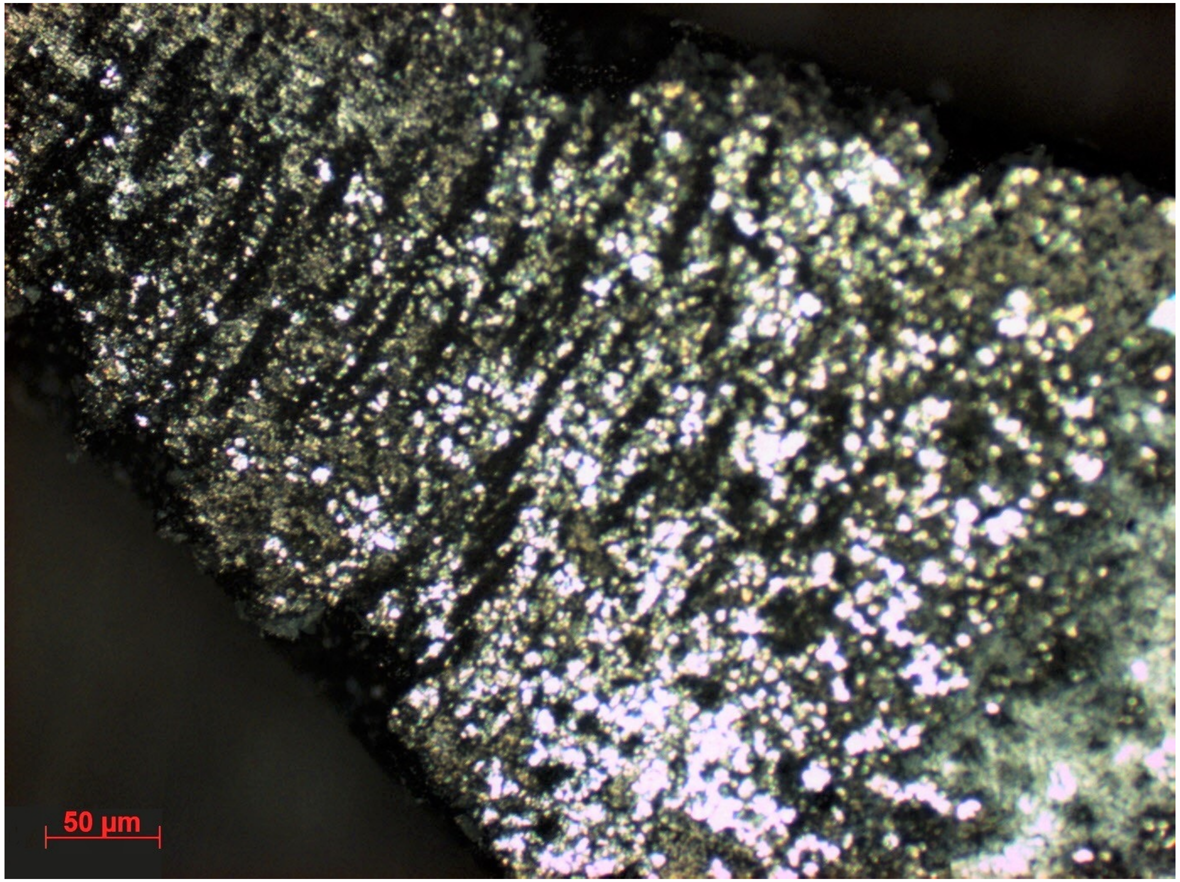


Fig. 6. Stress corrosion cracks on the surface of the a self loading tensile sample

# Trial test

A very rough 304 sample (240 grit) was held at 90% of yield and the solution (1000ppm thiosulphate and 1440ppm Cl solution) was heated to 70 °C for 7 hours. Some crack like features were observed on the edge of the sample.

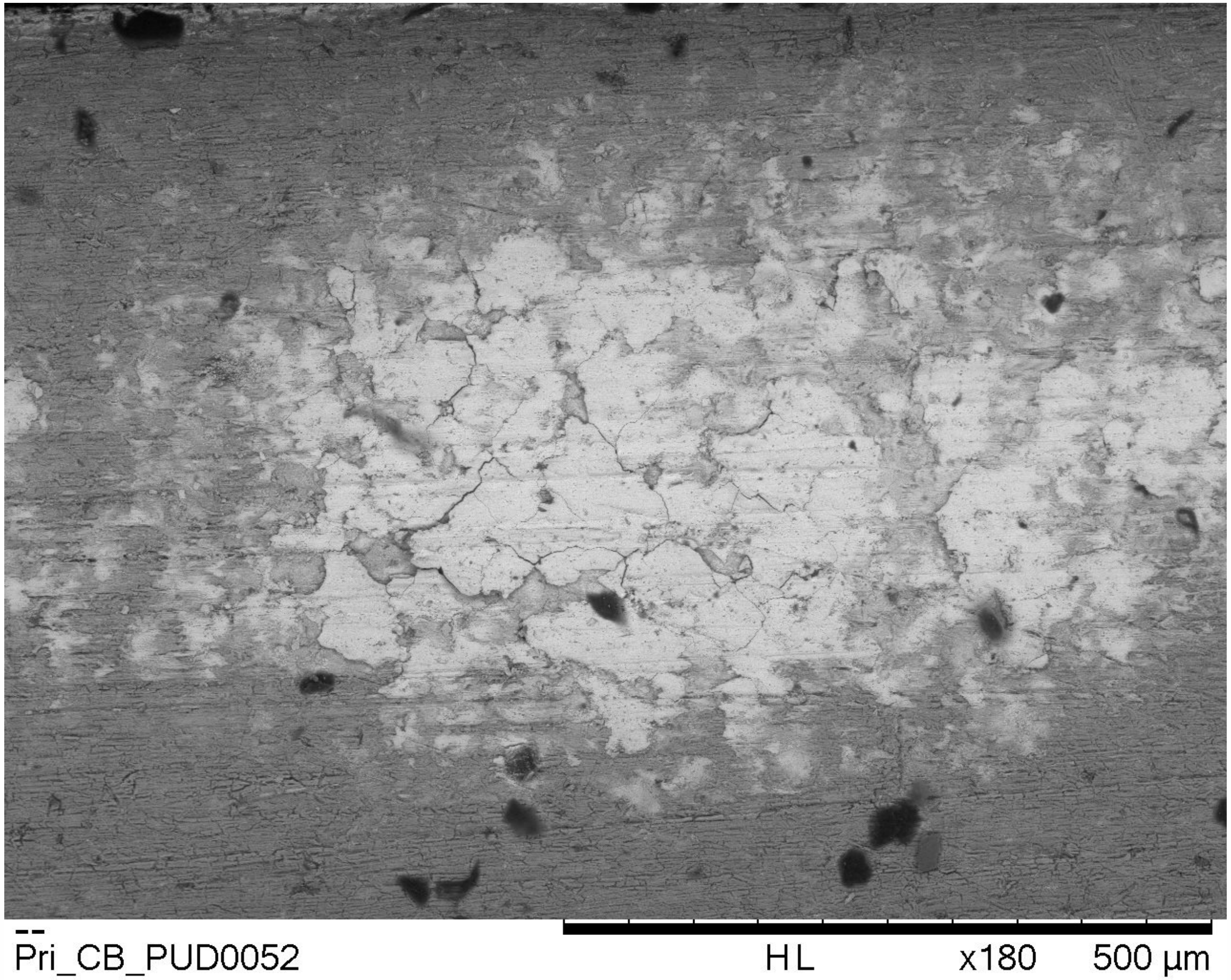


Fig. 7. SEM image of the trial sample

# Experiment

Four samples were planned to test:

| Sample | 1 | 2 | 3 | 4 |
|---|---|---|---|---|
| Material | 304 | 304 | 20/25/Nb | 20/25/N b |
| Surface finish | Rough | Mixed | Mixed | Mixed |
| Solution | Corrosiv e | Corrosive | Corrosive/ inhibitor | Corrosive |
| Duration (hours) | 10 | 18 | 12/6 | 18 (only 9 hours tested) |

All solutions were heated to 70°C and all samples were loaded and held to around 90% of yield.

Tomography was taken every 30 minutes and point diffraction was taken between each tomography.

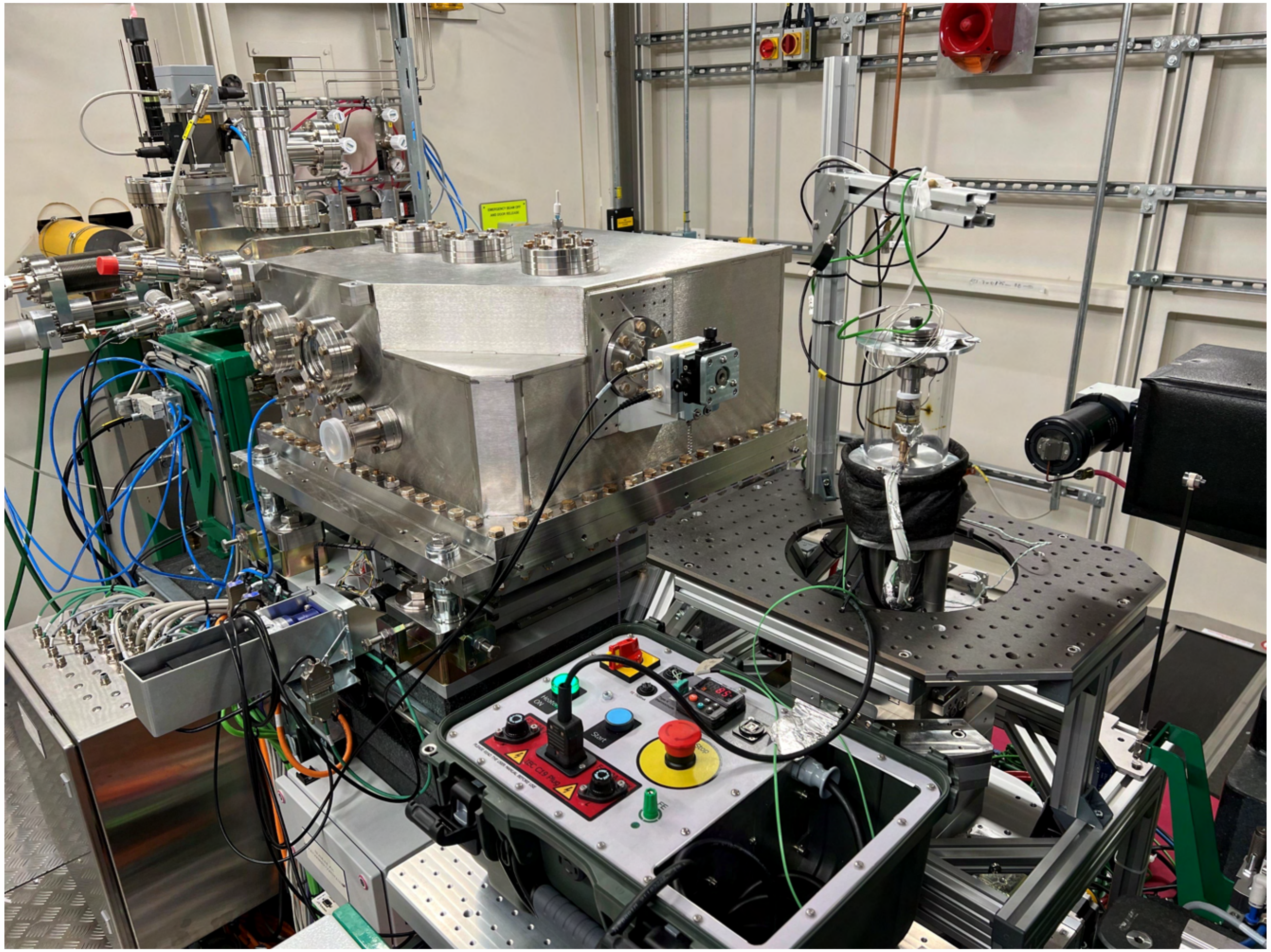

Fig. 8. Setup on the turning stage

# Results: radiographs

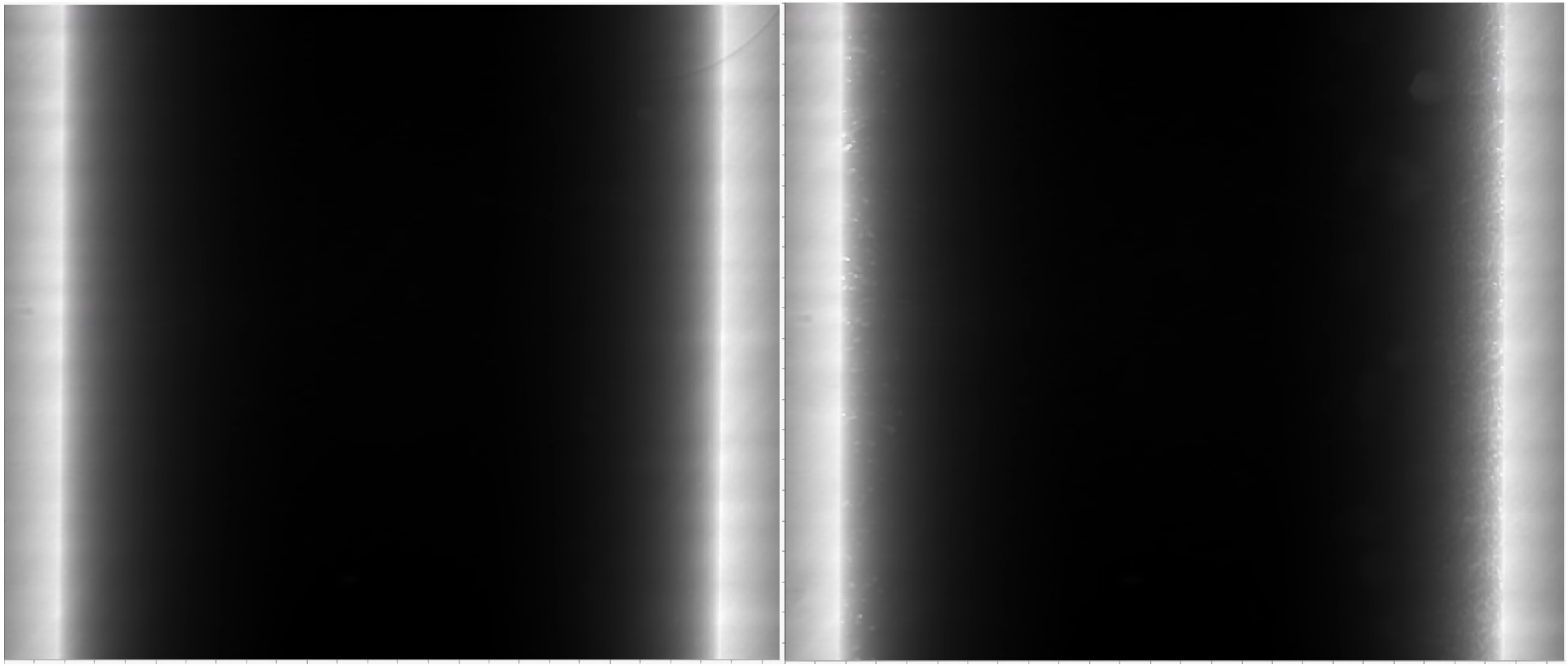

Fig. 9. radiographs of sample 1 (rough 304 stainless steel):
(left) at the beginning of the experiment, (right) at the end of the experiment

# Results: radiographs

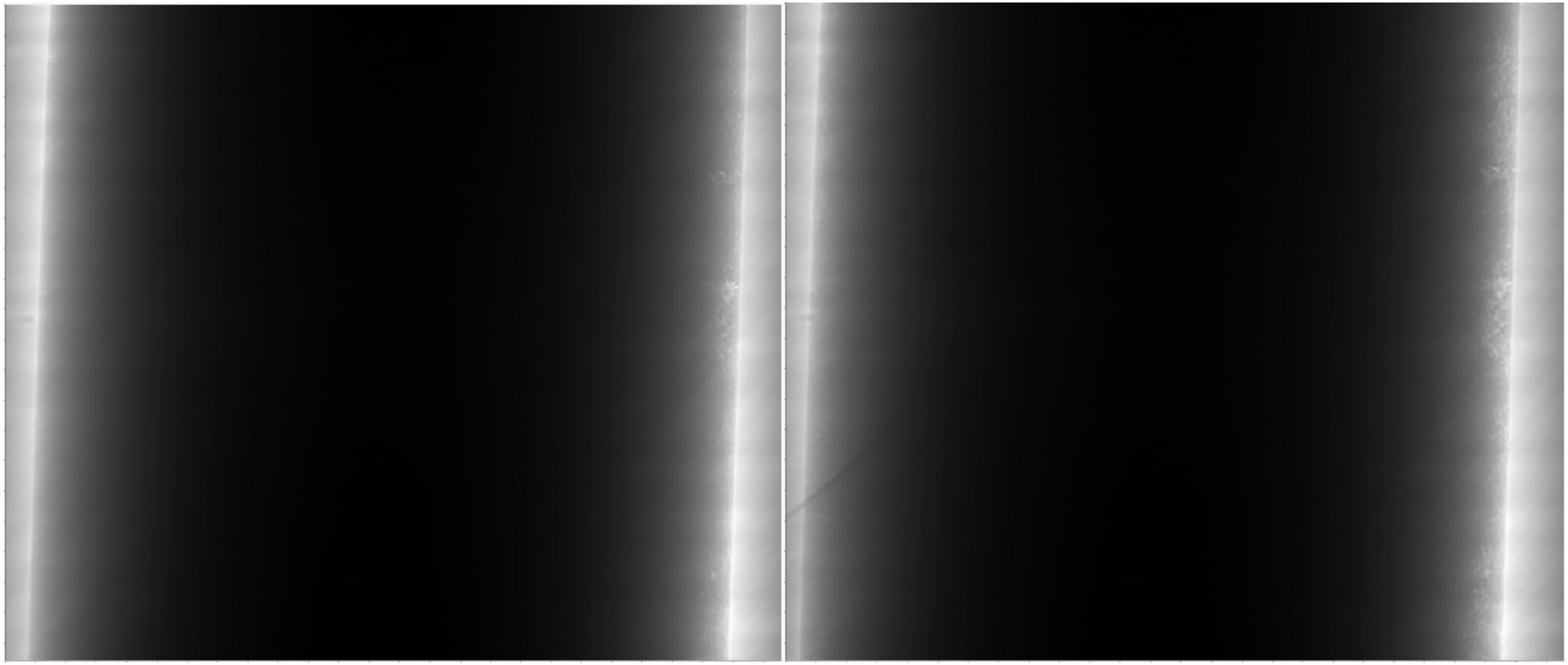

Fig. 10. radiographs of sample 2 (mixed 304 stainless steel): (left) at the beginning of the experiment, (right) at the end of the experiment

# Results: radiographs

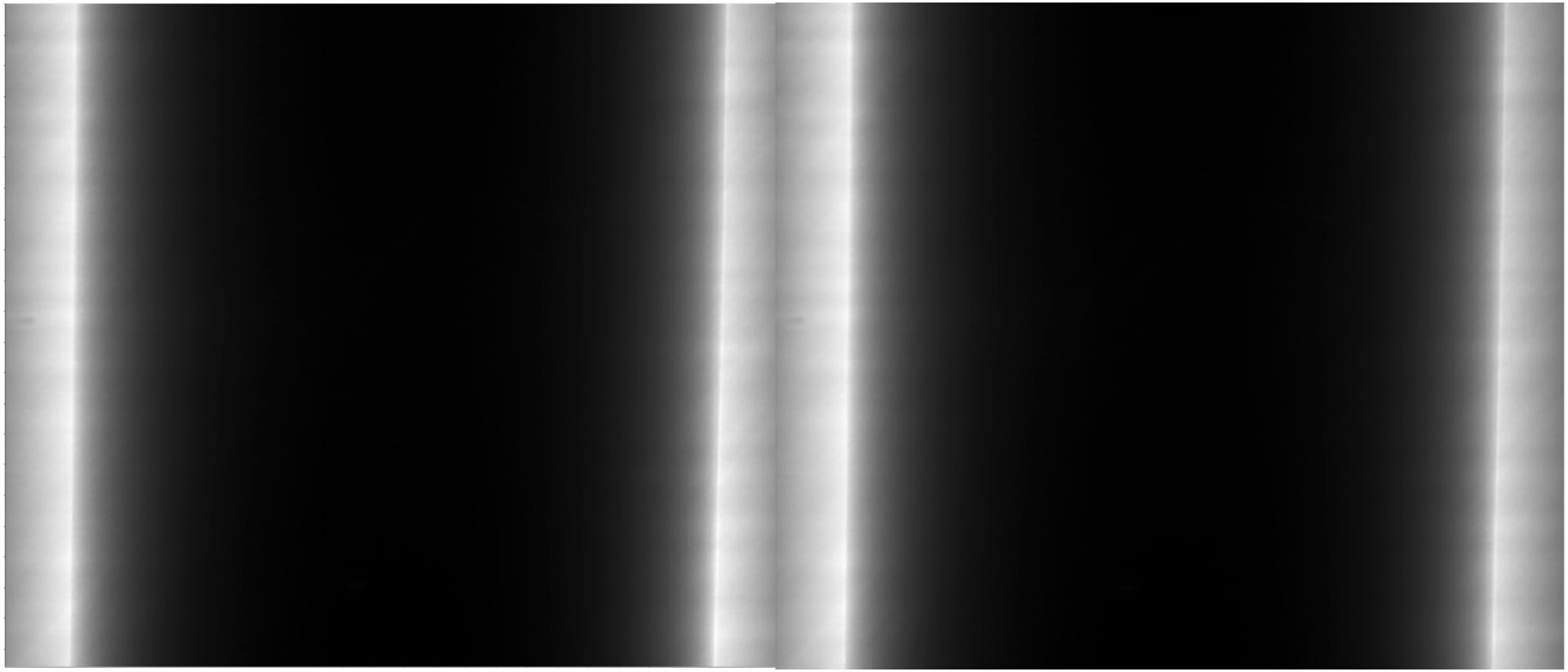

Fig. 11. radiographs of sample 3 (mixed 20/25/Nb with solution change):
(left) at the beginning of the experiment, (right) at the end of the experiment

# Results: tomographs

Sample 2 (304 ss with mixed surface roughness) successfully developed IGC/IGSCC during the experiment. Most cracks initiated on two rough surfaces, especially near the corner of the sample. Cracks started to initiate at the early stage of corrosion.

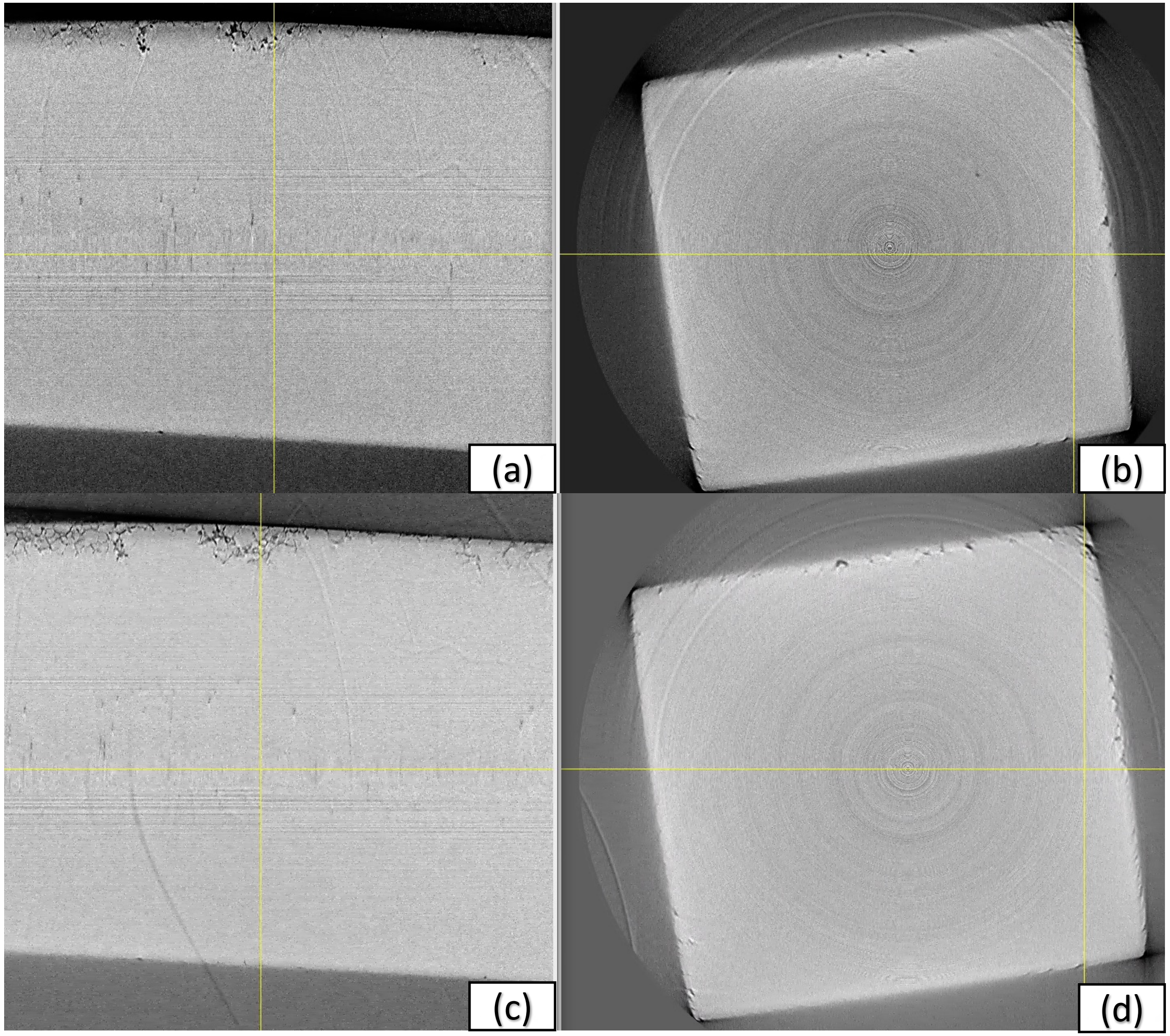


Fig. 12. slice and top views of the sample 2 (mixed 304):
(a), (b) after 3 hours and (c), (d) after 16 hours

# Results: tomographs

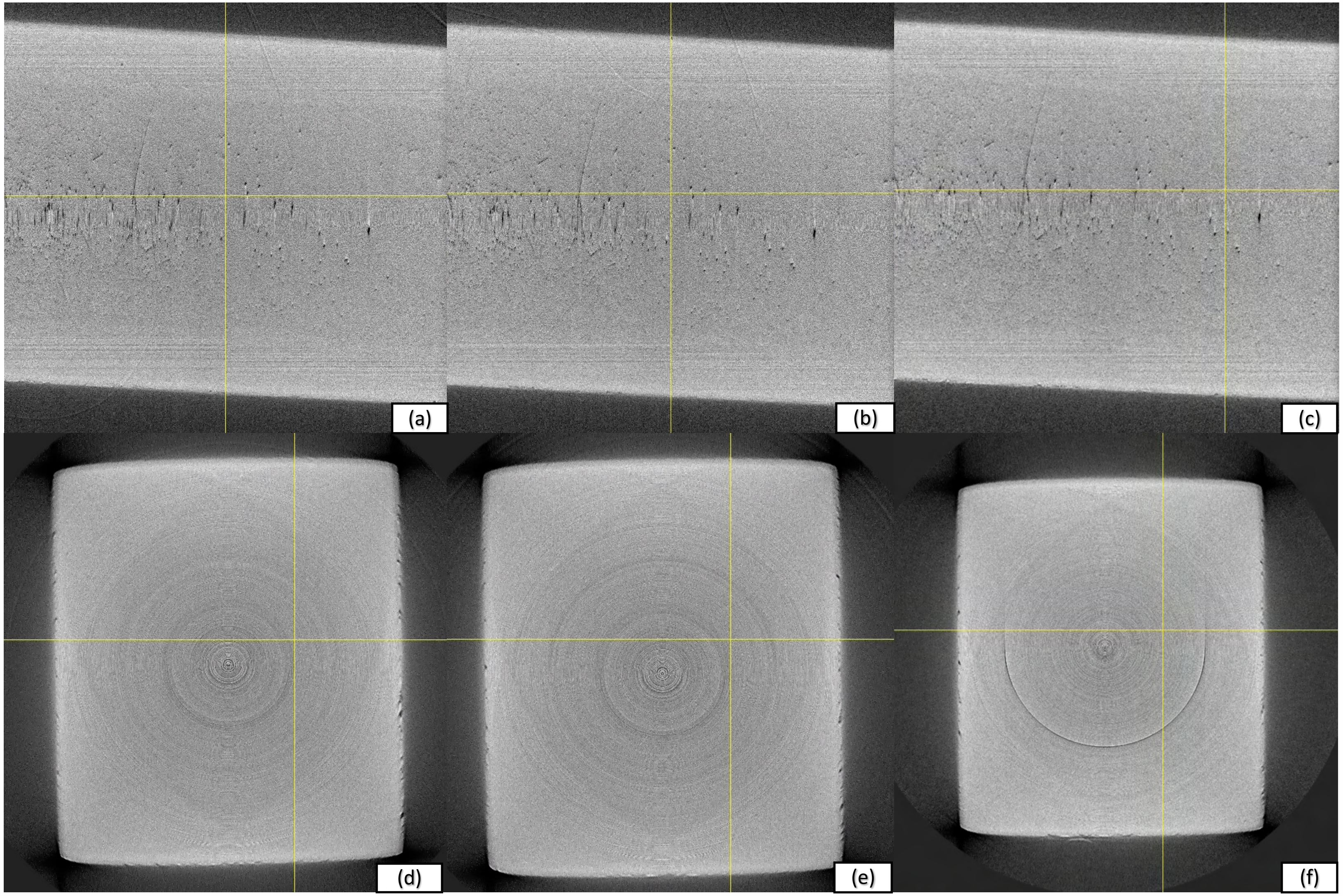


Fig. 13. slice and top views of sample 3 (mixed 20/25/Nb with solution change):
(a), (d) after 1.5 hours; (b), (e) after 12 hours; (c), (f) after 18 hours

# Results: tomographs

The rough surface of sample 3 (mixed 20/25/Nb with solution change) shows some levels of intergranular corrosion and potentially intergranular cracking. Further analysis is needed to tell if they are cracks.

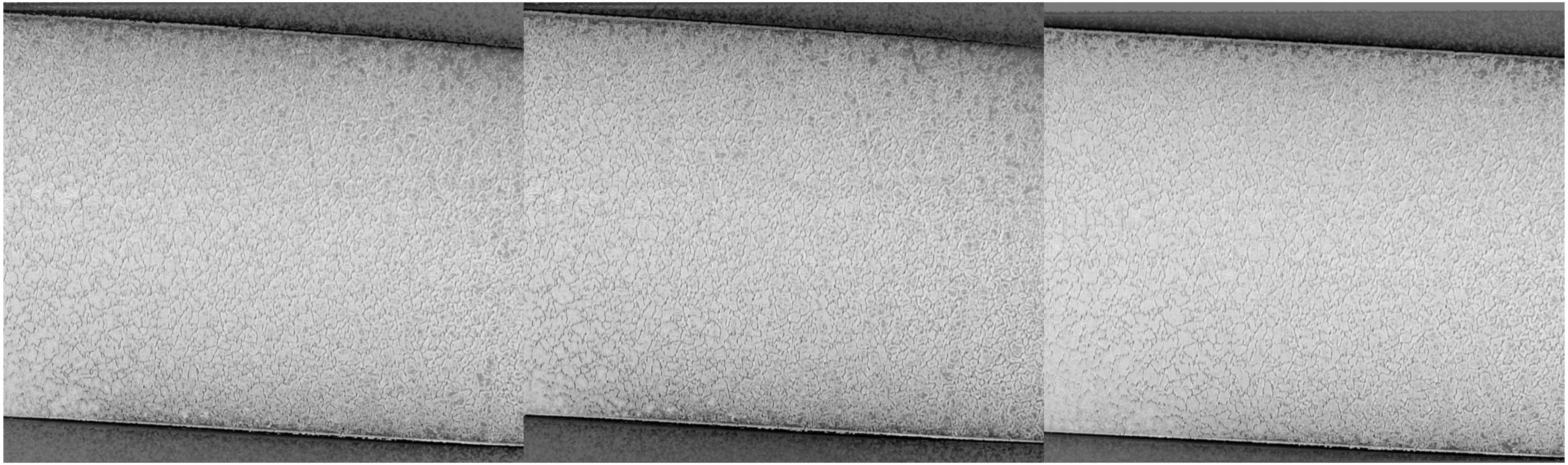

Fig. 14. rough surface of sample 3 (mixed 20/25/with solution change):
(a) after 1.5 hours; (b) after 12 hours; (c) after 18 hours

# Results: SEM

Sample 1 (304 sample with rough faces) was heavily corroded. Intergranular corrosion and TGSCC/IGSCC developed. Some grains have been removed from the edge of the sample, forming large voids.

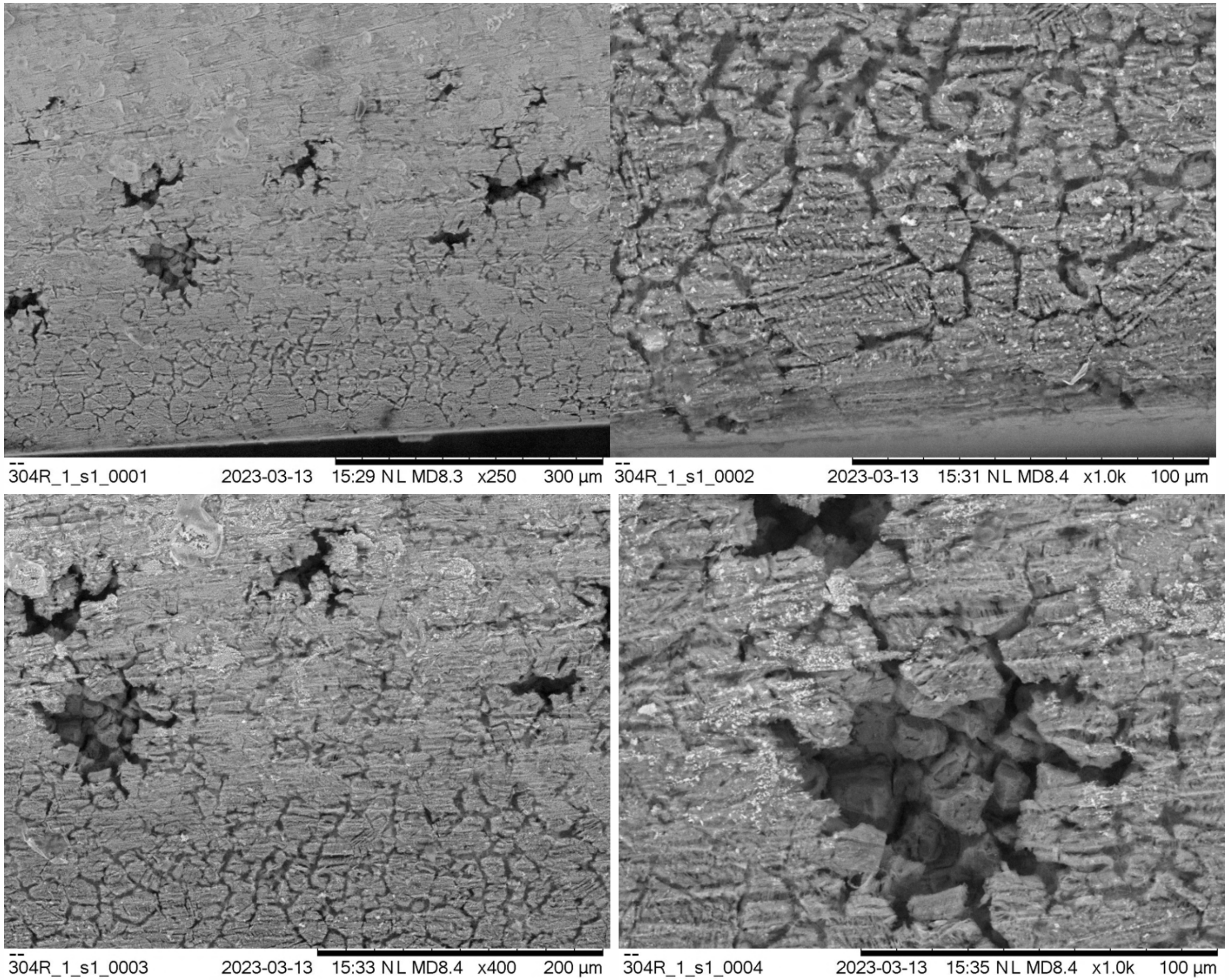


Fig. 15. SEM images of the edge of the sample 1 (rough 304 sample)

# Results: SEM

The fine surfaces of sample 2 (mixed 304 sample) show very different cracking:
The finer intergranular cracks developed on the faces, and the cracks on the rougher edge are both intergranular and transgranular.

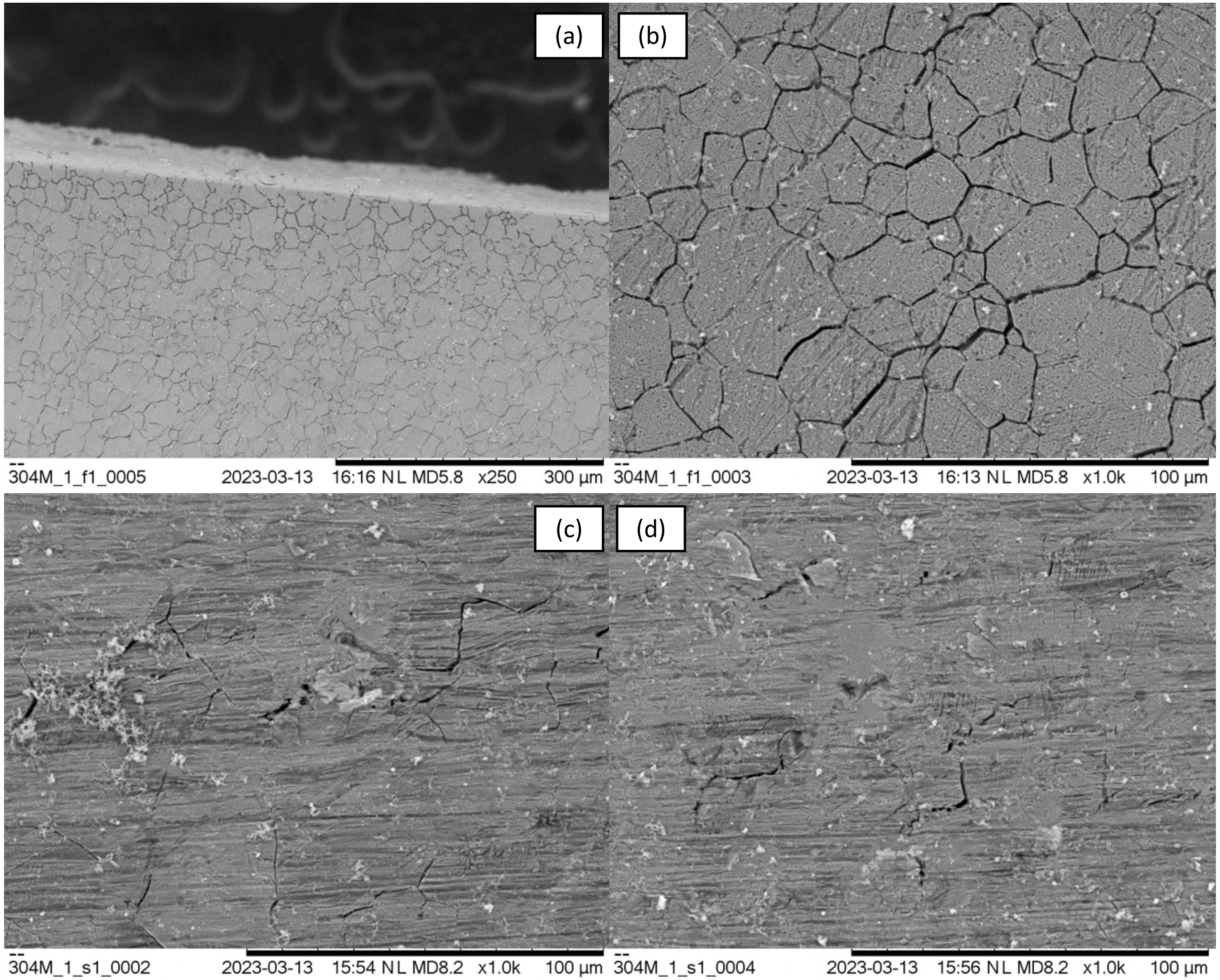


Fig. 16. SEM images of the fine surfaces of sample 2 (304 with mixed surface finish): (a), (b): face; (c),(d) edge

# Results: SEM

The fine face of sample 2 (mixed 20/25/Nb stainless steel with solution change) showed less corrosion than the fine face of 304 stainless steel with fewer cracks. SEM images on the rough face will be taken to confirm SCC on 20/25/Nb.

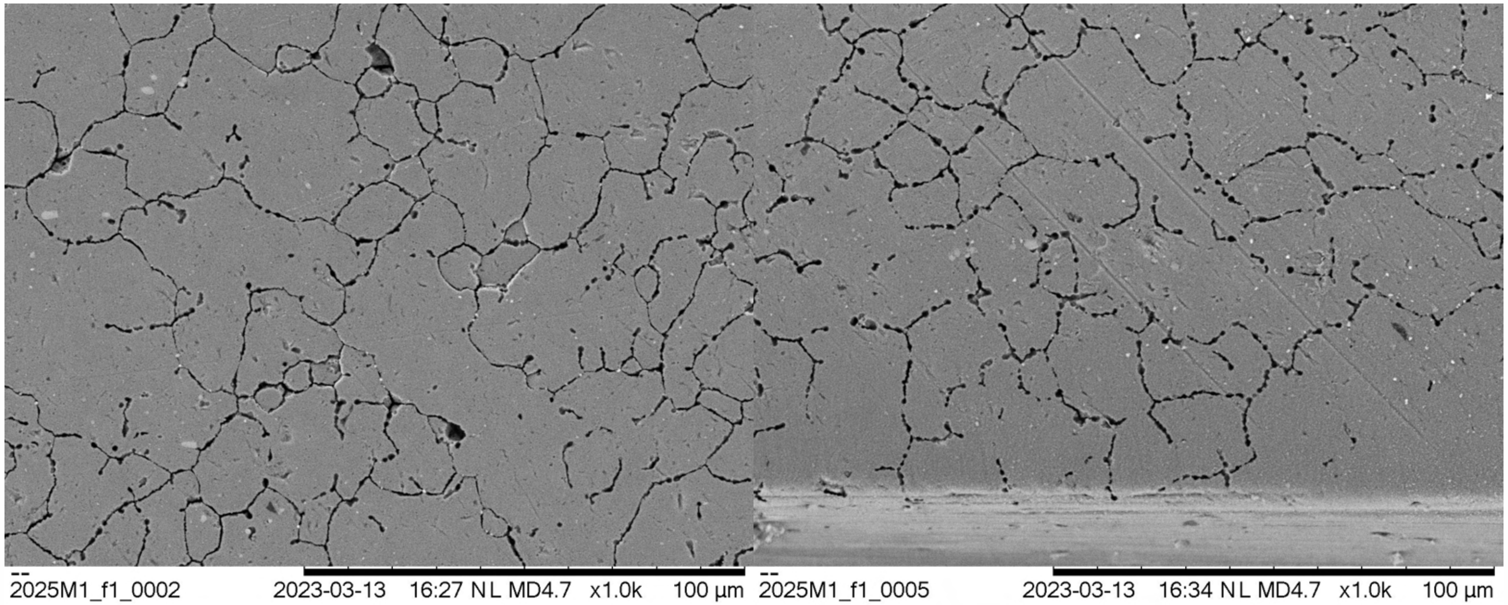


Fig. 17. SEM images of the fine face of the sample 3 (mixed 20/25/Nb with solution change)

# Conclusions and Plans

- In-situ corrosion synchrotron experiment has been carried out and IGC/SCC successfully developed in a short period of time.
- Surface roughness has strong effects on the severity of SCC and other form of corrosion
- 20/25/Nb is more resistant to corrosion than 304, and SCC will be confirmed with further analyses.
- A 3D volume will be reconstructed and DVC (digital volume correlation) will be used to study the crack growth rates of different materials and different environmental conditions.
- The composition of the crack area can be studied with diffraction results.
- The cracked area will be FIB-milled to study the relationship between crack growth and grain boundary properties.

TRANSCEND

Transformative Science and Engineering for Nuclear Decommissioning

## Team members:

Ron Clark, Xavier van Heule, Cemal Ozturk, Simon Mckendrey and Mehdi Mokhtarishirazabad

## Beamline scientists:

Sharif Ahmed and Alberto Leonardi

## Supervisors:

Ron Clark and Mahmoud Mostafavi

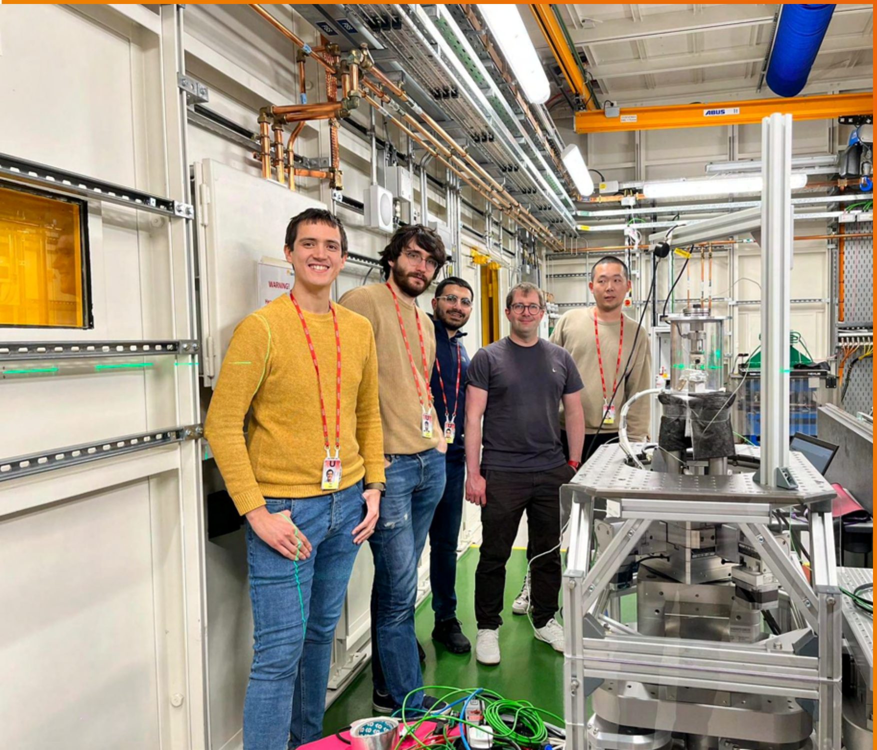

# Thank you

k.yuan@bristol.ac.uk

diamond

University of BRISTOL

NATIONAL NUCLEAR LABORATORY

Transformative Science and Engineering for Nuclear Decommissioning

# EFFECT OF SHEAR RATE ON POLYMER-INDUCED FLOCCULATION FOR BEHAVIOURAL MODIFICATION TECHNIQUES

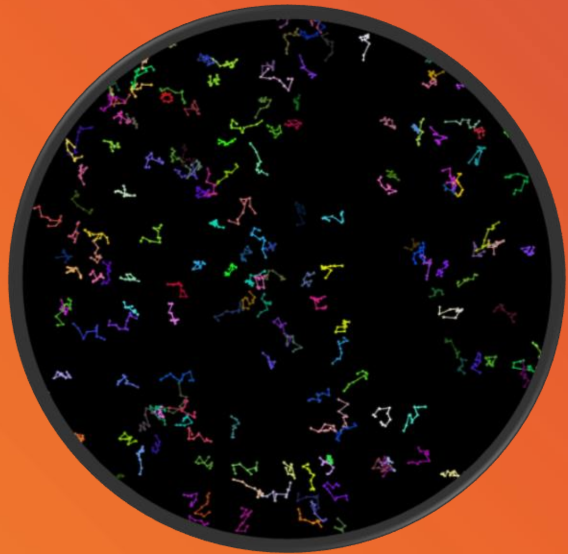


Dr. Lee Mortimer, University of Leeds

Prof. Mike Fairweather, University of Leeds


24th April 2023
London, UK

**TRANSCEND ANNUAL MEETING**

Energy
For a Low Carbon Future

# BEHAVIOURAL MODIFICATION

*Pile fuel storage pool at Sellafield* - IAEA Nuclear Energy Series No. NW-T-2.6 - Decommissioning of Pools in Nuclear Facilities, IAEA.

- At present, waste transportation and settling processes are executed sub-optimally and carried out with caution due to the complex nature of the wastes and a lack of understanding of their flow or interaction behaviour.
- In practice, the behaviours associated with these activities are sensitive to the chemical and material properties as well as flow conditions and **presence of other phases**.
- This sensitivity is capable of being exploited and the modification of such quantities to obtain a desired outcome is referred to as **behavioural modification**.

## MOTIVATION

- In developing such techniques, solutions can be generated to discourage or encourage **waste particle agglomeration** within transport flows and settling tanks, ultimately controlling the extent of long-term particle migration, interaction and **flocculation events**.

# MOTIVATION

- That said, to develop beneficial behavioural modification techniques the **system response to deviations in key parameters** must be known.

- It is difficult to probe the effects of such variations experimentally for **specific parameter sets**.

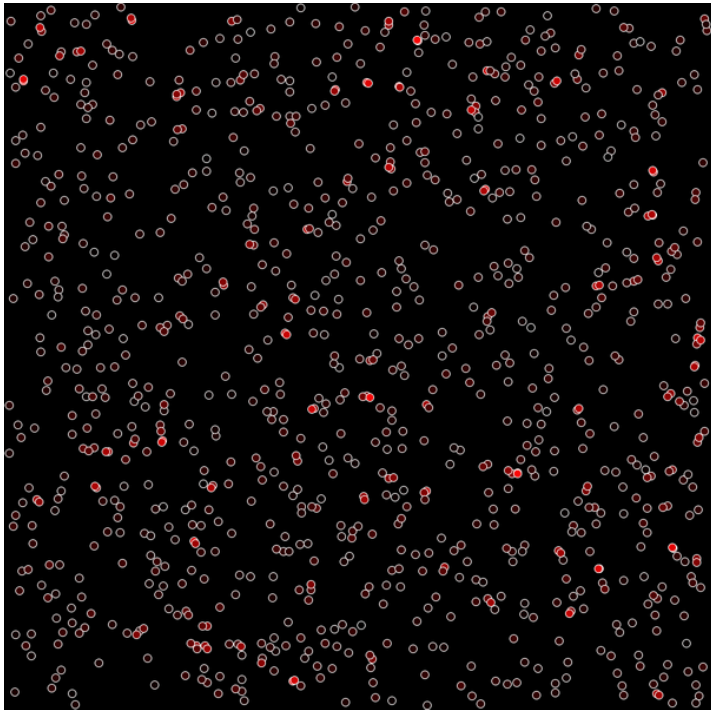

LOW HAMAKER CONSTANT

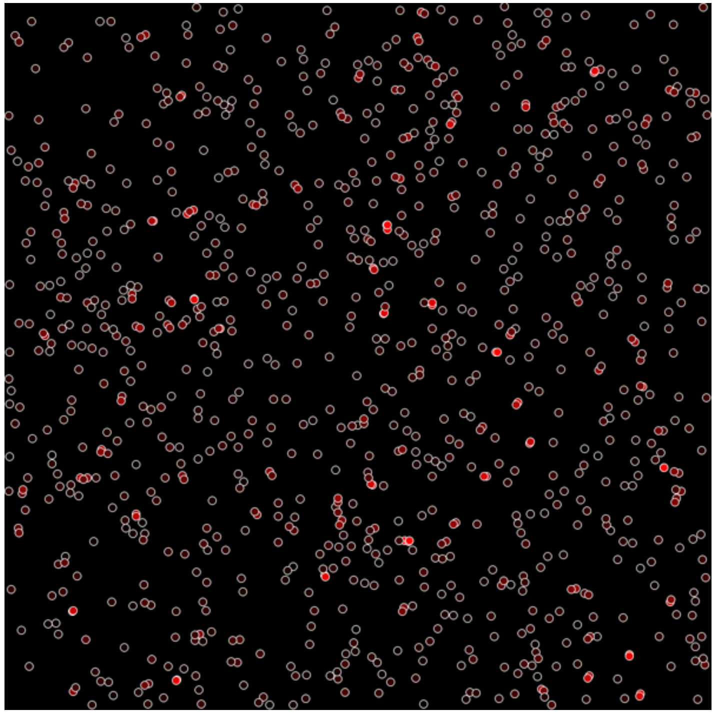

HIGH HAMAKER CONSTANT

- Computer simulations provide a means to overcome this difficulty by providing the capability to specify and explore the **impact of changes to a set of precise system parameters**.

# SIMULATION TECHNIQUES

- The accuracy and reliability of such calculations is based upon both the **order of the discretisation techniques** used for each phase, as well as the **fidelity of the models used** to predict the wide array of **interactions between the phases**.

## CONTINUOUS PHASE

**Direct numerical simulation (DNS)**

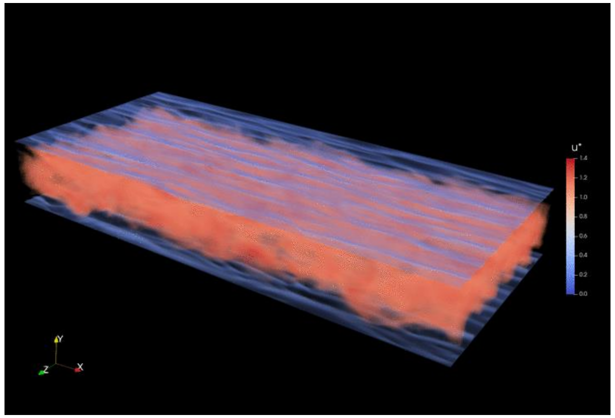

## PARTICULATE PHASE

**Lagrangian particle tracking (LPT)**
**Immersed boundaries method (IBM)**

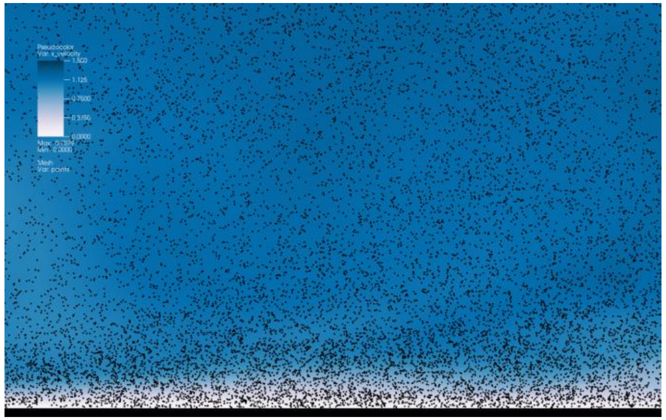

## POLYMERIC PHASE

**Finitely extensible nonlinear elastic model (FENE)**

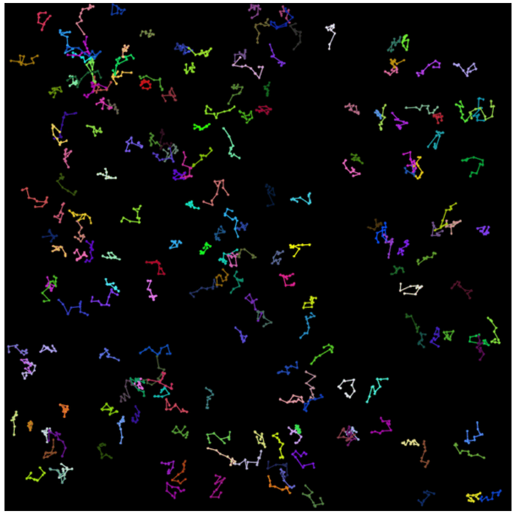

- Focus on coupling methods together to obtain a solver capable of predicting particle-fluid, particle-particle and particle-polymer interaction.

## POLYMERIC SYSTEMS

- Polymers are chemical compounds with molecules bonded together in **long repeating chains** of monomers.
- Both **synthesized** and **naturally occurring.**
- Possess **important advantageous properties** surrounding the way in which they interact with both themselves and other materials.
- In the present case, we are interested in how they **interact** and beneficially **modify behaviour** of both the fluid and particles.

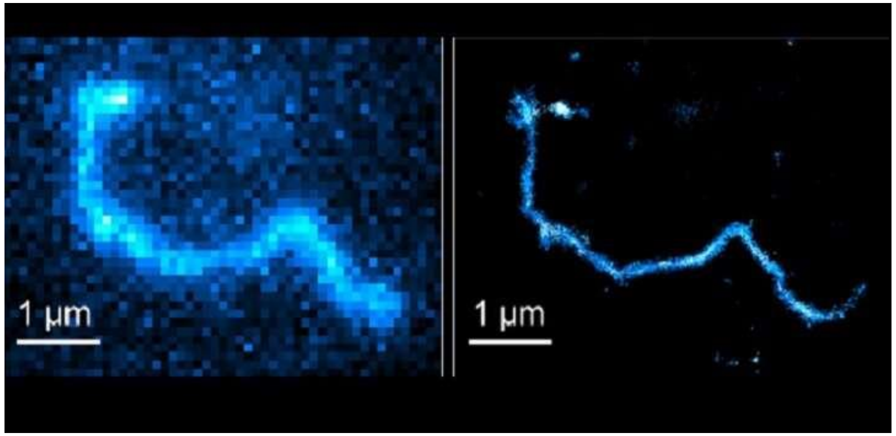


**Super-resolution fluorescence microscopy of Lambda DNA.**
[Abadi et al. Entangled polymer dynamics beyond reptation, *Nature Communications* (2018).]

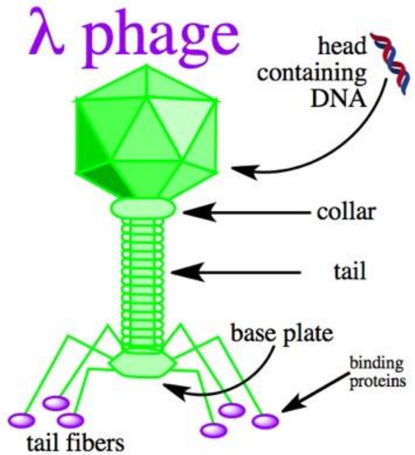

# POLYMER-PARTICLE INTERACTION

- Polymer flocculants **induce flocculation** by neutralizing the surface charge of the particles or by forming bridges between individual particles.

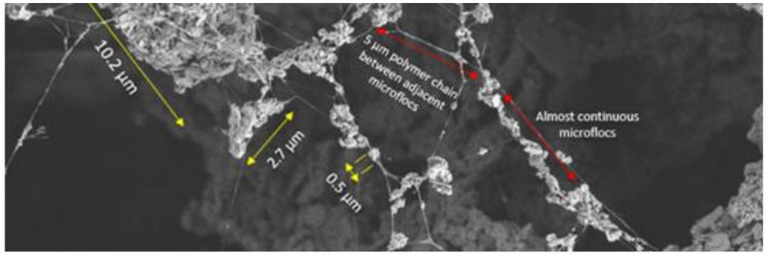


**Microstructure of kaolinite floc as revealed by cryo-SEM** - Sharma, S., Lin, C. L., & Miller, J. D. (2017). Multi-scale features including water content of polymer induced kaolinite floc structures. Minerals Engineering, 101, 20-29.

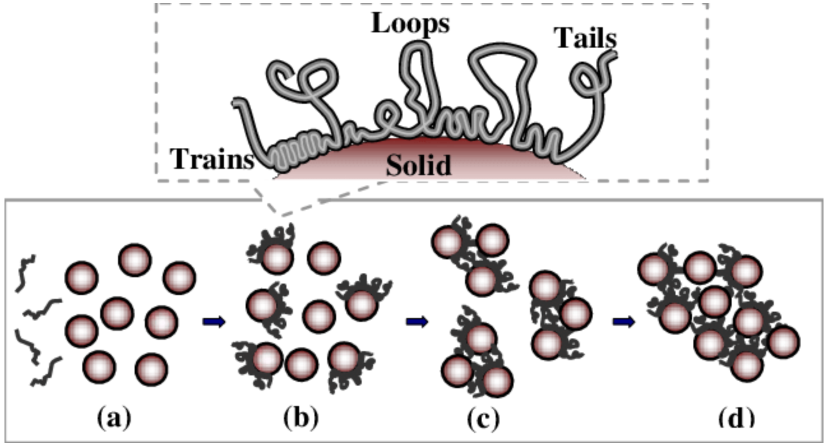


- The **adsorption mechanism** is modelled, current literature is sparse and so this interaction mechanism needs to be developed.

- The **bridging mechanism** will hence be implicit from adsorption.

- Adsorption is determined by attachment process, **hydrophobic** or **electrostatic interaction**.

- Hence attachment mechanism upon collision will rely on **electrochemical properties** of surface of particle and the polymer charge distribution.

# LANGEVIN DYNAMICS

- FENE (finitely extensible nonlinear elastic) chain model represents the polymer as a sequence of beads connected by nonlinear springs.

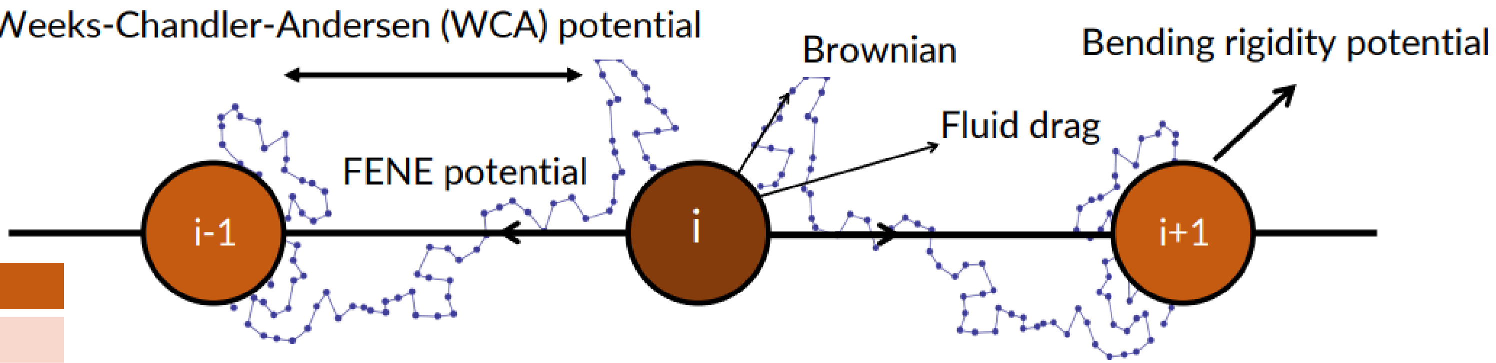


| Symbol | Meaning |
|---|---|
| $m$ | Mass |
| $\boldsymbol{r}$ | Position |
| $t$ | Time |
| $V_i$ | Potential |
| $\boldsymbol{\eta}_i(t)$ | Brownian noise |
| $\zeta$ | Drag coefficient |
| $k_B$ | Boltzmann's constant |
| $T$ | Temperature |
| $K_{BEND}$ | Bending potential |
| $\theta_i$ | Bead angle |
| $\sigma$ | Bead diameter |
| $r_{ij}$ | Bead separation |

$$\underbrace{m\frac{d^2\boldsymbol{r}_i}{dt^2}}_{\text{Inertia}} = \overbrace{-\boldsymbol{\nabla}\mathrm{V_i}}^{\text{Interaction potentials}} \underbrace{-\,\zeta\frac{d\boldsymbol{r}_i}{\mathrm{dt}}}_{\text{Fluid drag}} + \overbrace{\sqrt{2k_BT\zeta}\,\boldsymbol{\eta}_i(t)}^{\text{Brownian motion}}$$

$$\mathrm{V_i} = \underbrace{-\frac{K_{FENE}R_0^2}{2}\ln\left[1-\left(\frac{r_{i,i+1}}{R_0}\right)^{\mathbf{2}}\right]}_{\text{FENE bead-spring}} + \underbrace{K_{BEND}(1+\cos\theta_i)}_{\text{Bending rigidity}} + 1 + \underbrace{4\left[\left(\frac{\sigma}{r_{ij}}\right)^{12}-\left(\frac{\sigma}{r_{ij}}\right)^{6}\right]}_{\text{WCA potential}}$$

# LANGEVIN DYNAMICS

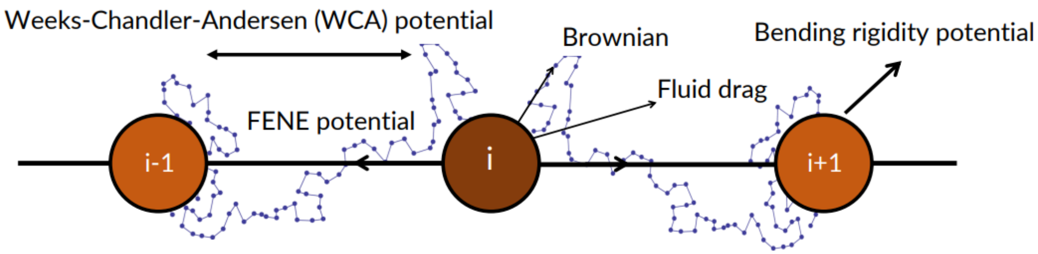


| Symbol | Meaning |
|---|---|
| $m$ | Mass |
| $\boldsymbol{r}$ | Position |
| $t$ | Time |
| $V_i$ | Potential |
| $\boldsymbol{\eta}_i(t)$ | Brownian noise |
| $\zeta$ | Drag coefficient |
| $k_B$ | Boltzmann's constant |
| $T$ | Temperature |
| $K_{BEND}$ | Bending potential |
| $\theta_i$ | Bead angle |
| $\sigma$ | Bead diameter |
| $r_{ij}$ | Bead separation |

Right: Potentials for typical polymer system using $K_F^* = 30, R_0^* = 1.6$

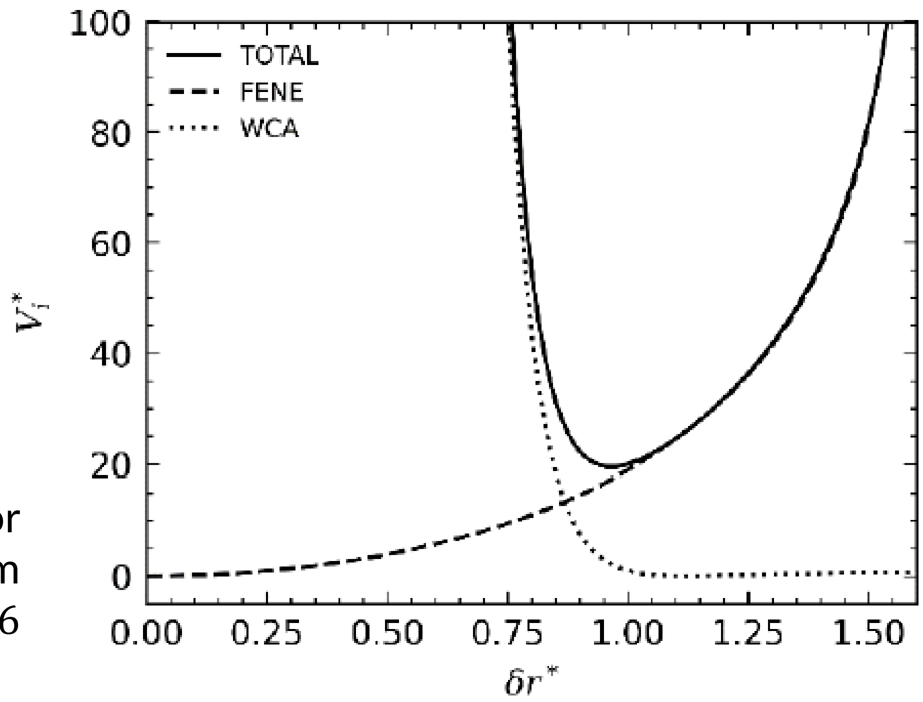


$$\mathrm{V_i} = \underbrace{-\frac{K_{FENE}R_0^2}{2}\ln\left[1-\left(\frac{r_{i,i+1}}{R_0}\right)^2\right]}_{\text{FENE bead-spring}} + \underbrace{K_{BEND}(1+\cos\theta_i)}_{\text{Bending rigidity}} + \underbrace{1 + 4\left[\left(\frac{\sigma}{r_{ij}}\right)^{12} - \left(\frac{\sigma}{r_{ij}}\right)^{6}\right]}_{\text{WCA potential}}$$

# POLYMERS UNDER EQUILIBRIUM CONDITIONS

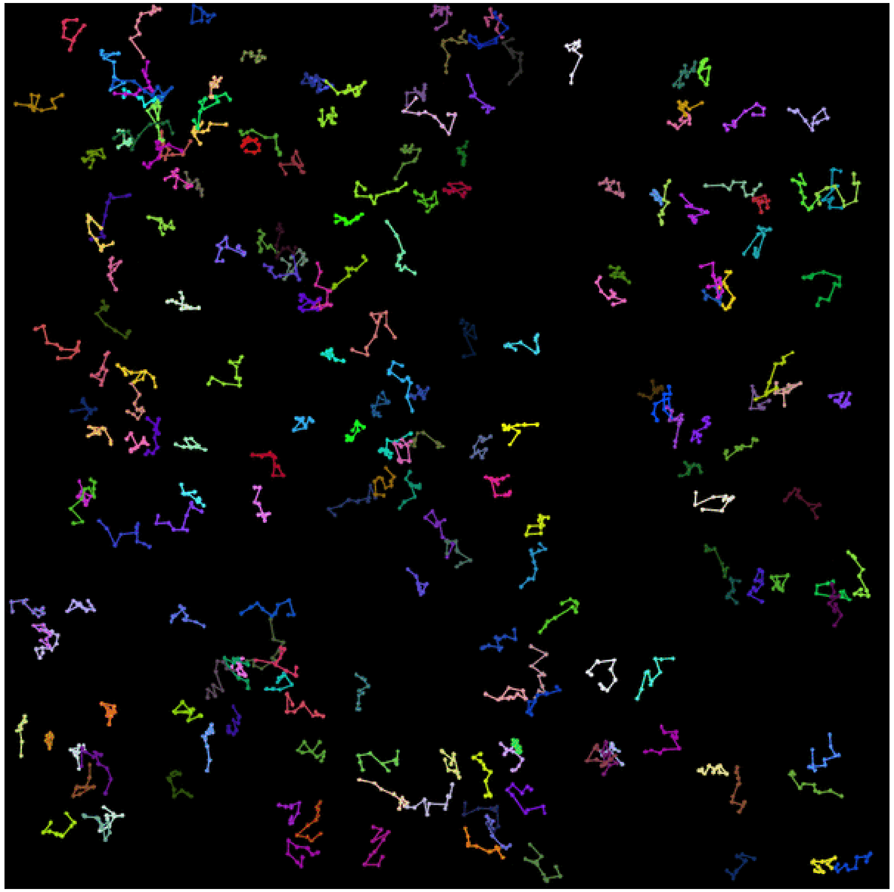

Validation data from M. Chopra and R. G. Larson, *J. Rheol.*, 2002, 46, 831–862

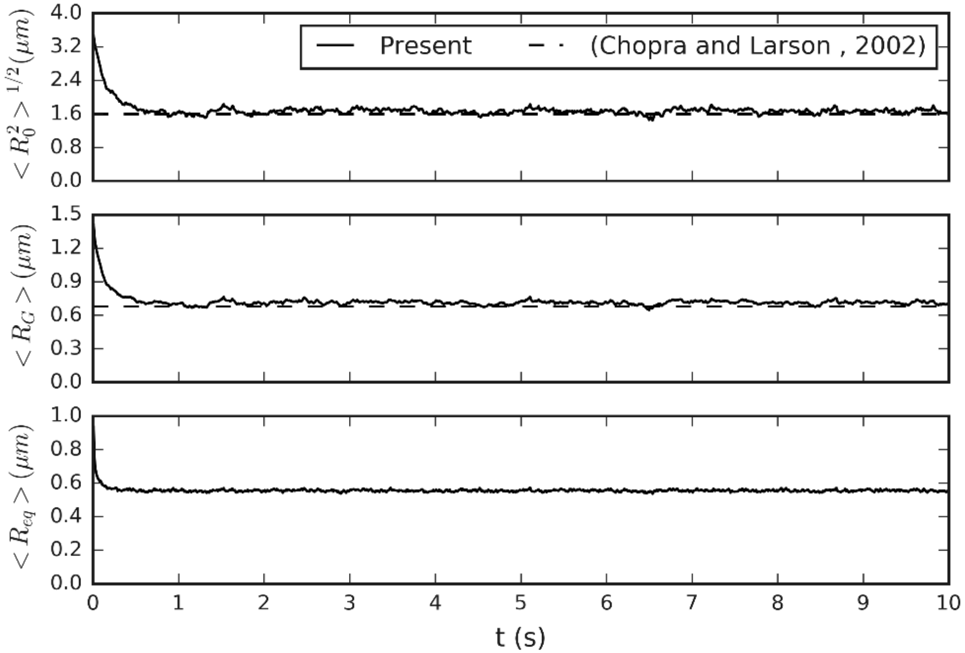


End-to-end distance vector

$$< R_0^2 >^{\frac{1}{2}} = \sqrt{\frac{\sum_p \left(\boldsymbol{X}_{N_B,p} - \boldsymbol{X}_{1,p}\right)^2}{N_P}}$$

Radius of gyration

$$< R_G^2 >^{\frac{1}{2}} = \sqrt{\frac{\sum_p \frac{\sum_b \left(\boldsymbol{X}_{b,p} - \boldsymbol{X}_{COM,p}\right)^2}{N_B - 1}}{N_P}}$$

Equilibrium stretch

$$< R_{eq}^2 >^{\frac{1}{2}} = \sqrt{\frac{\sum_p \frac{\sum_r \boldsymbol{R}^2}{N_B - 1}}{N_P}}$$

# EFFECT OF SHEAR ON POLYMER DYNAMICS

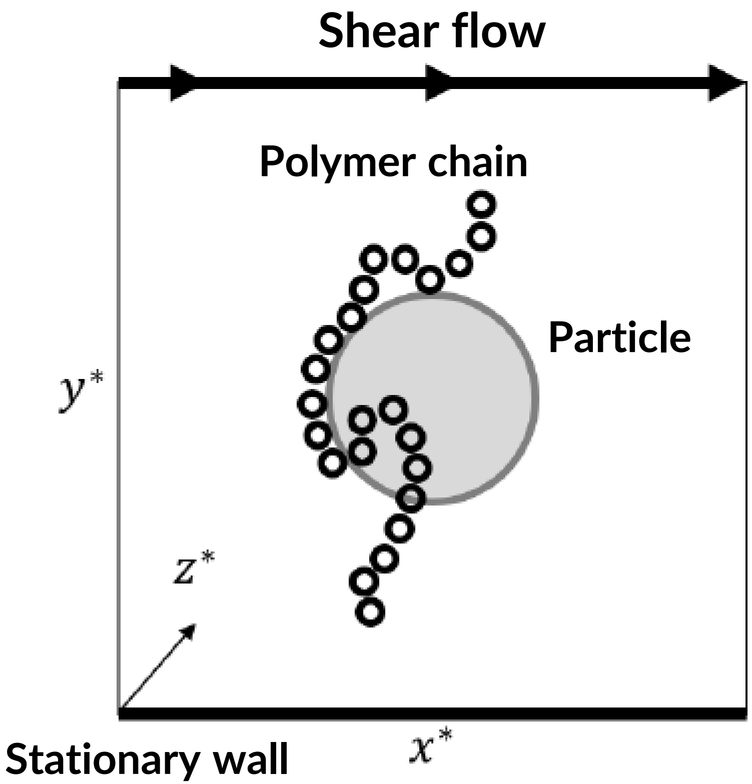


- For all simulations presented here, Monte-Carlo techniques were employed, meaning that multiple instances of the same simulation were performed with measurables averaged over all instances.
- To initialise, root beads were initially injected into a random $(y^*, z^*)$ location within the domain at the inlet.
- The polymer is then 'grown', taking care not to overlap beads.

# EFFECT OF SHEAR ON POLYMER DYNAMICS

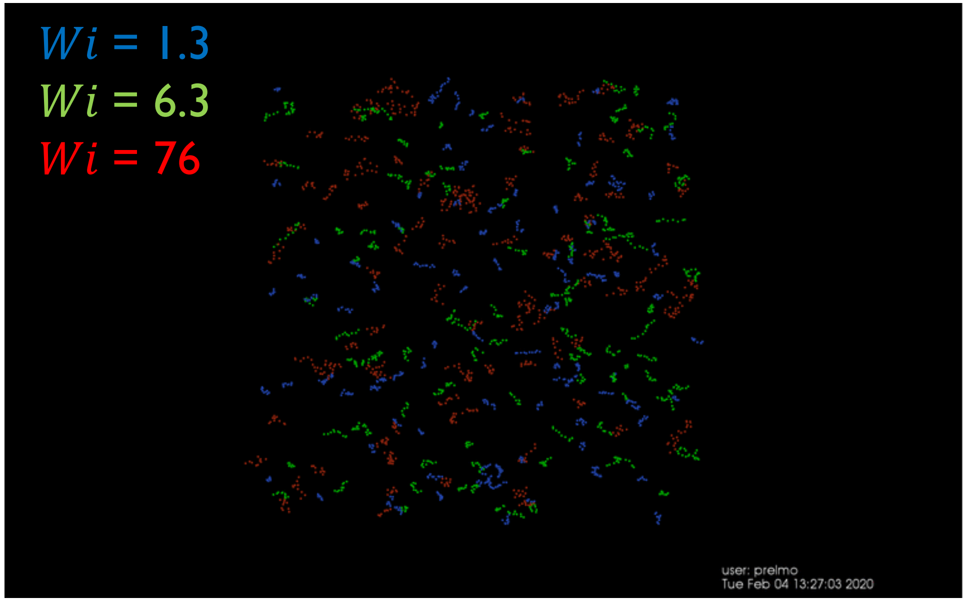


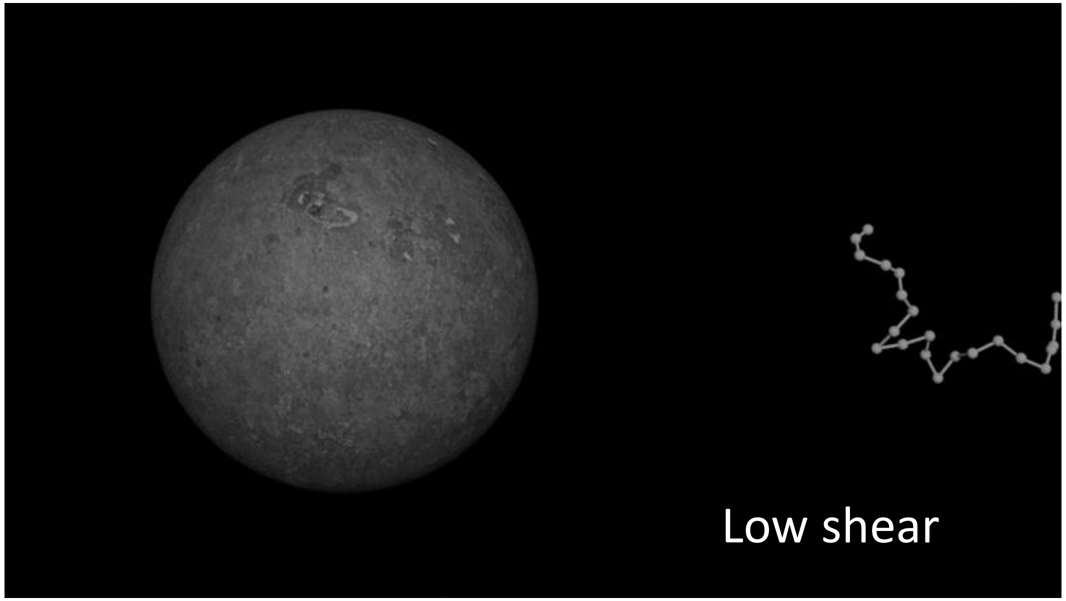


- Increased shear (Weissenberg number) leads to more stretched chain conformities. (Above)

- At low shear rates, polymers remain loosely bound to the particle.

- At increased shear, polymers are unable to adsorb onto the surface of the particle, even after a collision occurs.

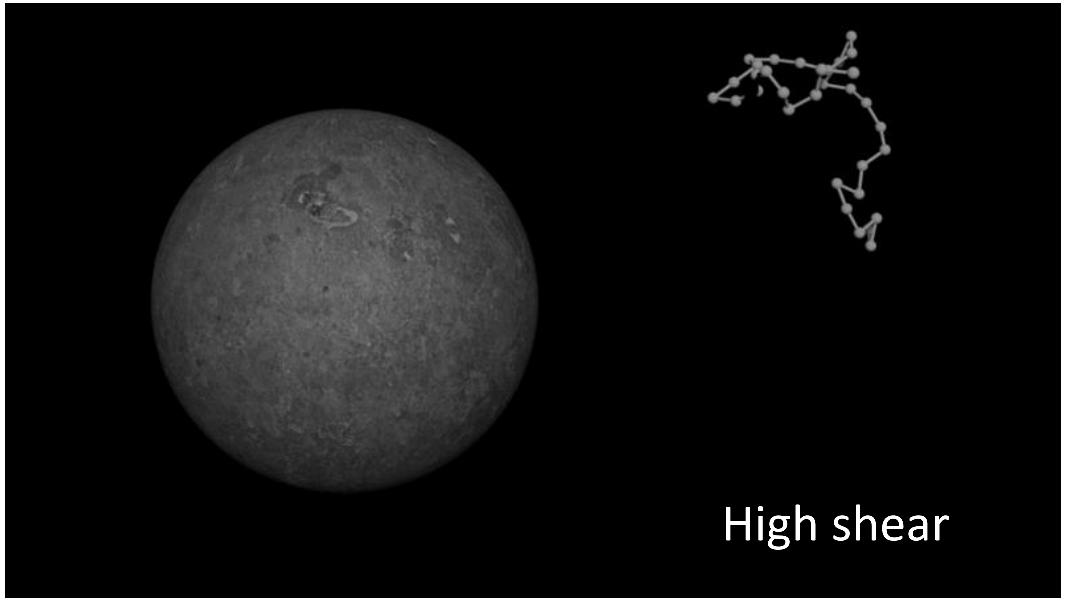


TRANSCEND

EPSRC
Engineering and Physical Sciences Research Council

# EFFECT OF SHEAR ON POLYMER DYNAMICS

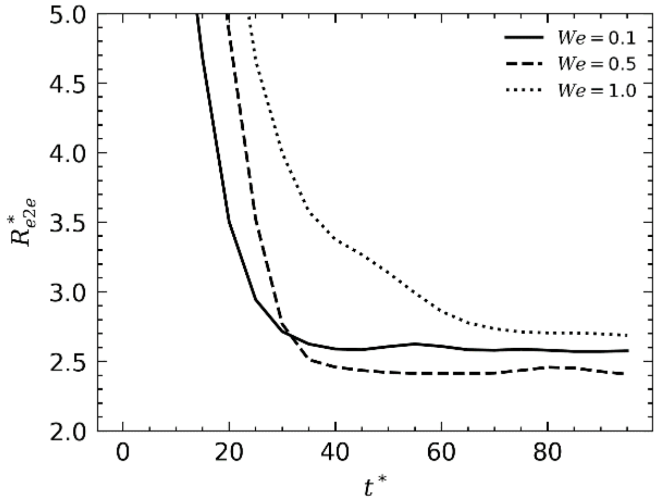


Effect of Weissenberg number, $We$, on temporal evolution of end-to-end polymer chain distance under shear flow conditions

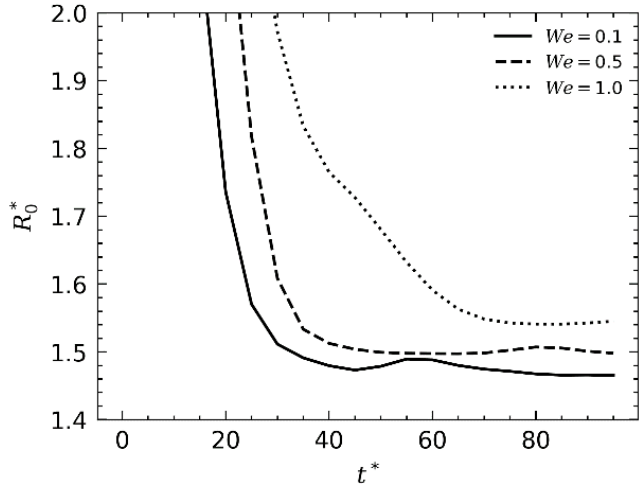


Effect of Weissenberg number, $We$, on temporal evolution of polymer chain radius of gyration under shear flow conditions

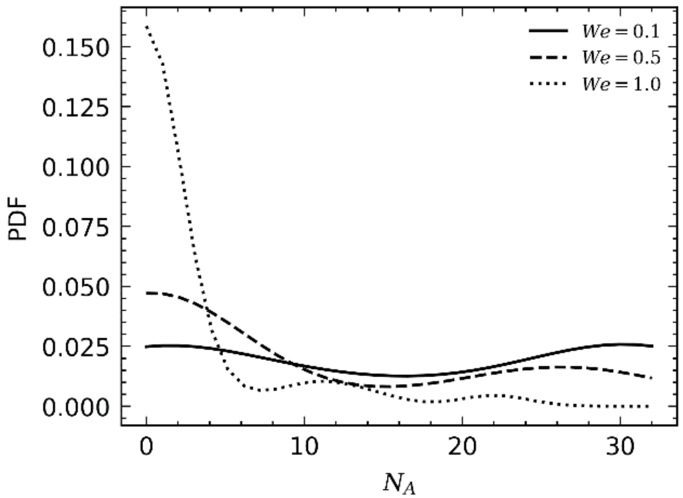


Probability density function of the number of adsorbed beads $N_A$. Effect of Weissenberg number is illustrated

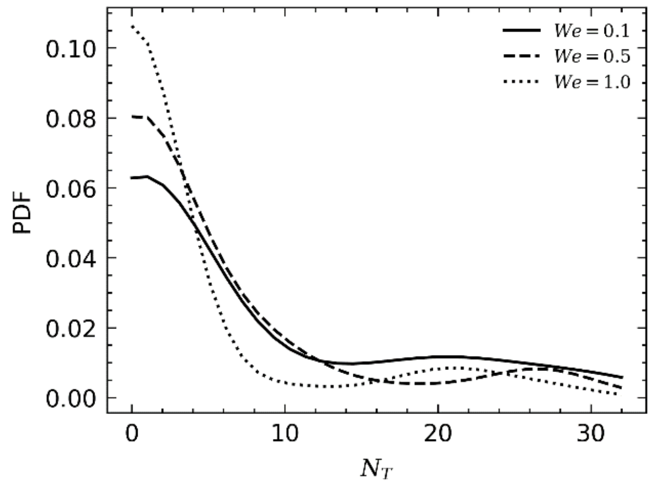


Probability density function of the number of tail beads $N_T$. Effect of Weissenberg number is illustrated

## MONTE-CARLO SIMULATION

- Statistics sampled over 100 Monte-Carlo instances
- Increased shear rates leads to higher end-to-end distances, although medium shear leads to a curling effect which minimises this quantity
- Low shear instigates adsorption events with increased chance of full ($N_A = 32$) adsorption, and fewer trains.

Adsorption efficiency dependence on Weissenberg number

| $We$ | % Adsorption |
|---|---|
| 0.1 | 67.4 |
| 0.5 | 37.6 |
| 1.0 | 12.1 |

TRANSCEND

EPSRC
Engineering and Physical Sciences Research Council

# MULTIPLE POLYMER INTERACTION

- Monte-Carlo studies were performed for 15 polymers adsorbing into particle surface

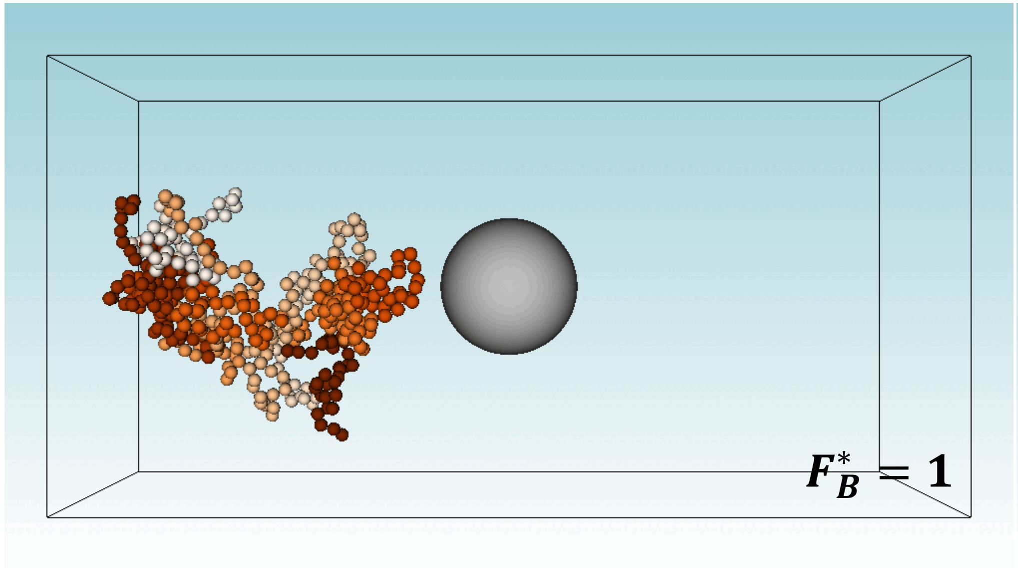


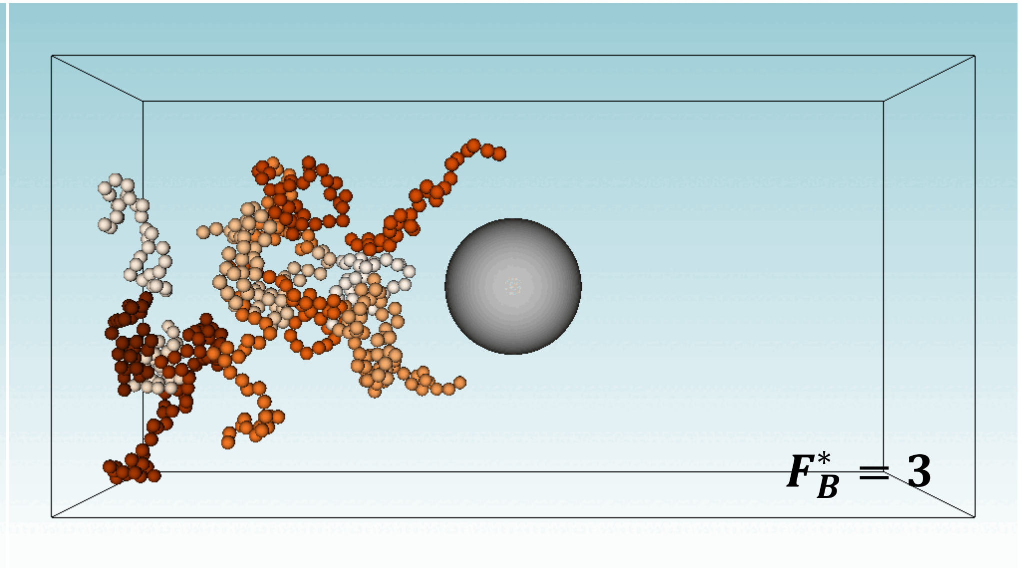


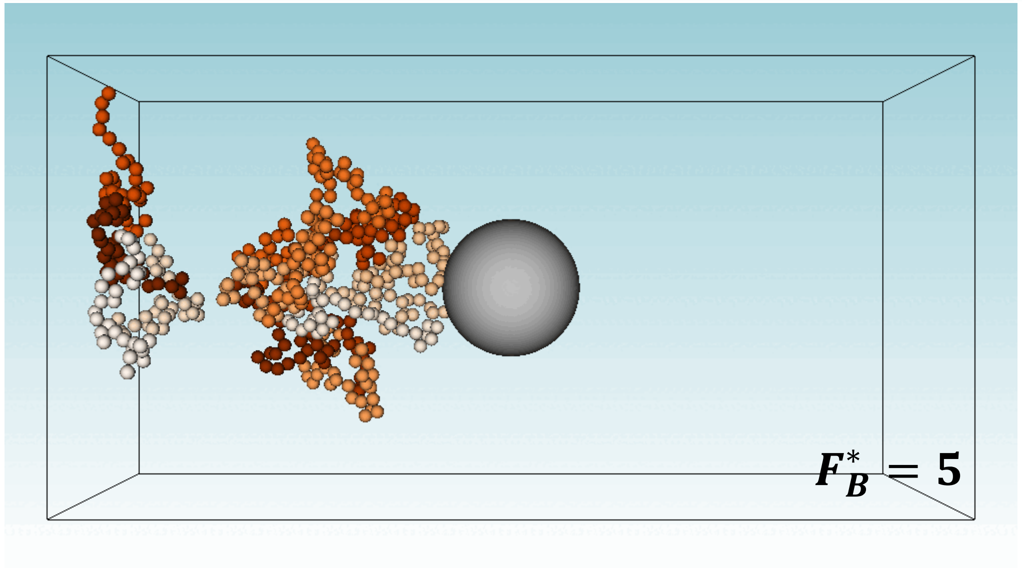


- At low bending rigidity, the result is that polymers are able to adsorb onto the particle with ease, flattening and spreading out across its surface.
- As the rigidity is increased, the inability to flatten out onto the particle leads to more cluster-like polymer conformities forming on the particle, and longer structures leading to longer tails. These also tend to form parallel to the streamwise direction.

TRANSCEND

# MULTIPLE POLYMER INTERACTION

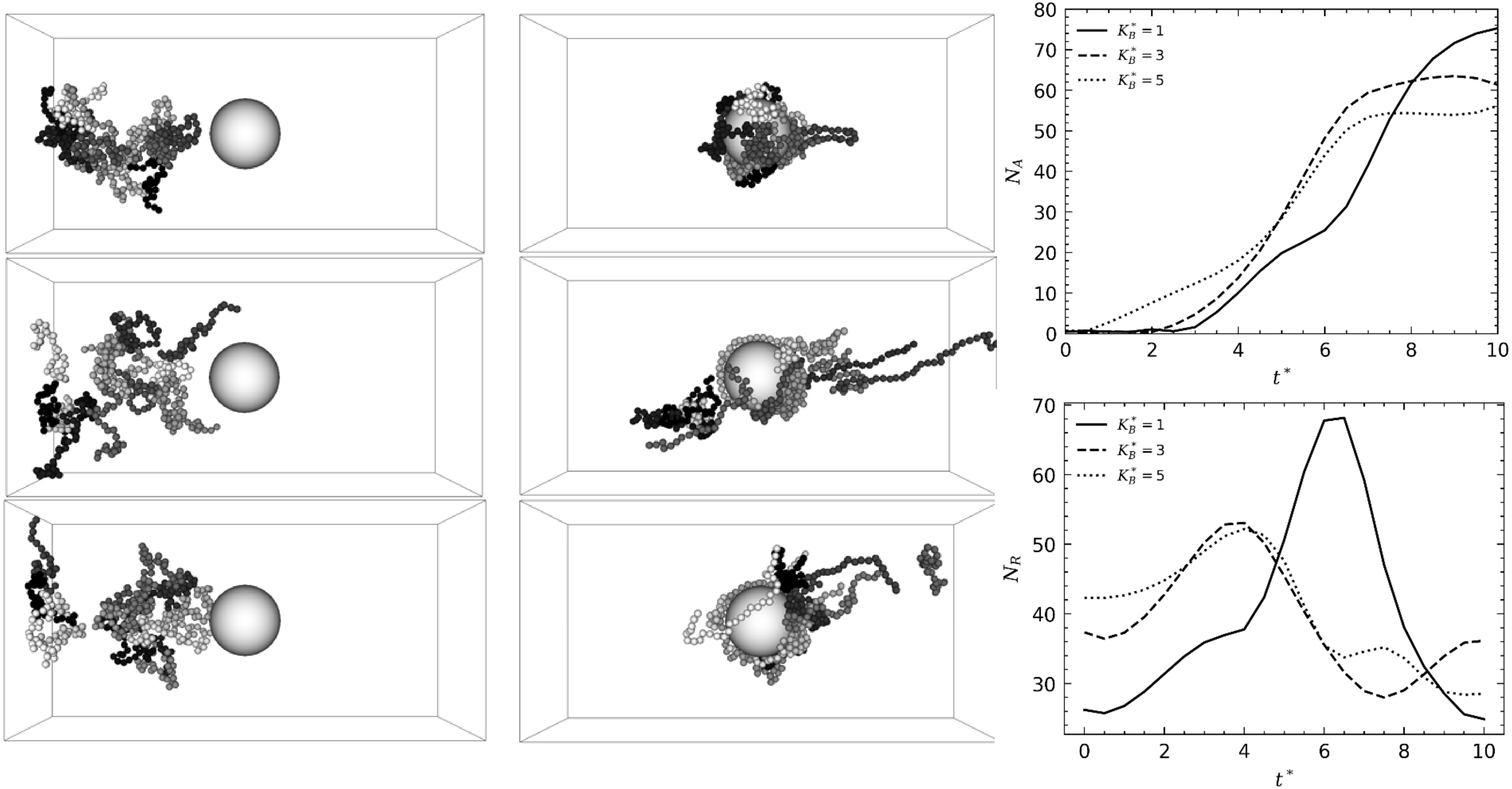


- For low bending rigidity, more monomers are capable of adsorbing onto the particle surface.
- As the potential is increased, the longer conformities present means that full adsorption onto the surface is less energetically favourable, and so the percentage is reduced

TRANSCEND

# CONCLUSIONS AND FURTHER WORK

- Novel, potential-based Langevin dynamics code, capable of predicting FENE bead-spring polymer- and particle-interactions model, has been developed, implemented and validated.

- Effect of polymer conformation and polymer-particle interaction has been further studied, with shear rate playing an important role in the conformation of polymer chains.

- A study into the effect of the Kratky-Porod bending rigidity potential indicates that polymer species with low bending rigidities tend to adsorb fully onto the particle surface, whereas increasing the rigidity leads to long tail-like structures forming and lower adsorption leaving further surface for more interactions to occur.

- Model is now being used to predict further flocculation with multiple particles in stagnant conditions, as well as low shear conditions, to determine effect of shear and other system properties on floc size (radii of gyration), fractal dimension and aggregate stability.

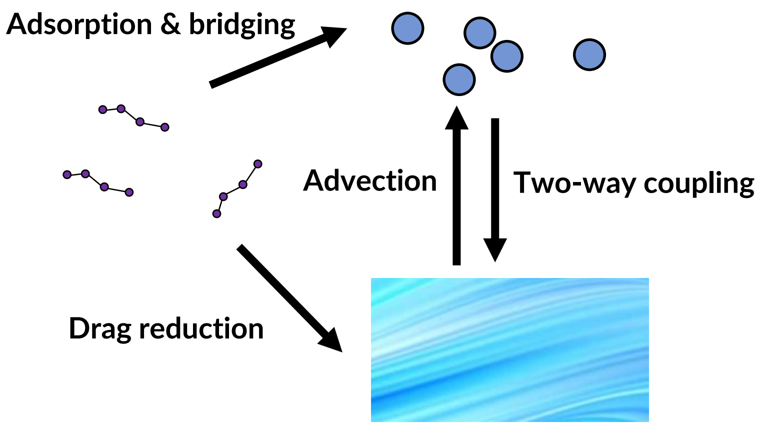


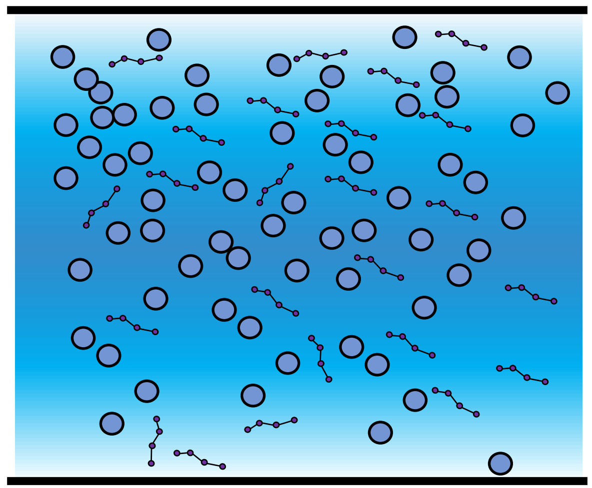

# PUBLISHED WORK ON BEHAVIOURAL MODIFICATION

***(*) Mortimer, L. F. , and Fairweather, M. Langevin Dynamics Prediction of the Effect of Shear Rate on Polymer-Induced Flocculation. Technische Mechanik-European Journal of Engineering Mechanics 43.1 (2023): 73-82.***

Mortimer L. F., Fairweather M., 2022. Prediction of polymer extension, drag reduction and vortex interaction in direct numerical simulation of turbulent channel flows. Physics of Fluids. (In review)

Mortimer, L. F. and Fairweather, M., 2021. Assessment of behavioral modification techniques through immersed boundary method simulation of binary particle interactions in isotropic turbulence. *Physics of Fluids.* 33 (3), 073307 doi: 10.1063/5.0049779

Mortimer, L. F. and Fairweather, M., 2020. Density ratio effects on the topology of coherent turbulent structures in two-way coupled particle-laden channel flows. *Physics of Fluids. 32* (10), 103302. doi: 10.1063/5.0017458

Mortimer L. F., Njobuenwu D. O. , Fairweather M., 2020. Agglomeration dynamics in liquid–solid particle-laden turbulent channel flows using an energy-based deterministic approach. *Physics of Fluids.* 32 (4) doi: 10.1063/5.0001596

Mortimer L. F., Njobuenwu D. O. , Fairweather M., 2019. Near-wall dynamics of inertial particles in dilute turbulent channel flows. *Physics of Fluids. 31 (6)* 063302 doi:10.1063/1.5093391

## ACKNOWLEDGEMENTS

This work is supported by a UK Engineering and Physical Sciences Research Council grant at the University of Leeds from the TRANSCEND (Transformative Science and Engineering for Nuclear Decommissioning) project.

UKRI Engineering and Physical Sciences Research Council

TRANSCEND

Thank you for your attention!
Questions?

**Dr. Lee Mortimer**
*PhD, PGDip, MPhys (Hons)*
Research Fellow
Office 2.22 Chemical and Process Engineering Building
School of Chemical and Process Engineering
University of Leeds
***l.f.mortimer@leeds.ac.uk***

Transformative Science and Engineering for Nuclear Decommissioning

# Off-Gas Emission Control from Vitrification of Radioactive Waste

Alex Stone, Sheffield Hallam University

*A. Scrimshire, F. Burrell, R. Marsh, A. Cundy, A. Holloway, S. Morgan, D. McKendrick, P. Bingham*

Transcend Annual Meeting
24th April 2023

# Introduction

High Temperature Glasses

Low Temperature Glasses

The Future

# The Problem

- The UK has 133,000 $m^3$ of radioactive waste in storage and an estimated 4,420,000 $m^3$ arising in the future[1]
- Intermediate level radioactive waste is high volume in the UK and more will arise from decommissioning
- High volume wastes of ILW classification:
  - SIXEP Sand/Clinoptilolite ion exchange material
  - Pond and Process Sludges (e.g. Magnox, THORP)
  - Plutonium Contaminated Material (PCM)
- Contaminated with Cs-137, I-129, Cl-stable from various decay/treatment processes

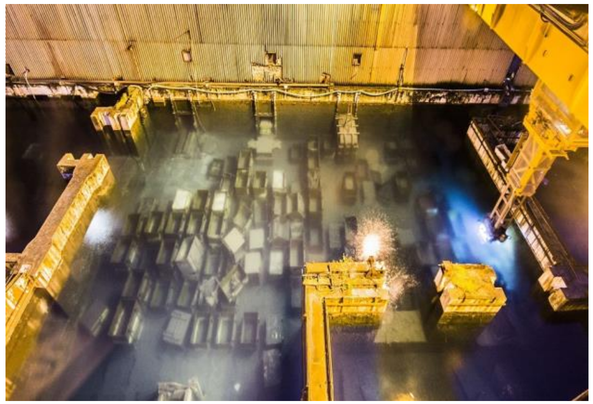

*Figure 1*. Magnox Storage Pond

# Thermal Treatment

- Vitrification as a waste treatment technique is already in use for HLW and has potential for ILW. This involves forming a glass or glass/ceramic product[2]
- Cold crucible ceramic, Joule Heated Ceramic and plasma melters are all being considered for treatment
- All require temperatures from 950-1500 °C which could volatilise some of the waste components
- A full inventory of radioactive material must be kept and reducing volatility reduces the error and risk associated with thermal treatment techniques

*Figure 2*. GeoMelt® Vitrification System

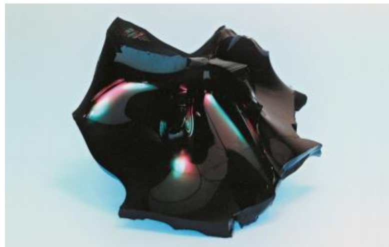

TRANSCEND

Transformative Science and Engineering for Nuclear Decommissioning

# Techniques

## Thermogravimetric Analysis

- Mass loss vs Temperature
- Maximum temperature 1200 °C

## X-Ray Fluorescence of resultant glasses

- Full elemental analysis
- Melting of sample in alumina crucible
- Maximum temperature 1450 °C

## Pyrolysis

- Active and inactive facilities available
- Designed for gaseous radionuclide analysis
- Maximum temperature 1000 °C


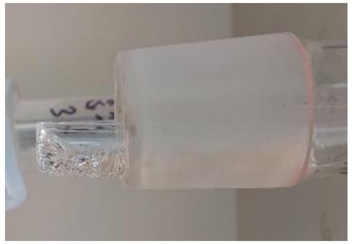

*Figure 3.* Raddec-6 Pyrolyser unit

*Figure 4.* Example of final sample product

| | Dopant | | | |
|---|---|---|---|---|
| | $^{127}I$ | $^{129}I$ | $^{137}Cs$ | $^{35.5}Cl$ |
| Base Glass (With Dopants) | 1 | 1 | 2 | 5 |
| Clinoptilolite 10-50wt% | 1 | 1 | 2 | 5 |
| Corroded Magnox Sludge 10-50wt% | 1 | 1 | 2 | 5 |
| Xanthan Gum Additive | 2 | 2 | 4 | 5 |
| Graphite Additive | 2 | 2 | 4 | 5 |
| Reduced Boron Frit | 3 | 3 | 4 | 5 |

*Table 1*. Table of experimental plan with priority order (1 high - 5 low)

# Glass Systems

Base glasses were selected for maximum relevance to the UK nuclear industry (MW and CaZn). These were then modified for processing of waste at lower temperatures and to increase waste loading.

Glass systems studied:

- MW
- CaZn
- 0% $SiO_2$ CaZn
- 30% $SiO_2$ CaZn

| | Nominal Composition (wt%) | | | |
|---|---|---|---|---|
| Oxide in Glass | MW | CaZn | 0% $SiO_2$ CaZn | 30% $SiO_2$ CaZn |
| $SiO_2$ | 61.74 | 47.6 | 0.00 | 30.00 |
| $Na_2O$ | 11.05 | 8.6 | 16.41 | 11.49 |
| $B_2O_3$ | 21.88 | 23.4 | 44.66 | 31.26 |
| $Li_2O$ | 5.33 | 4.2 | 8.02 | 5.61 |
| $Al_2O_3$ | - | 4.2 | 8.02 | 5.61 |
| ZnO | - | 6.0 | 11.45 | 8.02 |
| CaO | - | 6.0 | 11.45 | 8.02 |

Introduction

**High Temperature Glasses**

Low Temperature Glasses

The Future

# Thermogravimetric Analysis

- Caesium mass loss is **greater** in MW glass than CaZn glass
- The bulk of the mass loss is dependent on caesium addition releasing a **high temperature** gaseous species
- CaZn glass is better at retaining caesium than MW glass at a given temperature
- Little difference in thermal events other than decomposition of the $Cs_2CO_3$ reagent

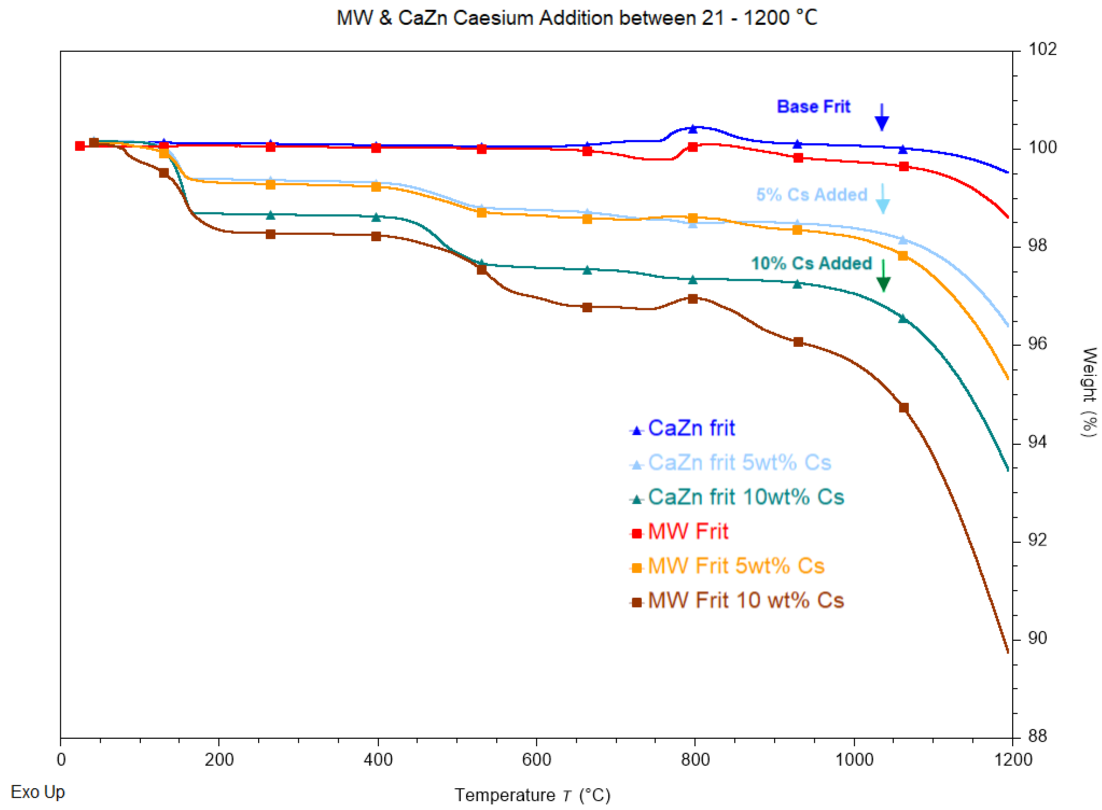


Introduction
**High Temperature Glasses**
Low Temperature Glasses
The Future

# Temperature dependance

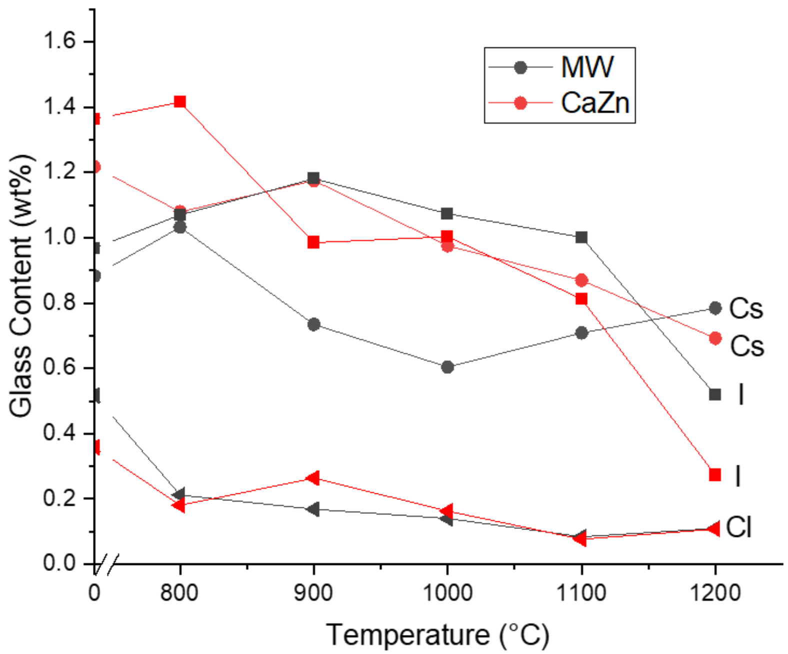


$$Frit + x \xrightarrow[Heat]{} Product$$

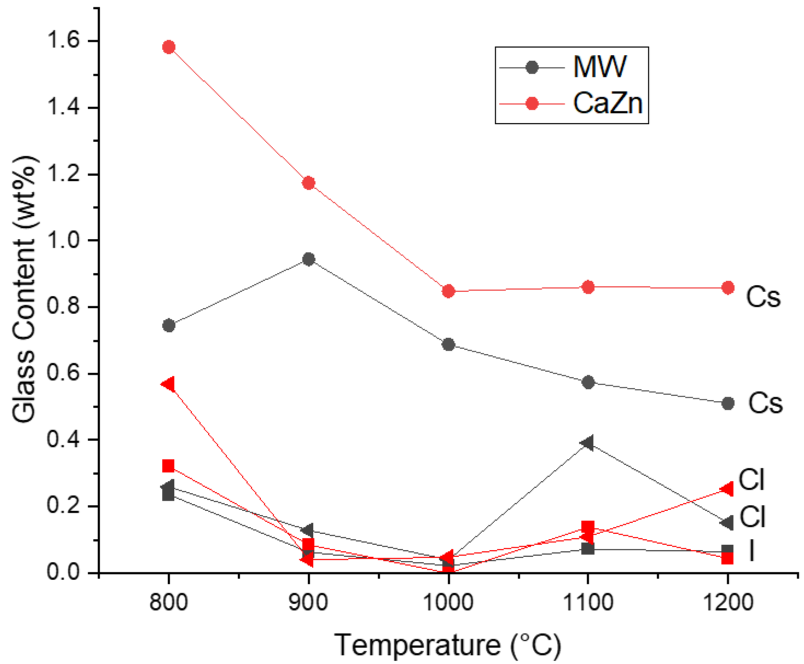


$$Frit + x \xrightarrow[Heat]{} Fritx \xrightarrow[Heat]{} Product$$

- Increasing temperature **accelerates** Cs, I and Cl loss from MW and CaZn glasses
- **Caesium retains better** in the glass structure for halides iodine and chlorine
- **CaZn glass retains better** overall for all samples and elements

# Waste Loading

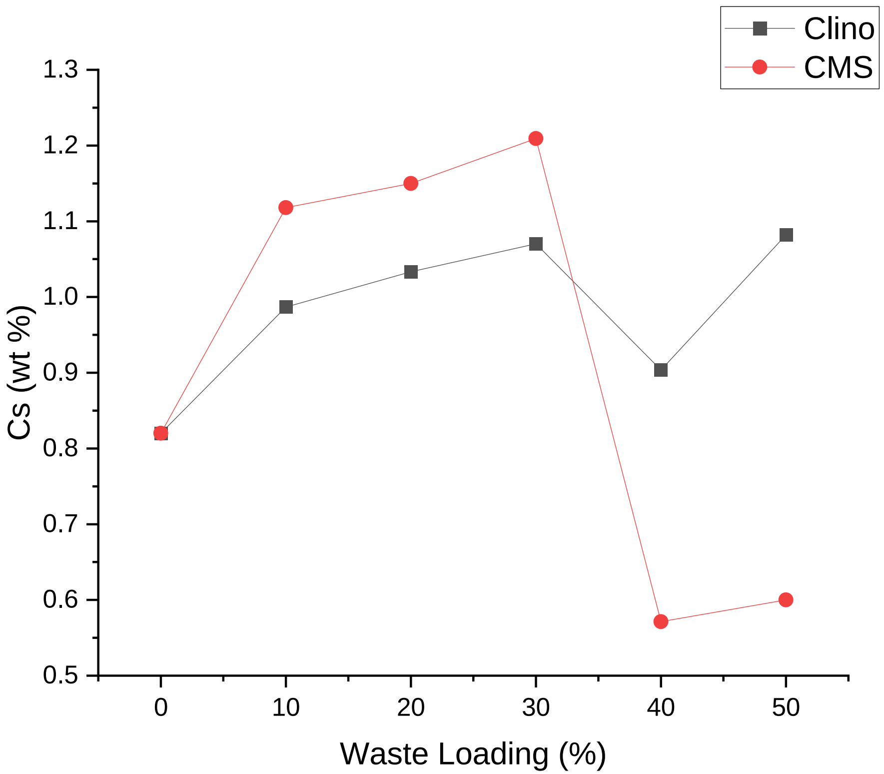


The effect of Waste loading of CaZn glass doped with caesium

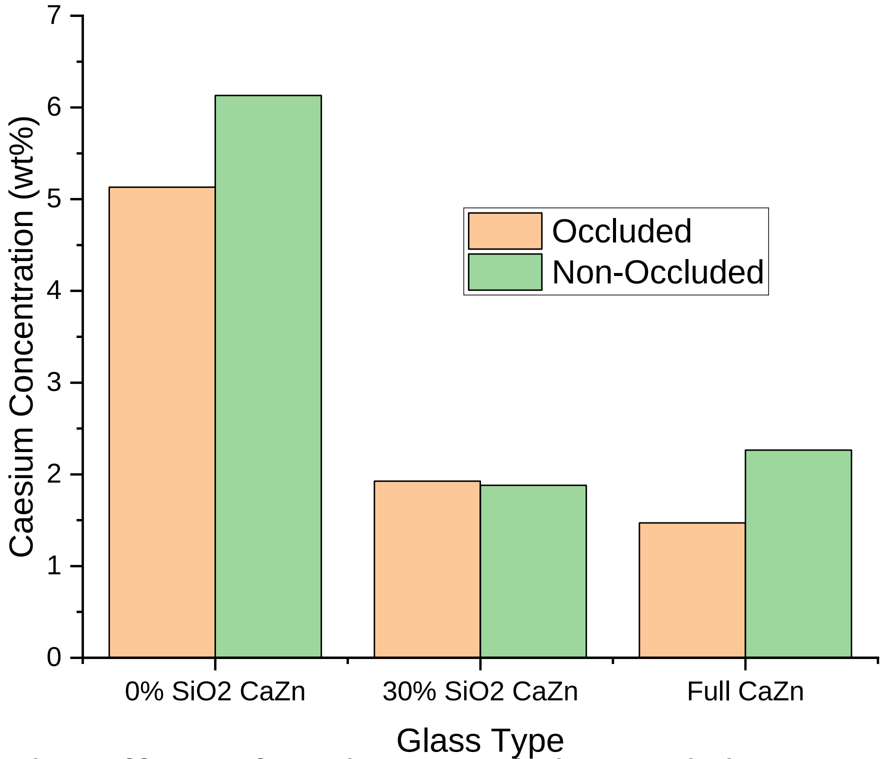


The effect of occlusion of clinoptilolite on caesium retention in three glass systems

- Waste additions between 10 – 30 wt % positively affect caesium retention
- Occlusion increases volatility of caesium

Introduction

High Temperature Glasses

**Low Temperature Glasses**

The Future

# Waste Loading

- Using pyrolysis adding the same concentration of each dopant we have been able to capture or retain **active** and inactive **caesium** and **iodine** in simulated wasteforms with **corroded Magnox sludge** and **clinoptilolite**
- Emissions reducing additives:
  - Carbon sources: Graphite, Xanthan gum, Starch
  - Glass formers and intermediates: $SiO_2$, ZnO,
- Initial results show **waste loading** has a large effect on retention of active iodine-129 in the silica free CaZn glass systems studied
  - Clinoptilolite has a positive effect on retention for both I and Cs

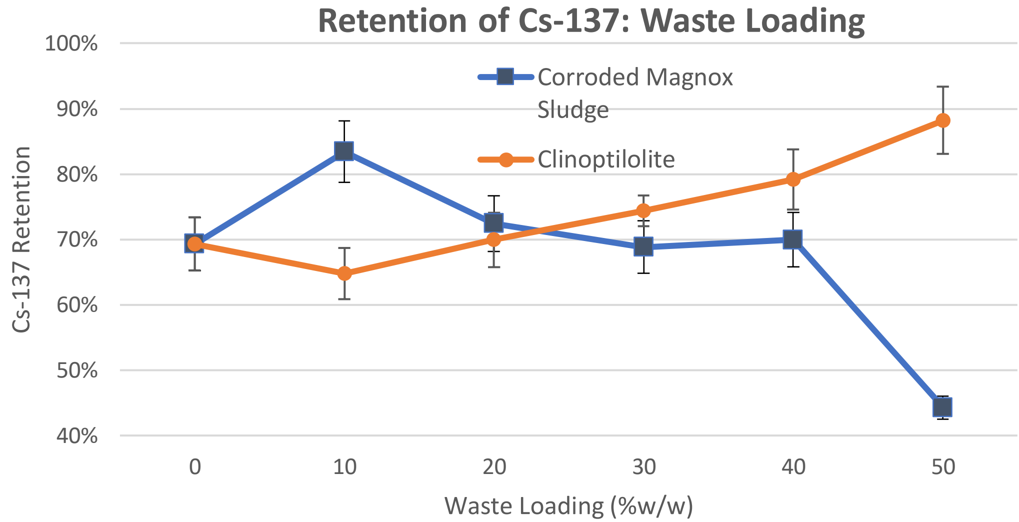


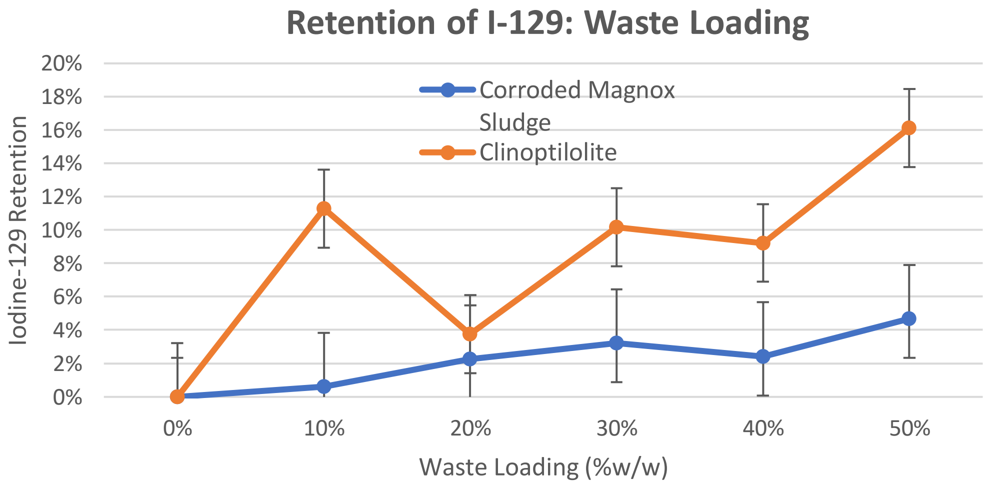

# Carbon and Nitrogen

- Carbon containing additives had very **little effect** on **iodine retention** but a small change for **caesium** in the borate glass
    - Xanthan gum and Starch **positively** changed the retention by 17% and 14% respectively for Cs-137
    - Graphite had little effect for both radionuclides
- Atmosphere above the melt has a **large influence** on **iodine volatility** but less of an impact on **caesium**
    - Nitrogen gas flow over the melt **increased retention** of I-129 by up to 74% and Cs-137 by 8%

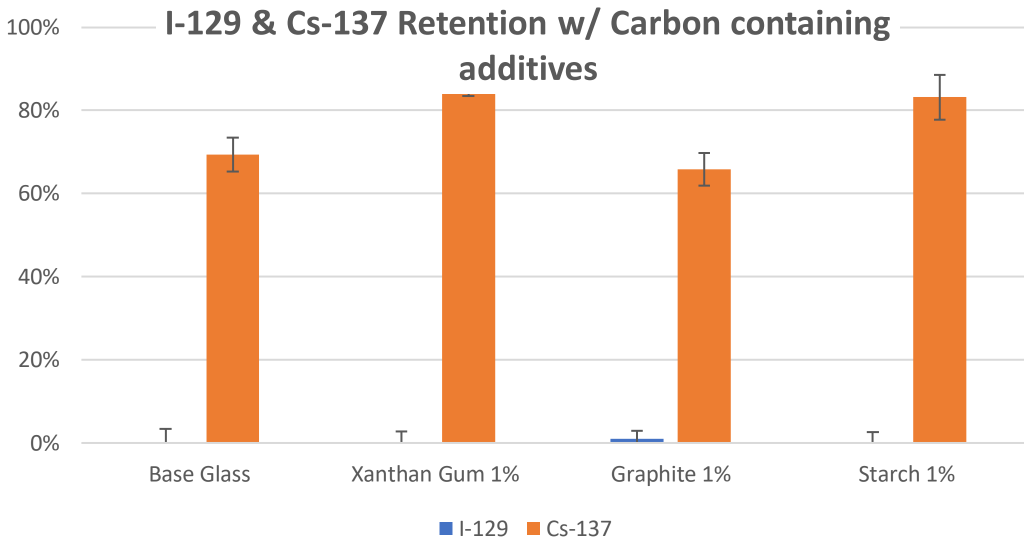


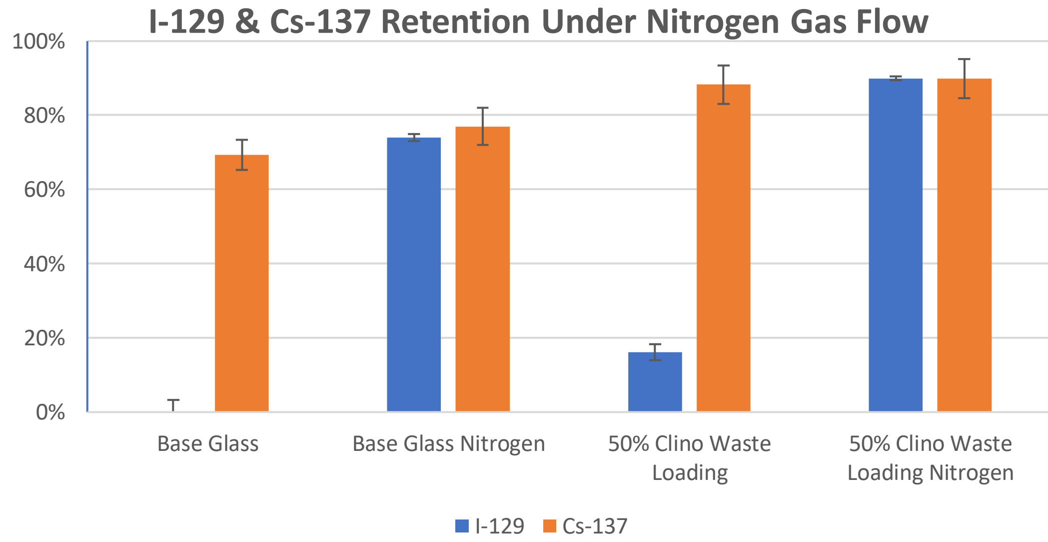

NNUF
National Nuclear User Facility

Nuclear Decommissioning Authority

NATIONAL NUCLEAR LABORATORY

Sheffield Hallam University

Thank you

alex.h.stone@student.shu.ac.uk

TRANSCEND

Transformative Science and Engineering for Nuclear Decommissioning

# Radiation effects on nuclear waste forms:
# How does the crystallinity of glass composite affect radiation tolerance?

Tamás Zagyva – The University of Manchester, Dalton Cumbrian Facility

Theme 1 Integrated Waste Management

24th April 2022
London

MANCHESTER 1824
The University of Manchester
Dalton Nuclear Institute

NATIONAL NUCLEAR LABORATORY

Energy
For a Low Carbon Future

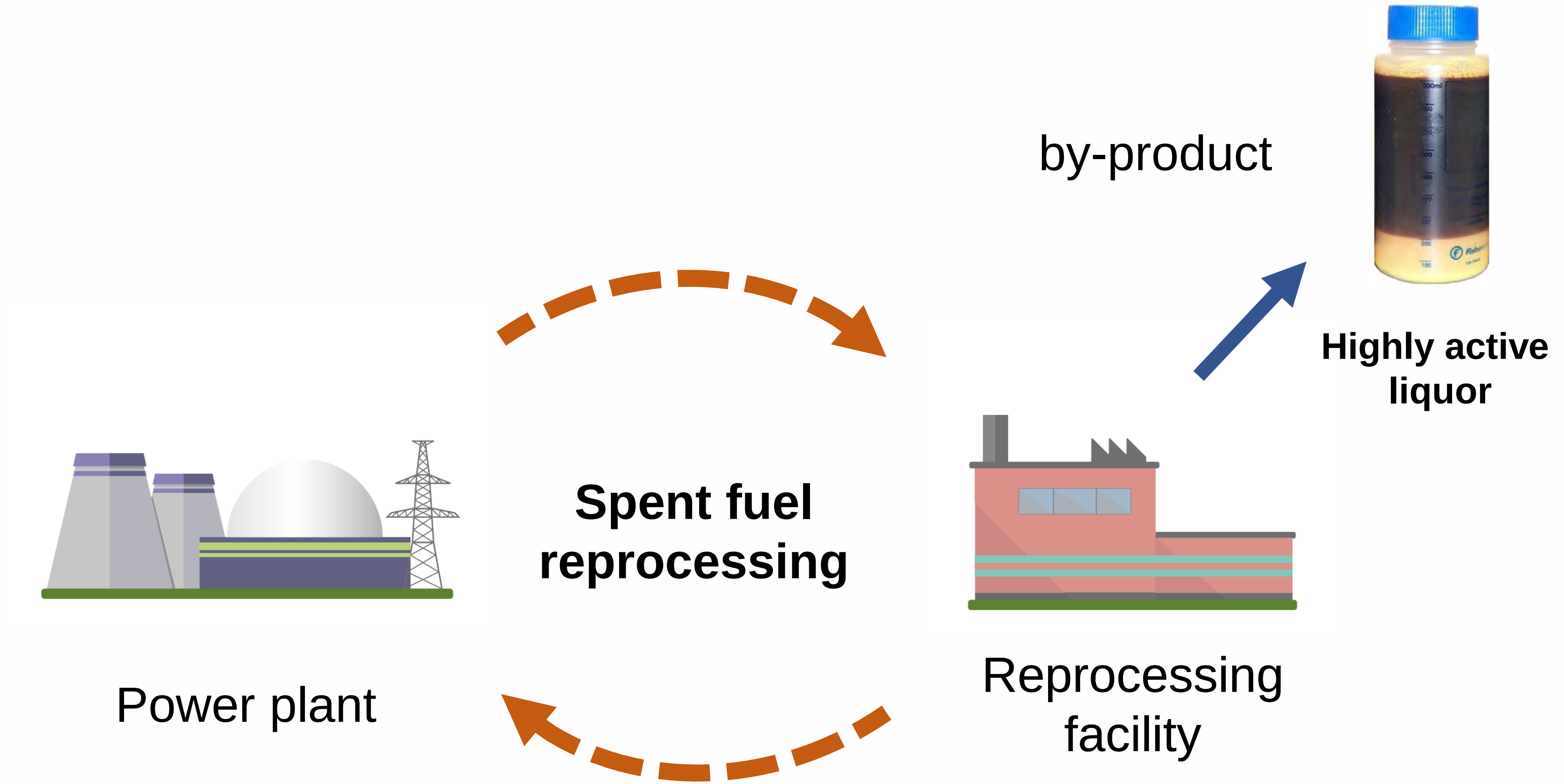
by-product
Highly active liquor
Spent fuel reprocessing
Power plant
Reprocessing facility

**Highly active liquor (HAL)**

**Vitrification**

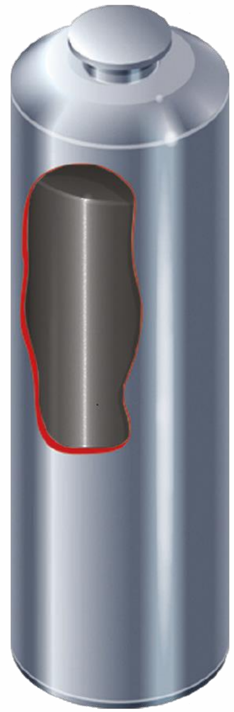

**Solid glass wasteform**


HAL with high Mo content

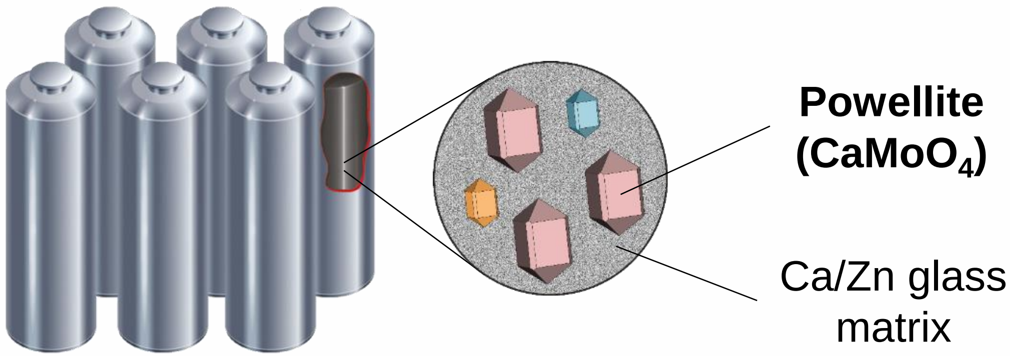


Glass composite high-level waste

**Goal of research:** evaluate the radiation tolerance of Mo-rich HLW glass composite materials.

α–radiation, β–radiation, γ–radiation

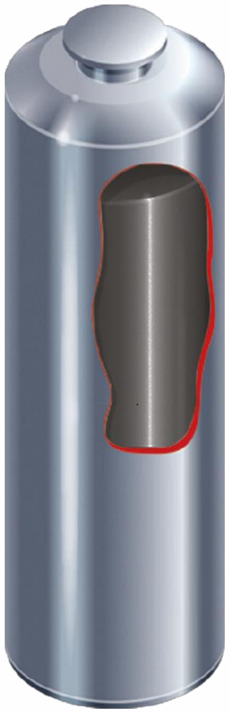

HLW
glass composite

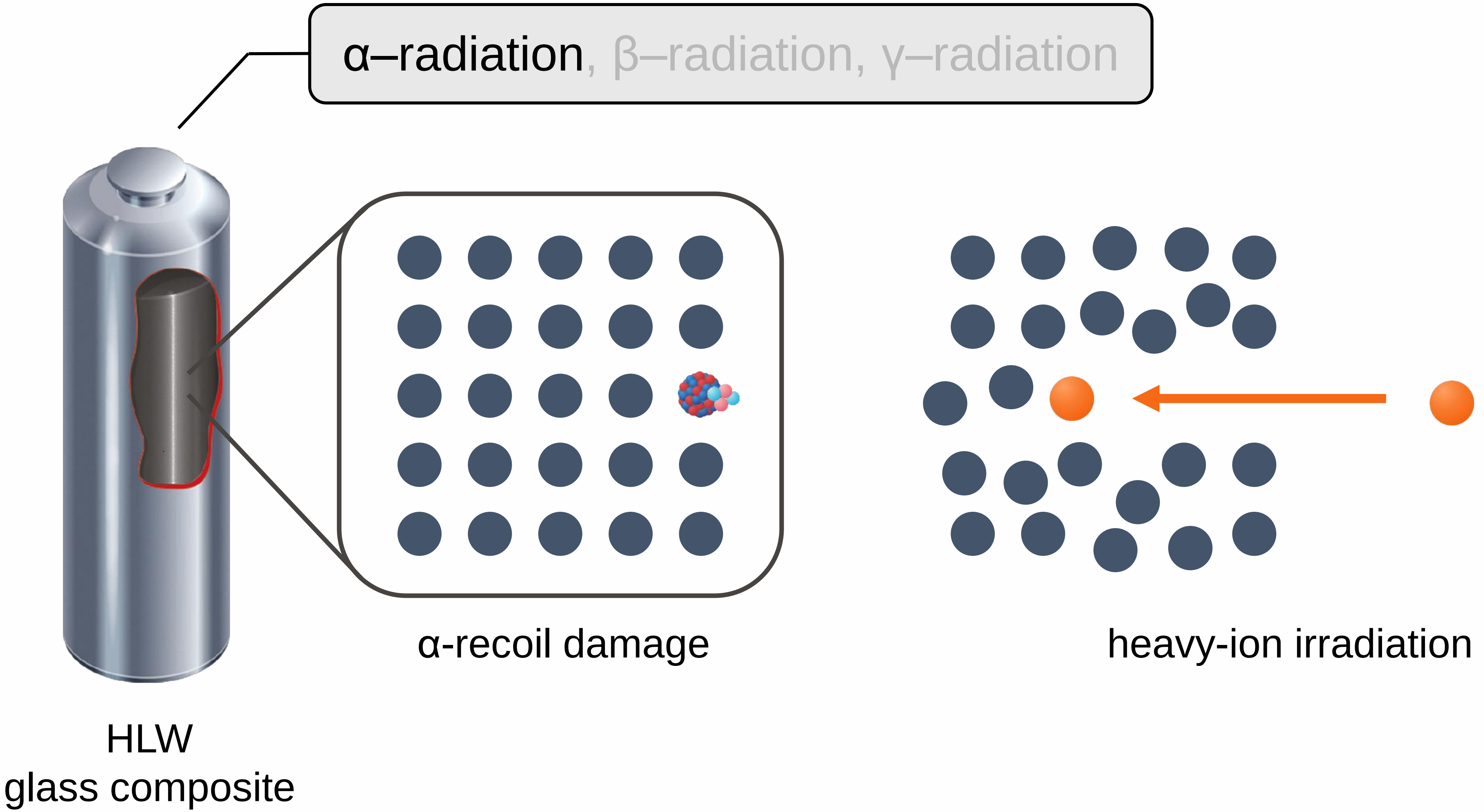
α–radiation, β–radiation, γ–radiation
α-recoil damage
heavy-ion irradiation
HLW
glass composite

## Nuclear waste simulant glass composite

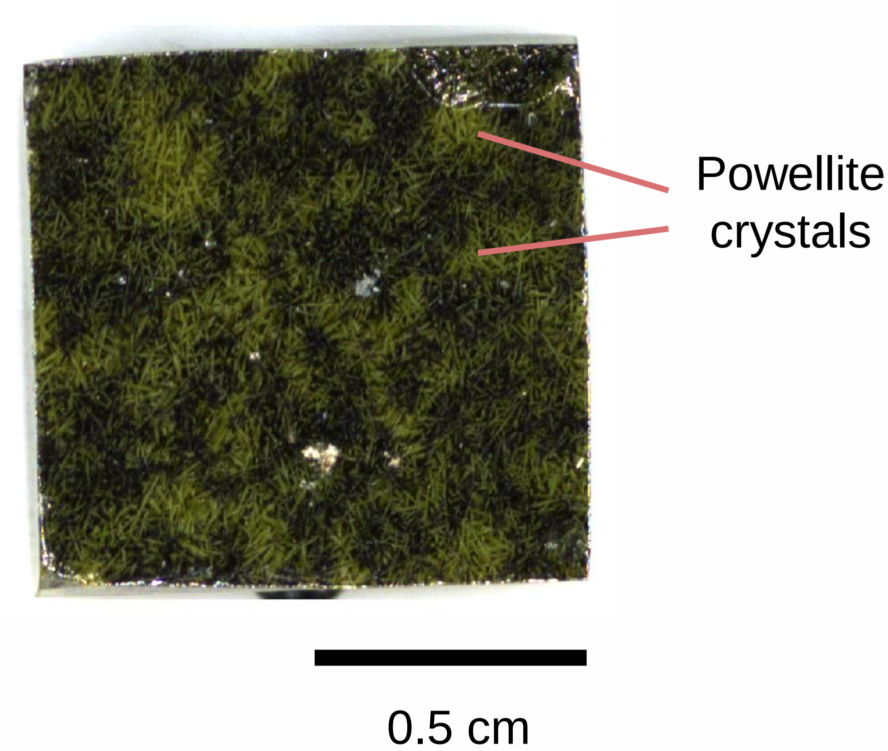


## Heavy-ion irradiation experiments

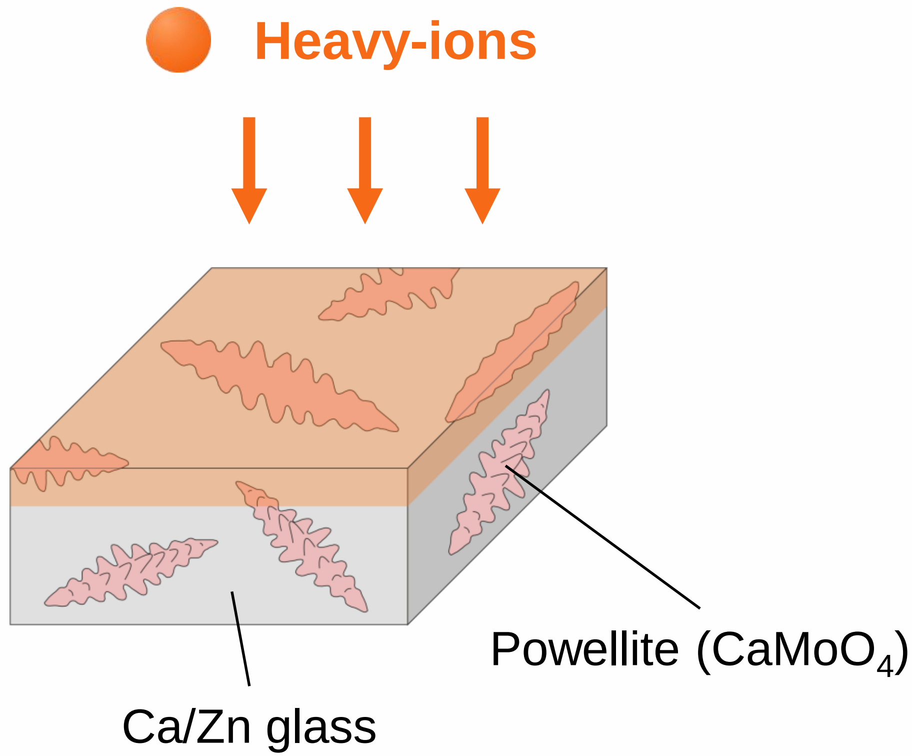

# Characterisation of glass composite samples

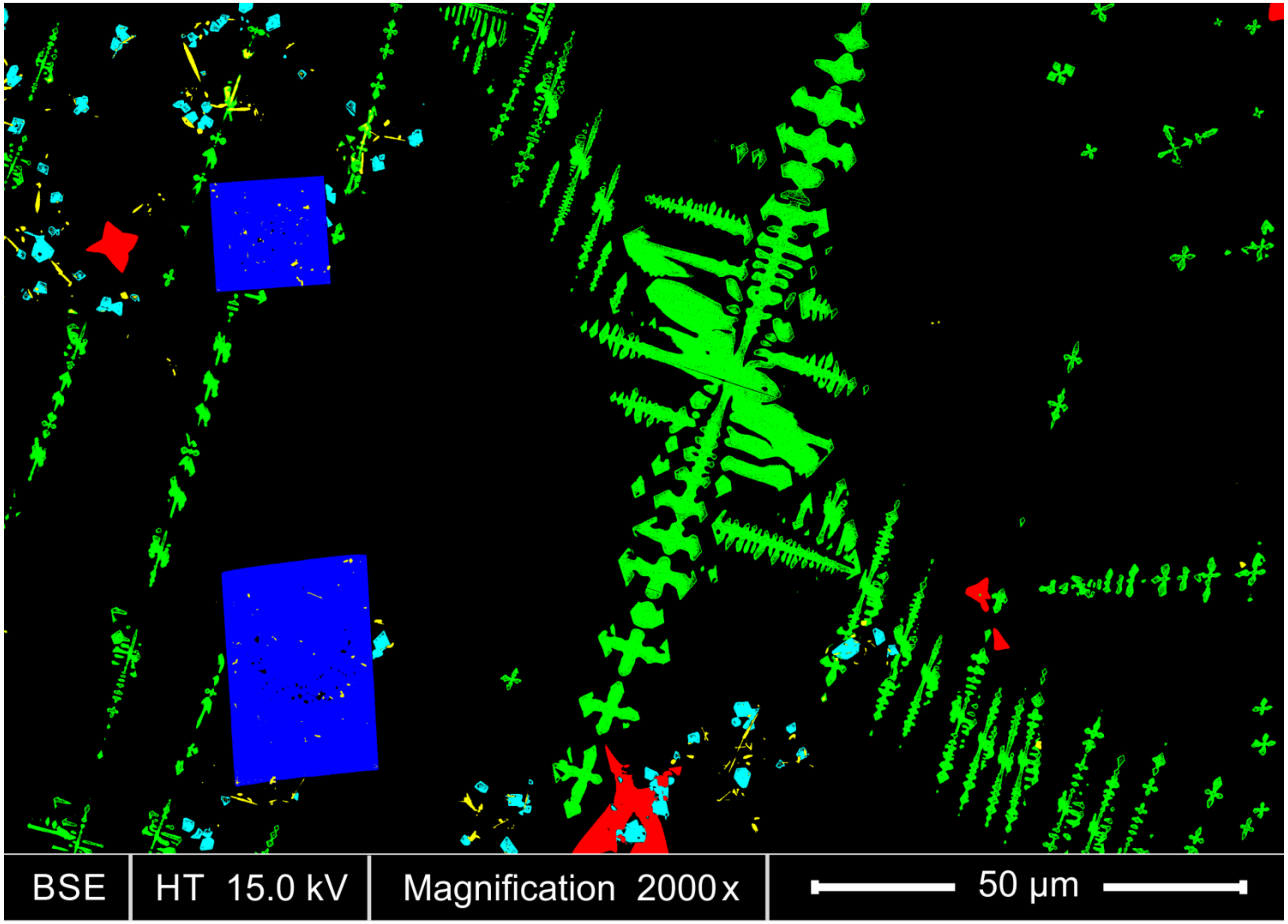


powellite

zircon

cerianite

zincochromite

ruthenium dioxide

crystallinity: 16%

## Gd elemental maps

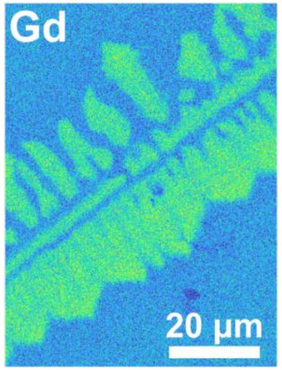


powellite

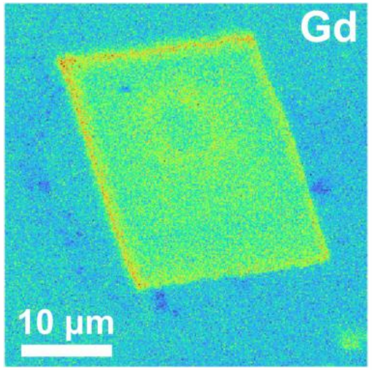


zircon

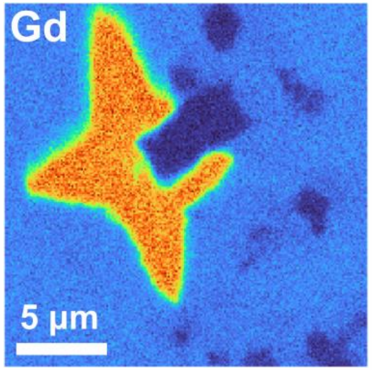


cerianite

**α-decaying actinides**

## Sr and Cs elemental maps

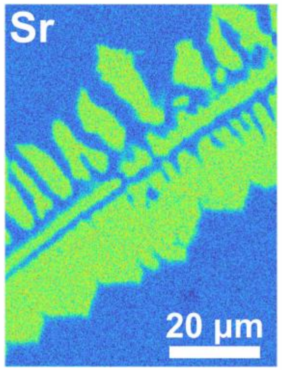


powellite

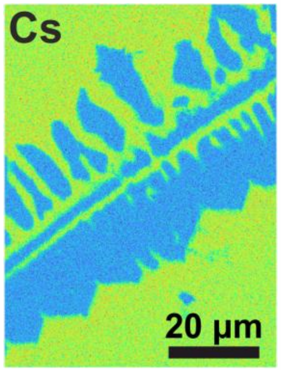


glass

**β-decaying fission products**

# Heavy ion irradiation experiments

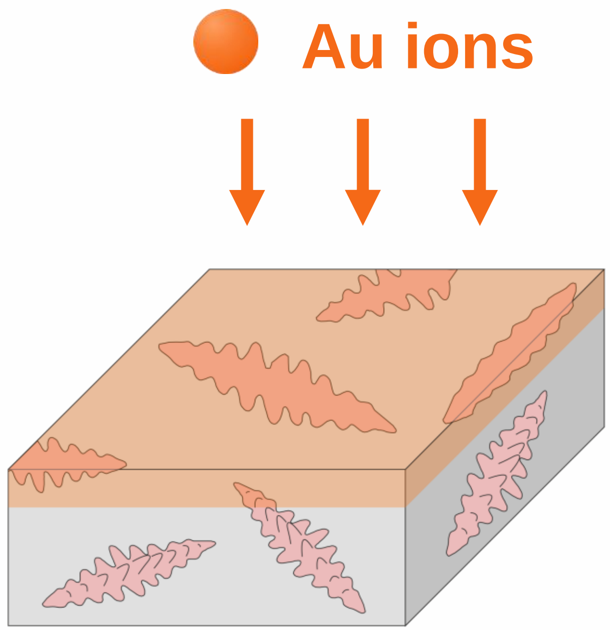


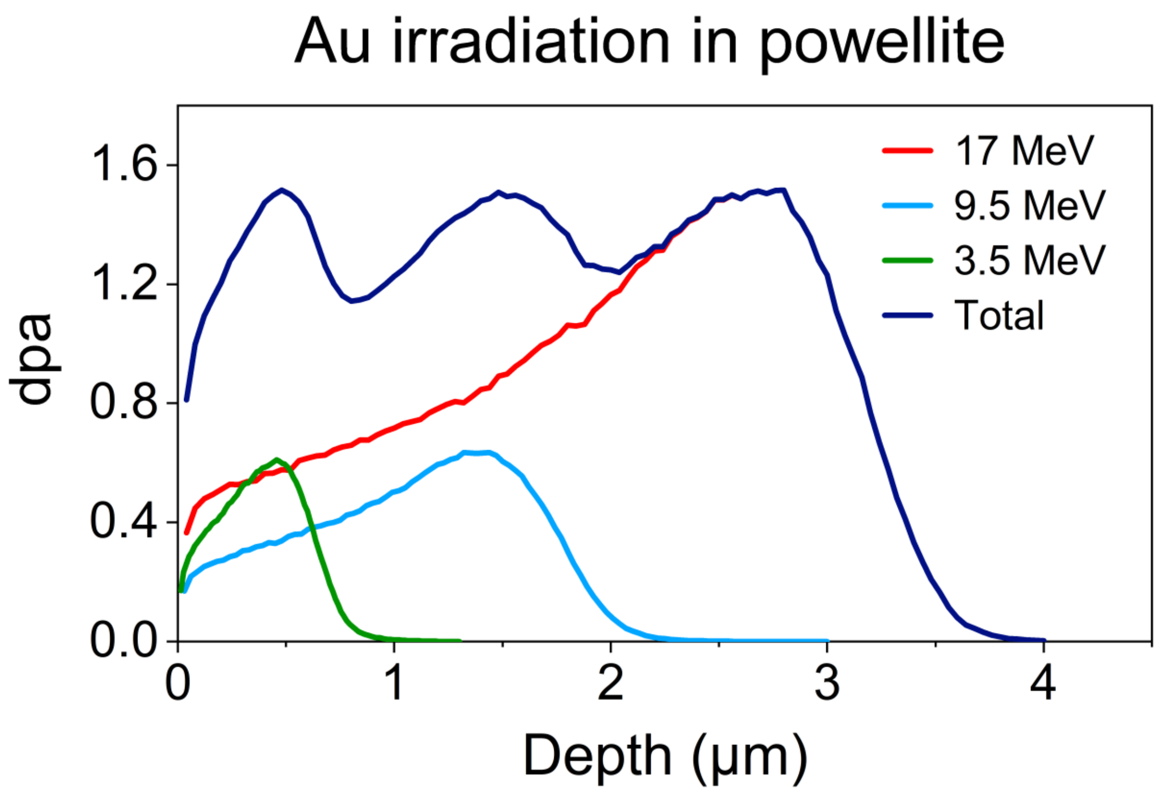

# Heavy ion irradiation experiments

**BEFORE Au irradiation**

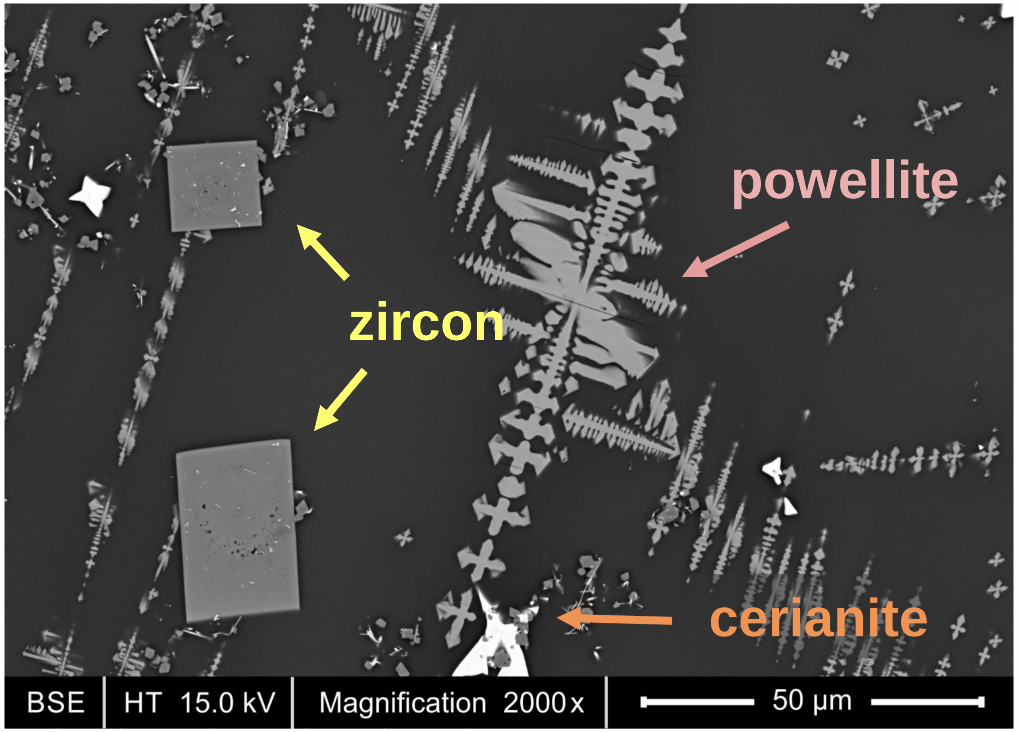


**AFTER Au irradiation**

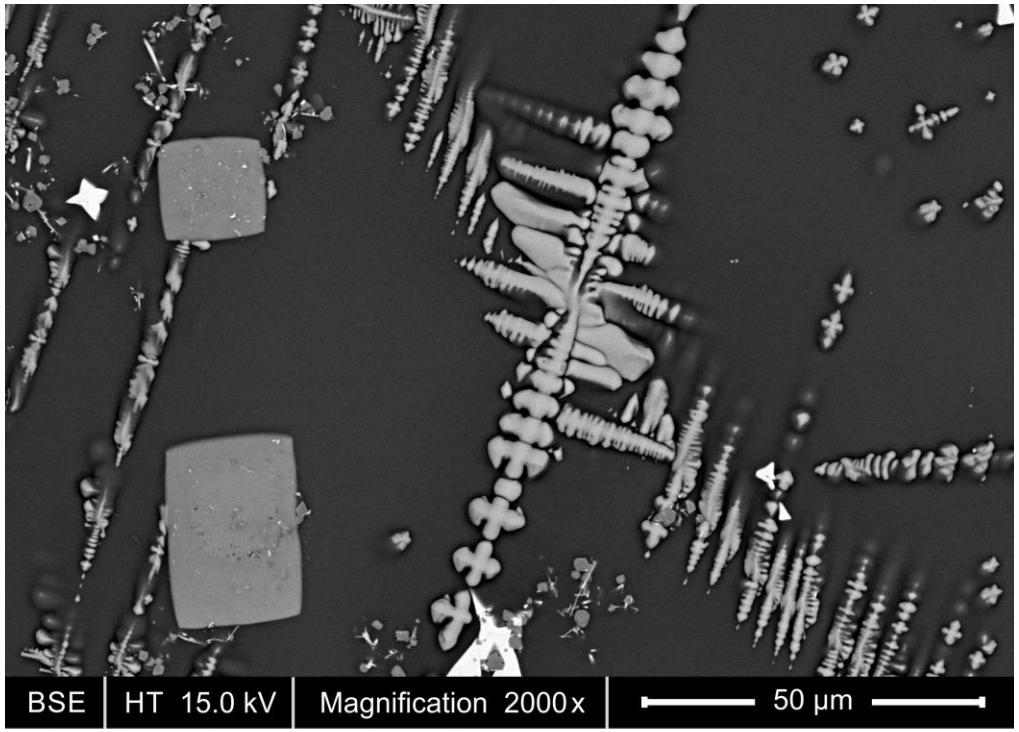


powellite and zircon – swelling

cerianite – no change

# Heavy ion irradiation experiments (EBSD)

cerianite | zincochromite | ruthenium dioxide | powellite | zircon

before **Au** irradiation

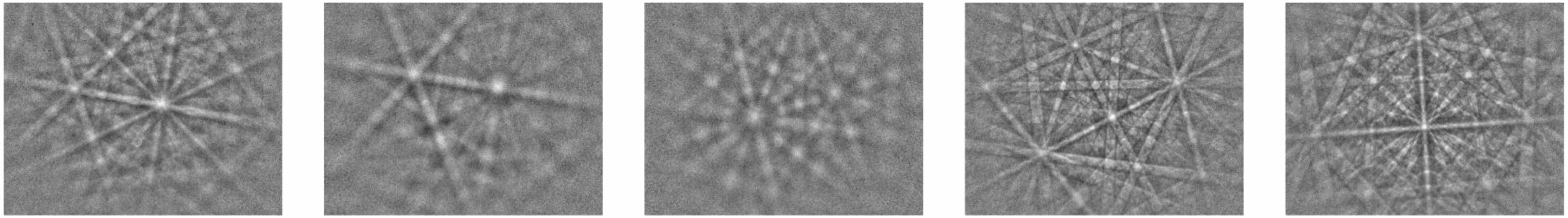

# Heavy ion irradiation experiments (EBSD)

| | cerianite | zincochromite | ruthenium dioxide | powellite | zircon |
|---|---|---|---|---|---|

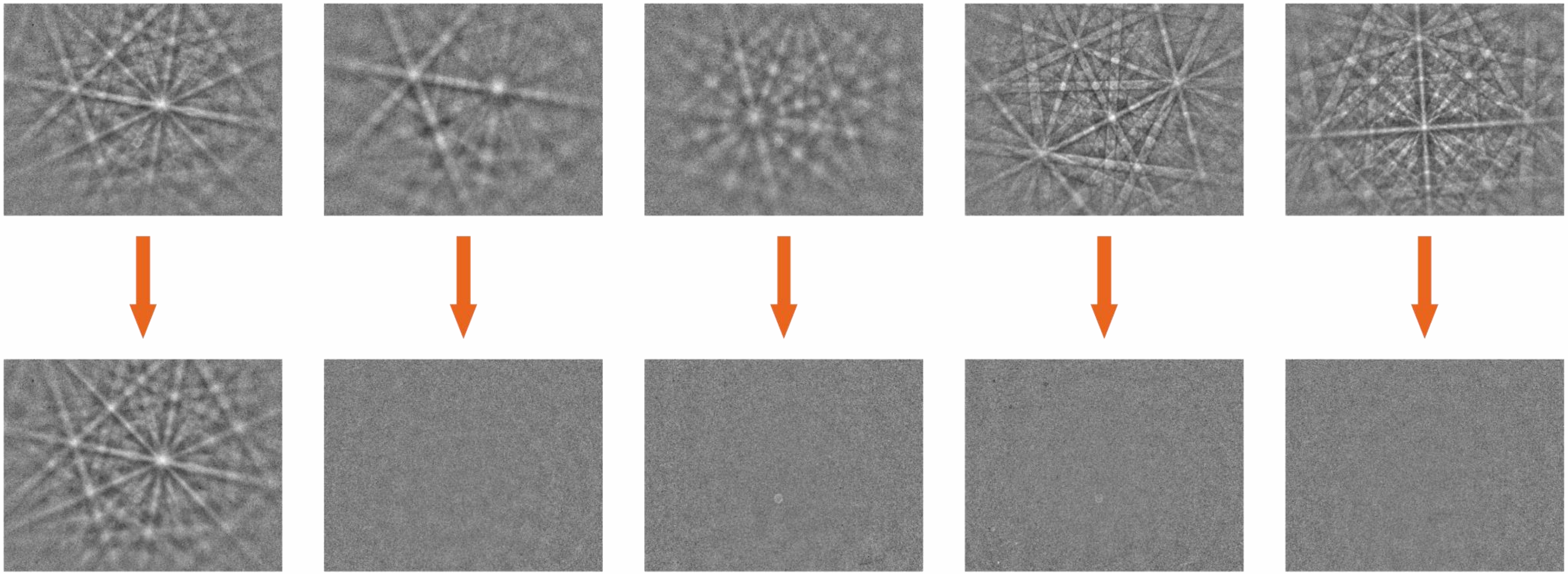

before **Au** irradiation

after **Au** irradiation

**no change** | **complete amorphisation** | **complete amorphisation**

# Heavy ion irradiation experiments

**GIXRD:** incident angle = 1.8°

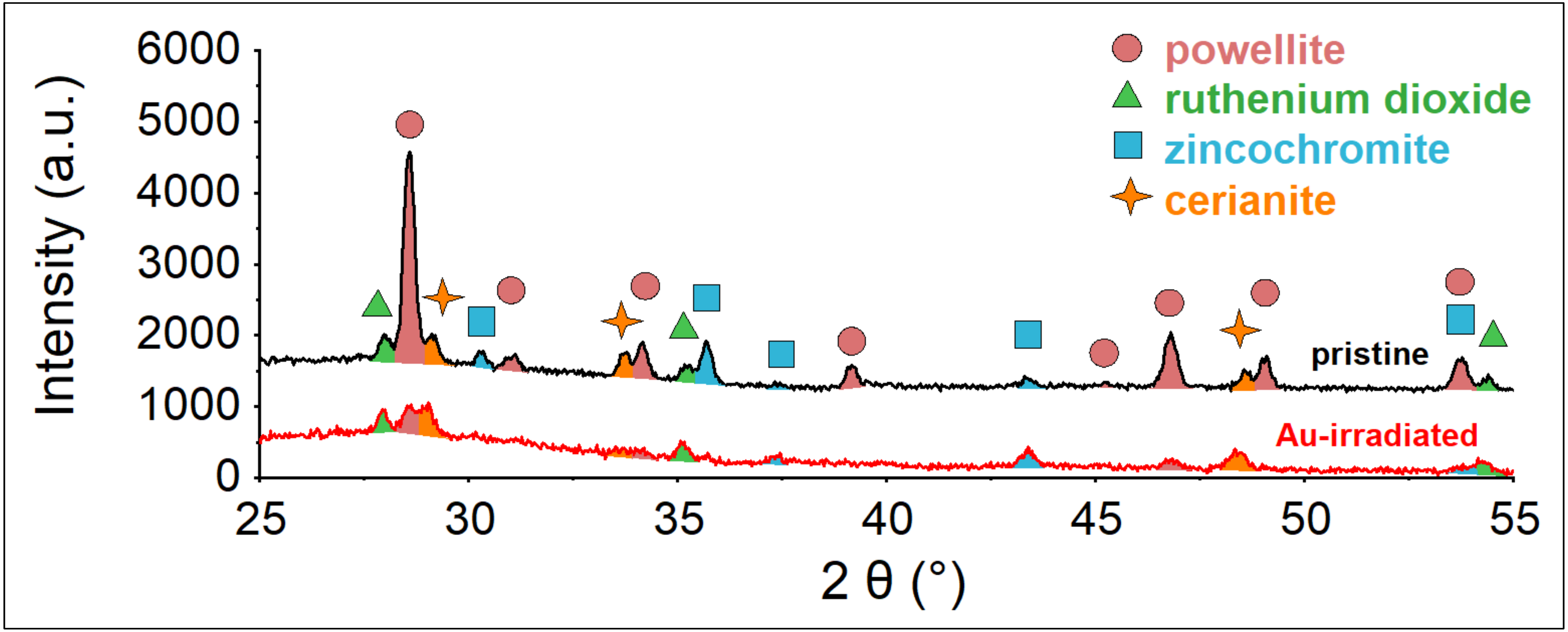

## Summary (1)

- relative radiation tolerance of crystals:

high

cerianite

zincochromite ≈ ruthenium dioxide

powellite ≈ zircon

low

- amorphised crystals swelled considerably
- **First evidence of powellite ($CaMoO_4$) amorphisation!**

→ TEM analysis with *in situ* **Ar** and **Xe** ion irradiation

# TEM with in situ Ar and Xe ion irradiation

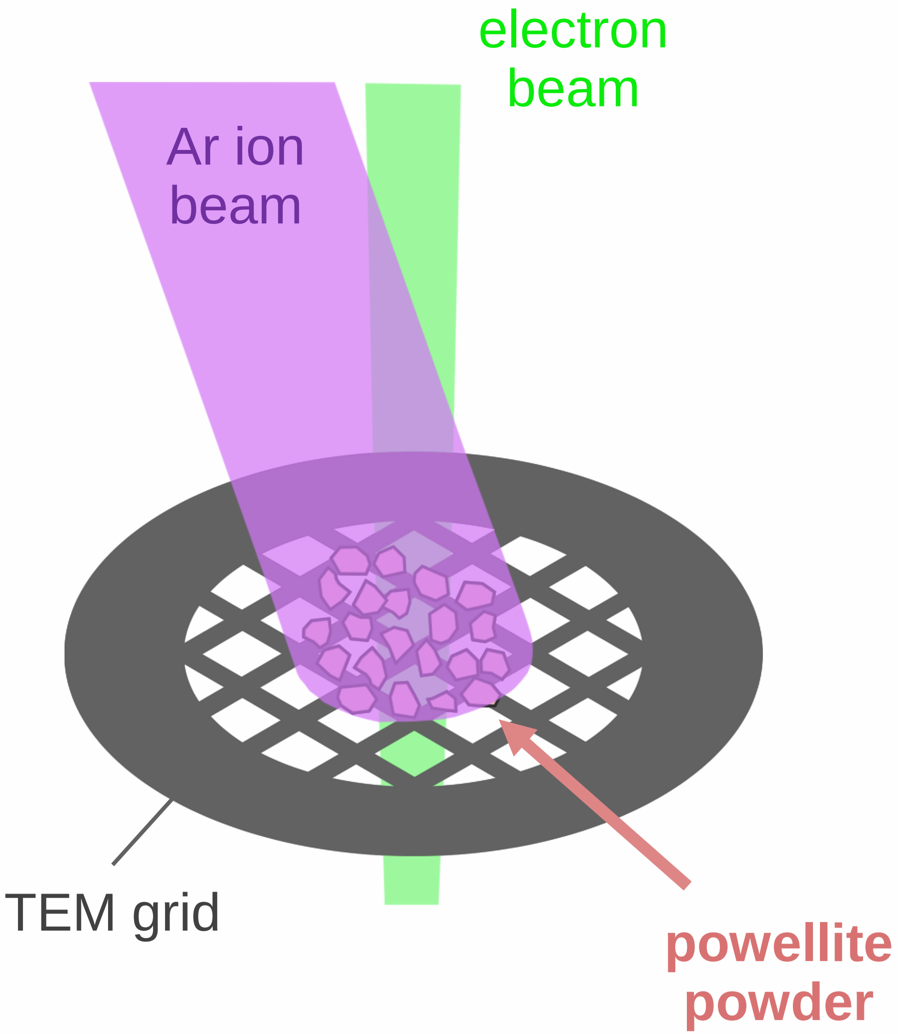


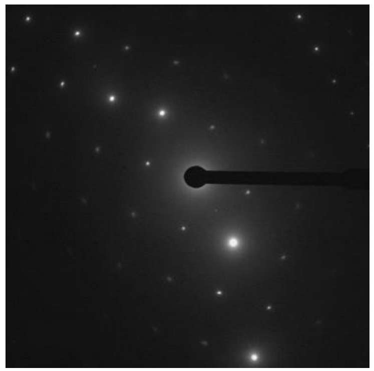

crystalline powellite
before irradiation

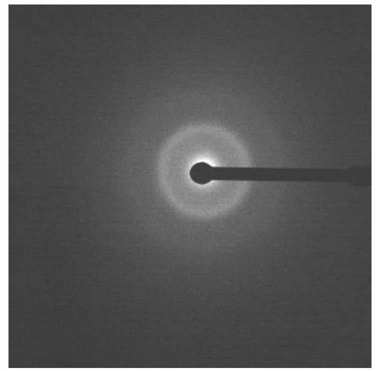

amorphous powellite
after irradiation

# TEM with in situ Ar and Xe ion irradiation

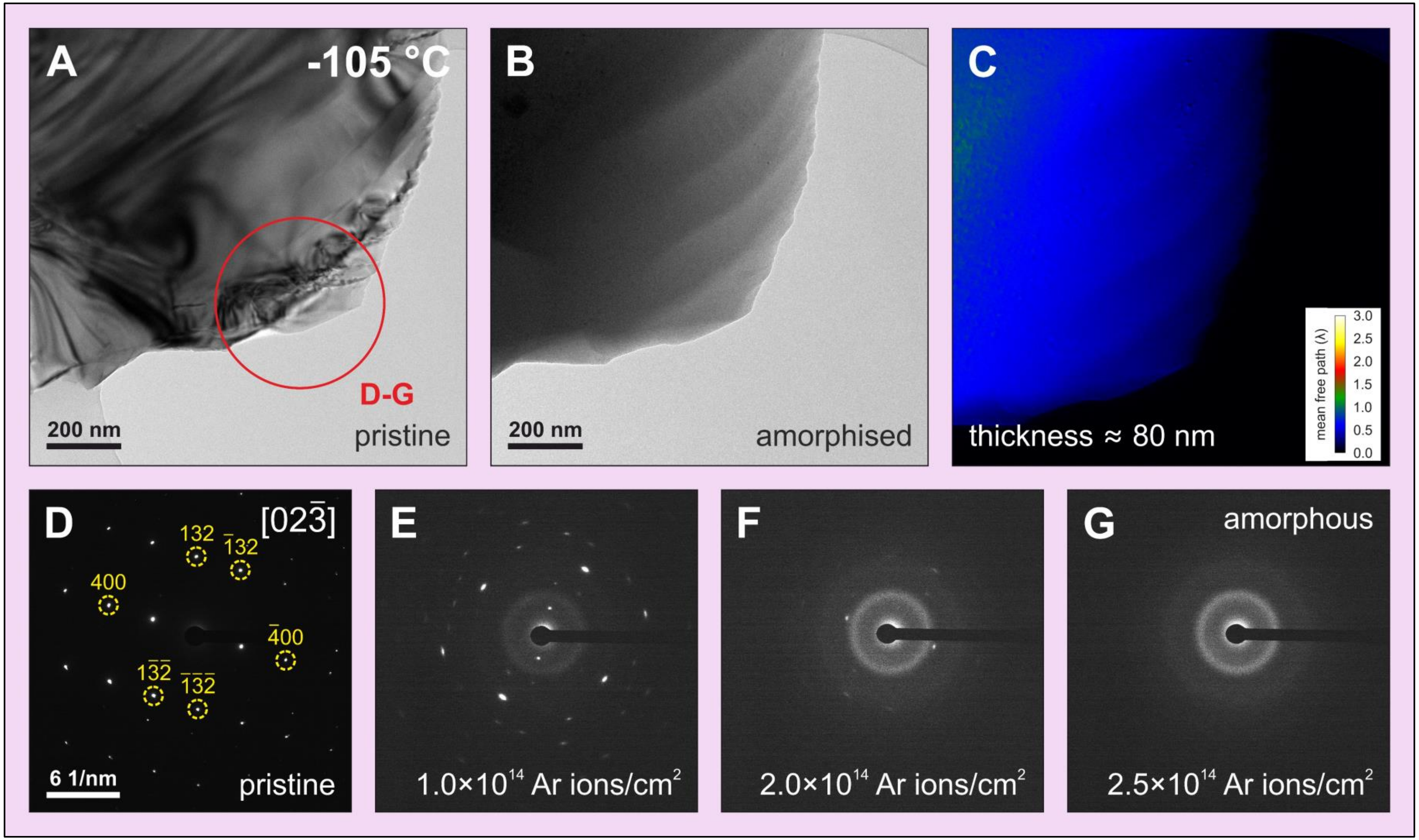

# TEM with in situ Ar and Xe ion irradiation

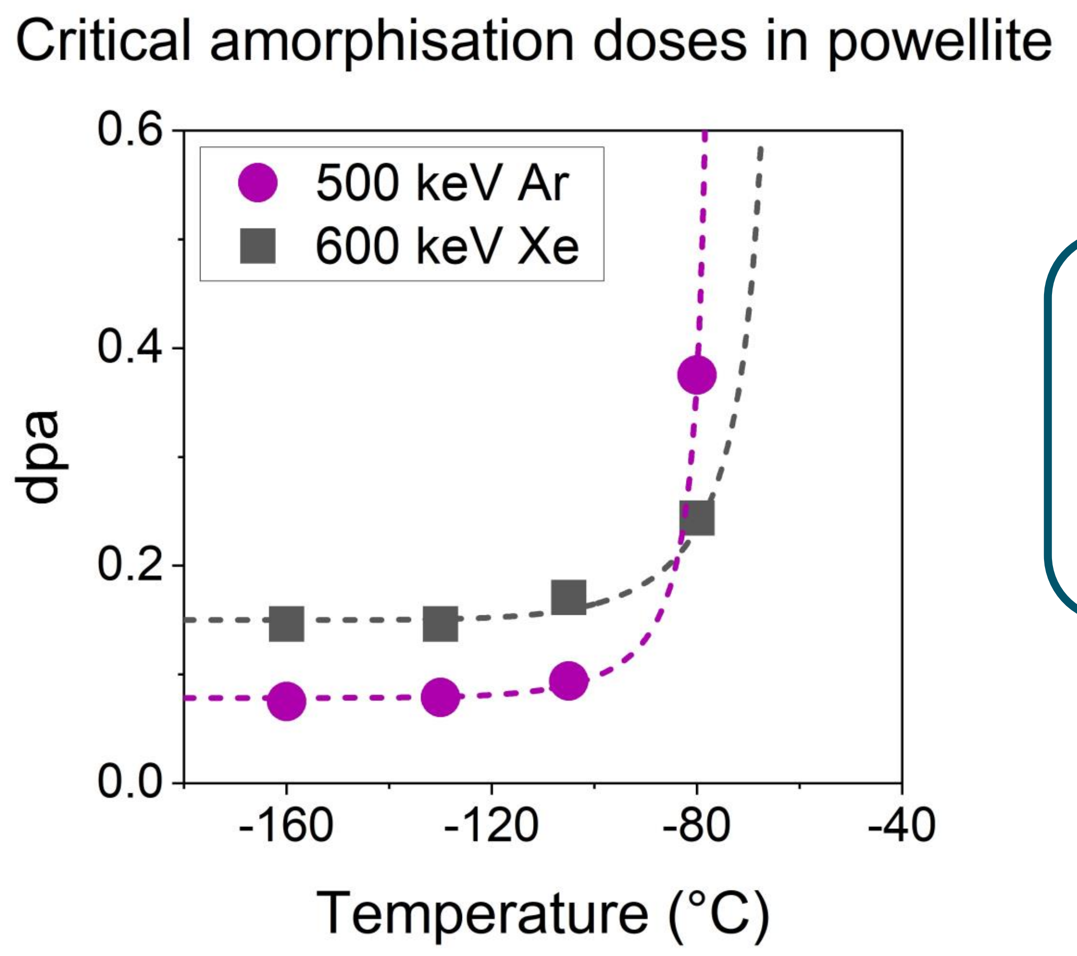


Dual defect annealing process

1. Thermal spike
2. Dynamic annealing

# Electron beam-induced recrystallisation

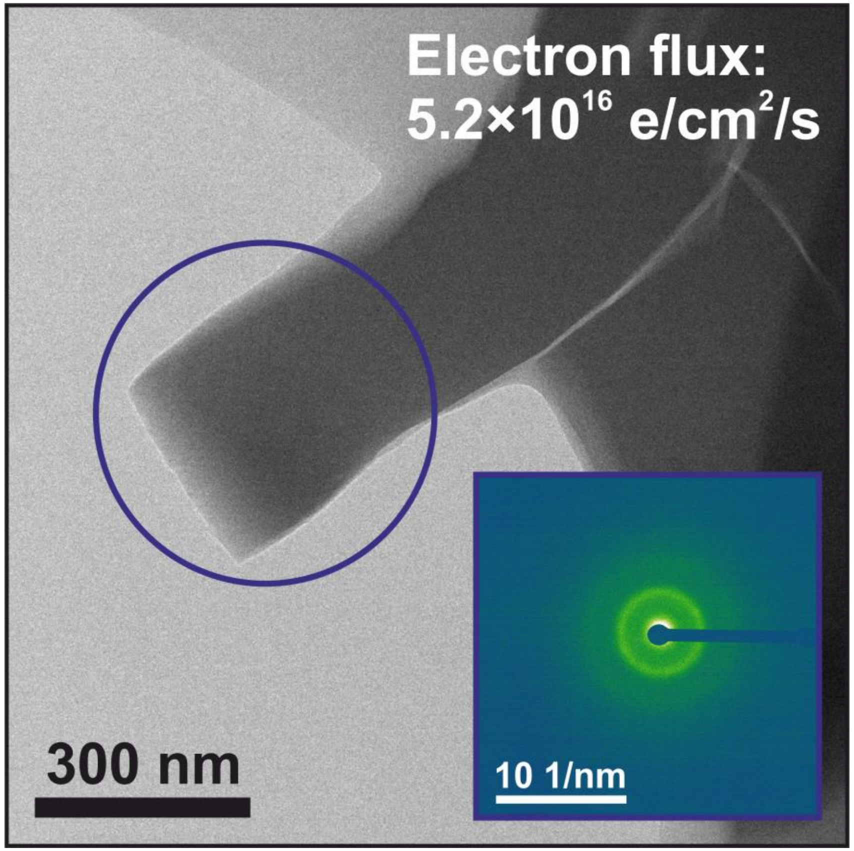


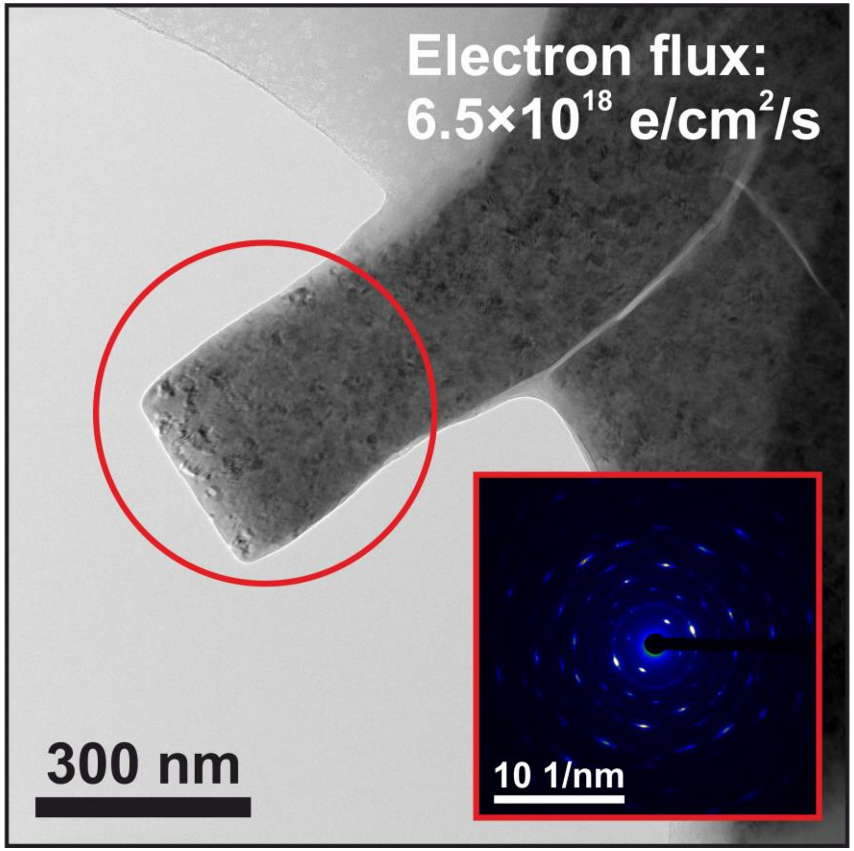

# Electron beam-induced recrystallisation

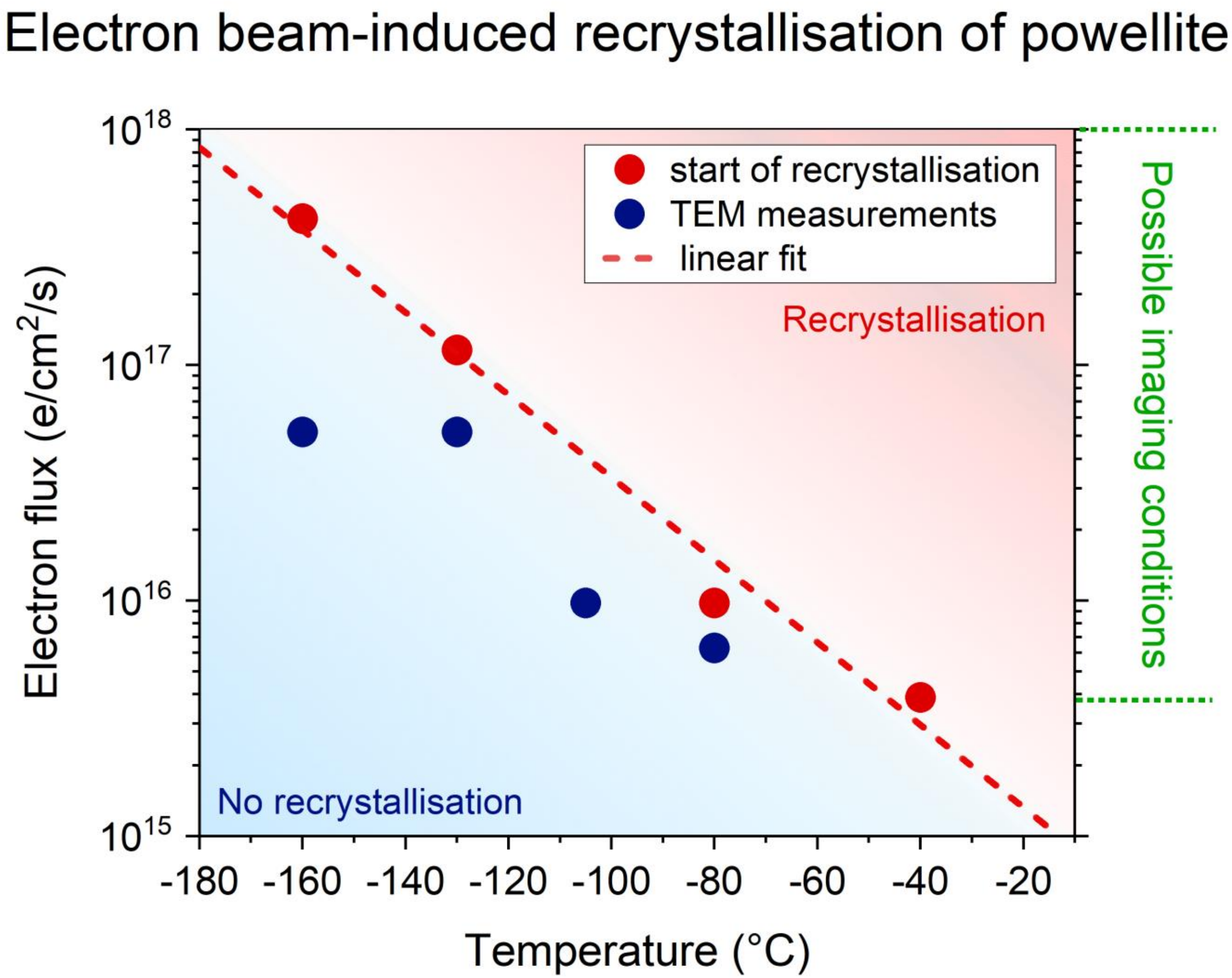

# Summary (2)

| Literature | | This study |
|---|---|---|
| 8 ion irradiation study (He, Ar, Kr, Xe, Au, Pb) **NO AMORPHISATION** | ⇔ | 4 ion irradiation study (Ar, Xe, Ni, Au) **AMORPHISATION** |
| 2 electron irradiation study **AMORPHISATION** | ⇔ | electron irradiation study **RECRYSTALLISATION** |

Mendoza et al. 2011 / Brinkman et al. 2013 / Tang et al. 2014 / Jagielski et al. 2014 / Wang et al. 2014 / Patel et al. 2020

## Conclusions

- First evidence of ion irradiation induced amorphisation in powellite and electron beam induced recrystallisation in amorphous powellite.
- Powellite is susceptible to amorphisation by alpha recoils in high level wastes; however, the relatively high temperature and the ionisation induced annealing may cause significant defect recovery.
- The irradiation induced swelling might be significant enough to cause further cracking.

## Outcome of research:

- 1$^{st}$ paper: Journal of Nuclear Materials – under review
- 2$^{nd}$ paper: Acta Materialia – under review
- (3$^{rd}$ paper: Journal of Nuclear materials – submission in 2023)

TRANSCEND

Transformative Science and Engineering for Nuclear Decommissioning

## Thank you for the help!

Robert Harrison
Brian O'Driscoll
Laura Leay

Tracey Taylor
Mike Harrison

NATIONAL NUCLEAR LABORATORY

Anamul Haq Mir
Felix Kaufmann
Paul Bingham
Prince Rautiyal
Györgyi Glodán
Chetna Tyagi
Samir de Moraes Shubeita

Special thanks for the support from National Nuclear Laboratory.

NATIONAL NUCLEAR LABORATORY

Thank you

Contact Details
tamas.zagyva@postgrad.manchester.ac.uk

# The effect of the alkali metals on The CAS glass system

Lucas-Jay Woodbridge[1], Daniel Bailey[1] and Russell Hand[1]

The University of Sheffield

[1]*Immobilisation Science Laboratory, University of Sheffield, Department of Materials Science and Engineering, Sir Robert Hadfield Building, Mappin Street S1 3JD, UK*

Transcend annual meeting – 24th & 25th April 2023



*lwoodbridge1@Sheffield.ac.uk

# Chemical system of $CaO-Al_2O_3$-SiO2

- Well known glass formers
- Pristine series created
- Reasons for selection of sample

Pristine sample CAS 50 10 40

Crystalline phases labelled for the phase diagram divisions

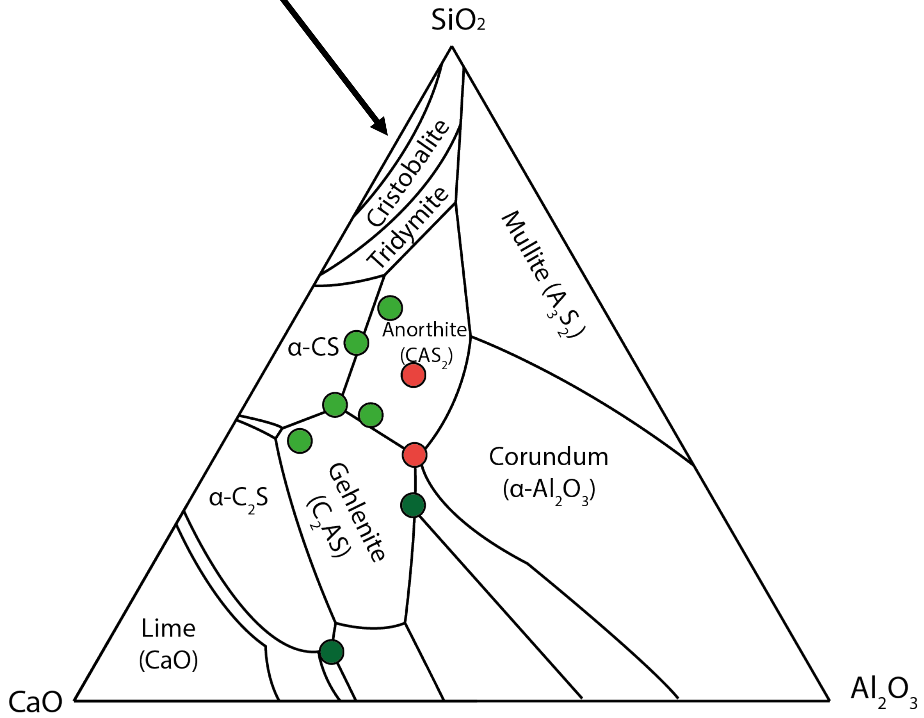


$CaO$, $Al_2O_3$, $SiO_2$ phase diagram with samples plotted
Edited from Khadilkar et al 2015.

| | C28Al12Si60 | C42Al12S46 | C42.4A15.5S42.1 | C50Al10Si40 | C35Al10Si55 |
|---|---|---|---|---|---|
| Oxide | Mol% | Mol% | Mol% | Mol% | Mol% |
| CaO | 28 | 42 | 42.4 | 50 | 35 |
| Al2O3 | 12 | 12 | 15.5 | 10 | 10 |
| SiO2 | 60 | 46 | 42.1 | 40 | 55 |
| Total | 100 | 100 | 100 | 100 | 100 |

Glass series chemistry in Mol%


*lwoodbridge1@Sheffield.ac.uk

[1]Glass formation in silicates: Insights from composition – Pascal Richet, Mathieu Roskosz & Jacques Roux – 2006

# Proof of a proven concept… or not

- Next step was Cs loading of these pristine glasses

Very uninspiring batch sandcastles


*lwoodbridge1@Sheffield.ac.uk

# Scope melt process

- For the interest of time scoping melts were undertaken
- Attempt to find the right temperature
- Attempt to see what the problem is

10g melt alumina crucibles to do 6 melts at a time



*lwoodbridge1@Sheffield.ac.uk

# Scope melt process

- Issues still found at max muffle furnace temperature
- Alkalis a problem across the board?
- Is it a size issue?


10g melt alumina crucibles most of which didn't melt


*lwoodbridge1@Sheffield.ac.uk

# Scope melt process

- Li, Na and K all perfect at loading level and temperature
- Rb not perfect but better than Cs
- Pollucite formation seen

Left- CAS 35 10 55 with 1 Mol% Cs and right 1, 5 and 10 Mol% K in CAS 50 10 40



*lwoodbridge1@Sheffield.ac.uk

XRD of glasses

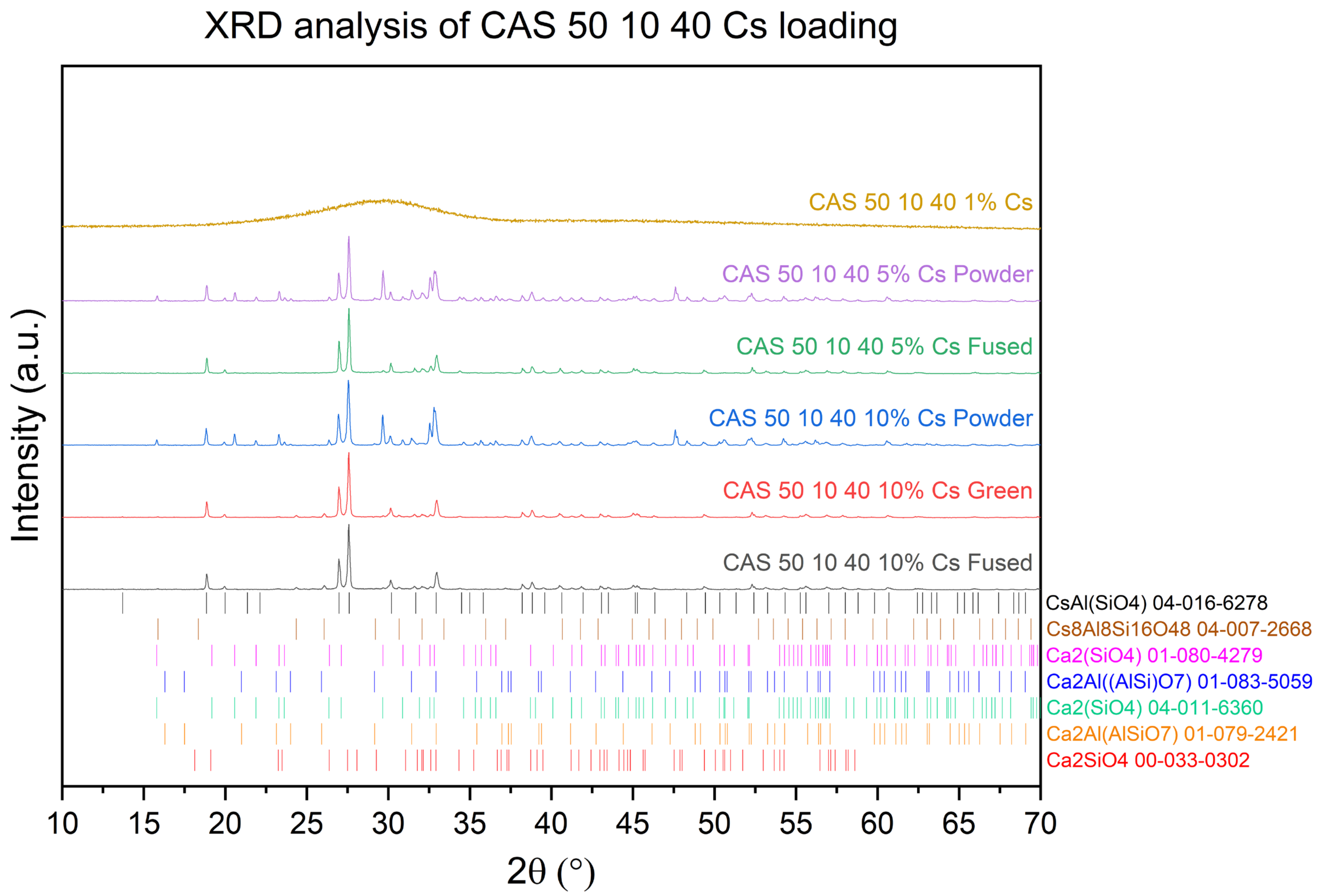


@ISL_Sheffield

# XRD of glasses

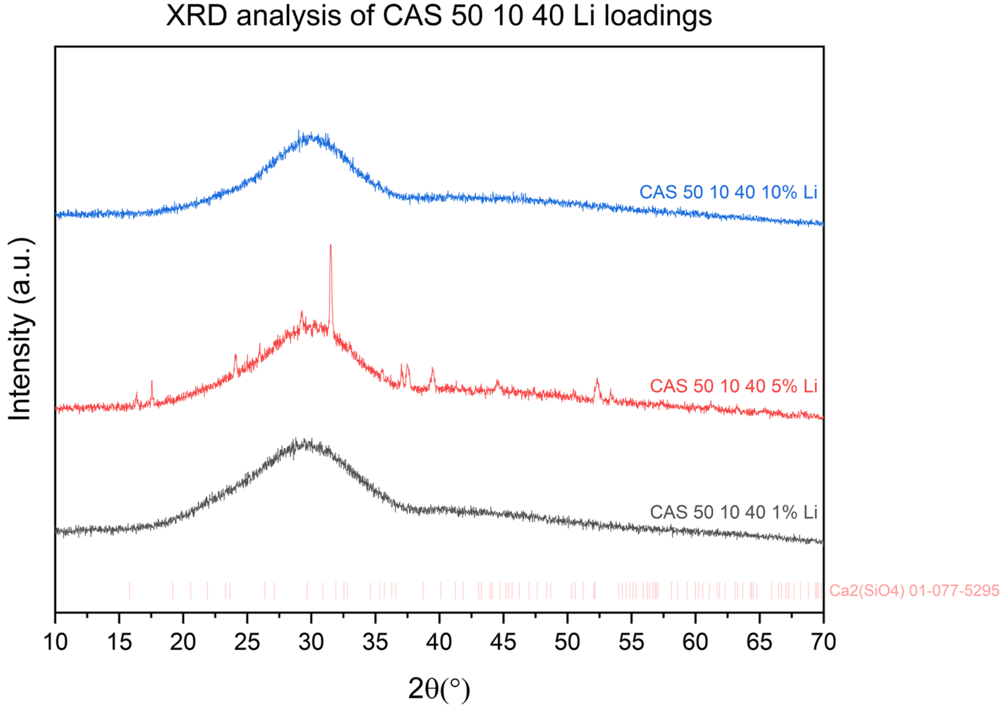


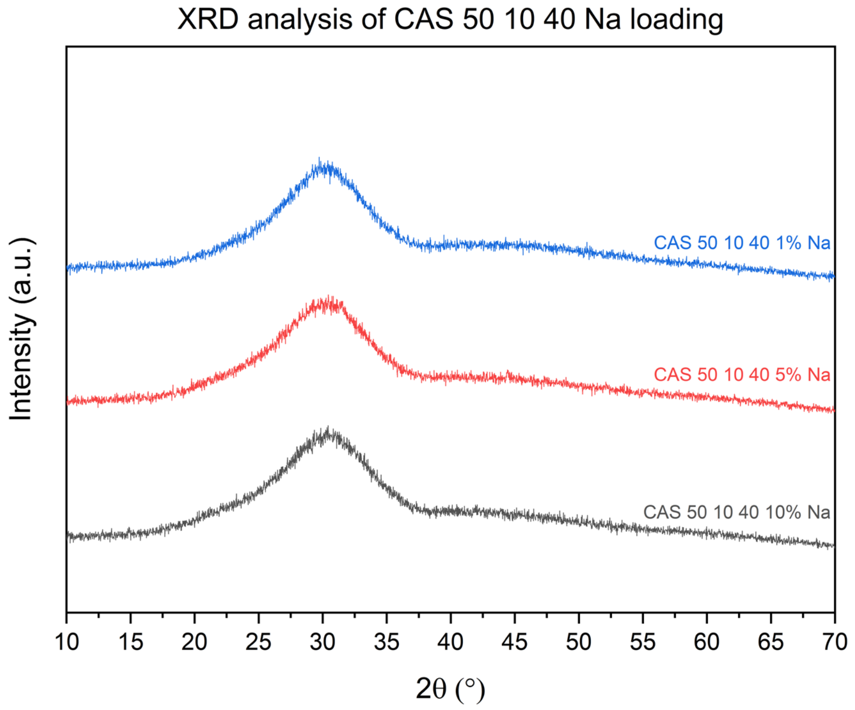


@ISL_Sheffield

# XRD of glasses

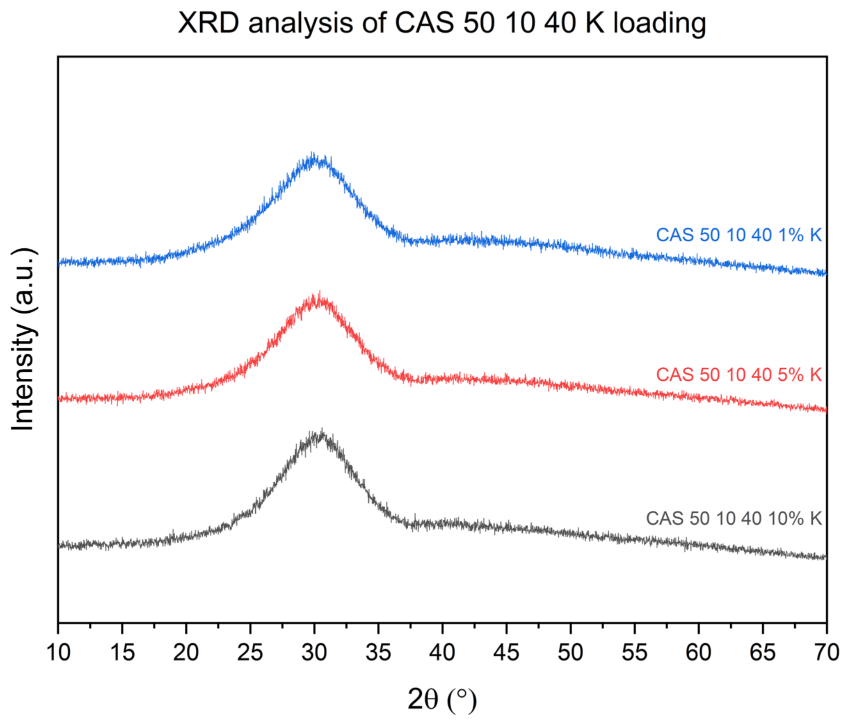


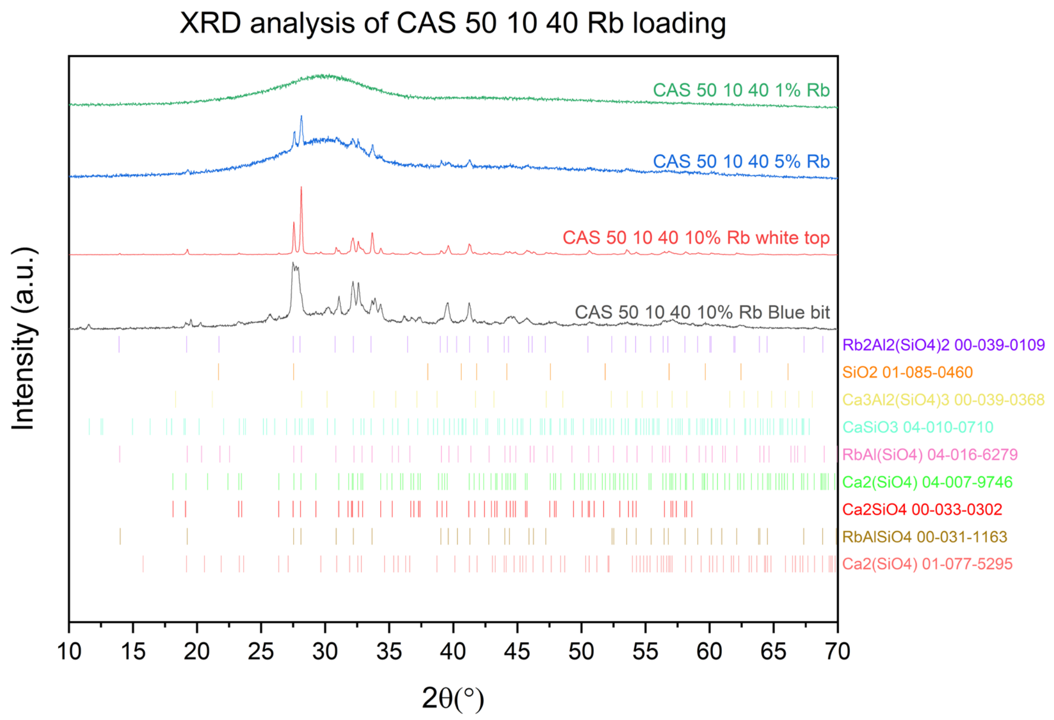


@ISL_Sheffield

# XRD of glasses

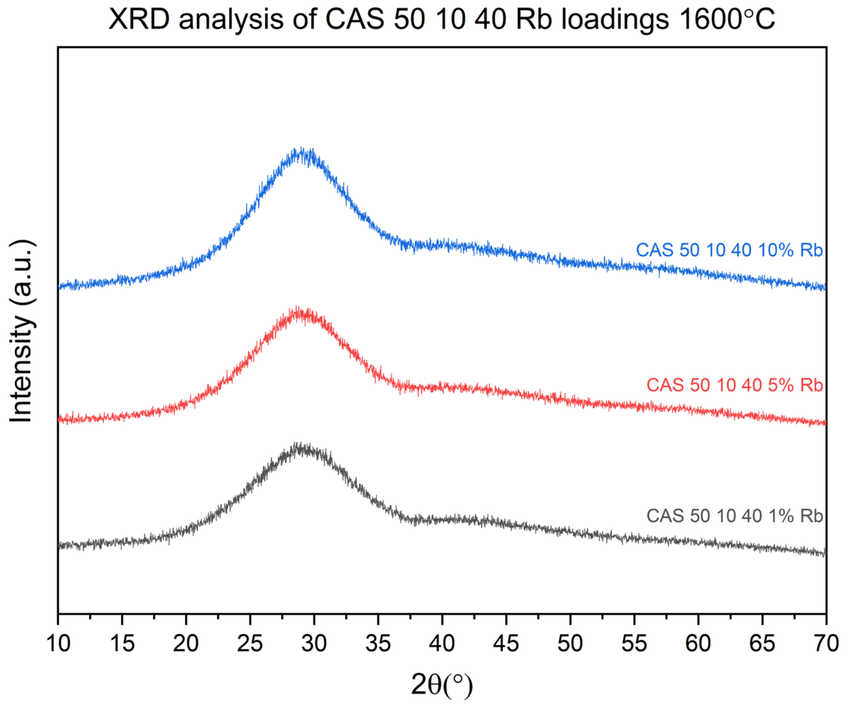


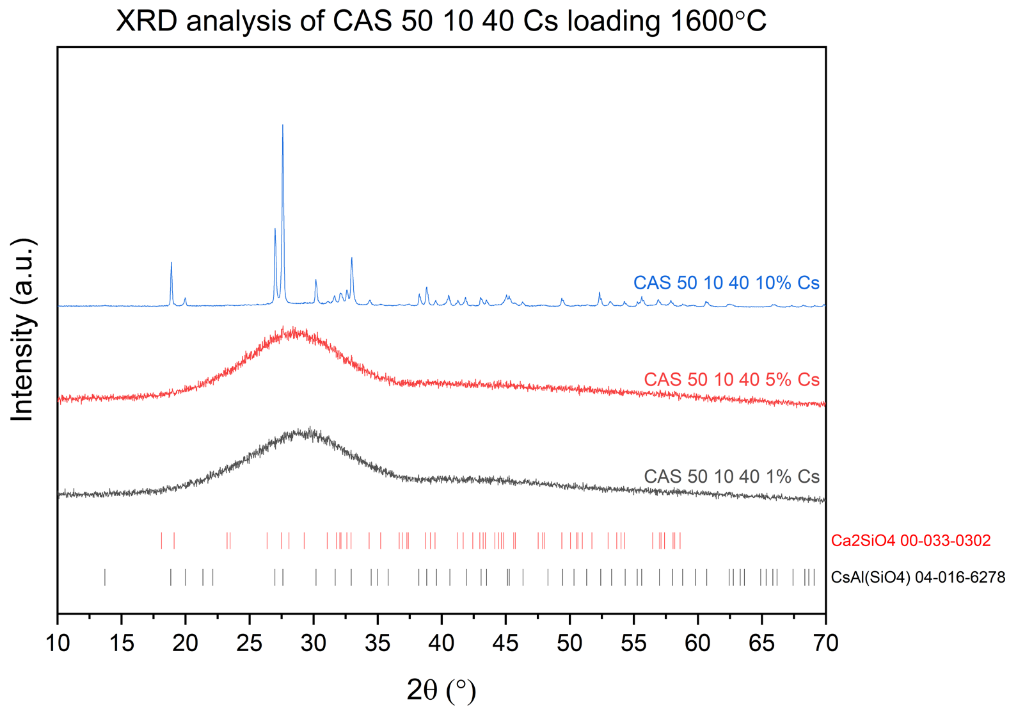

# Scope melt process

- Evidence from the literature that in other fields Li and Na are known to decrease viscosity and K increases it (Chang and Ejima 1987, Sukenaga et al 2006)

- Can you flux Cs into melt with Li or Na additions?


5% Li 5% Cs

3% Na 7% Cs

3% Na 7% Cs


*lwoodbridge1@Sheffield.ac.uk

# XRD of glasses

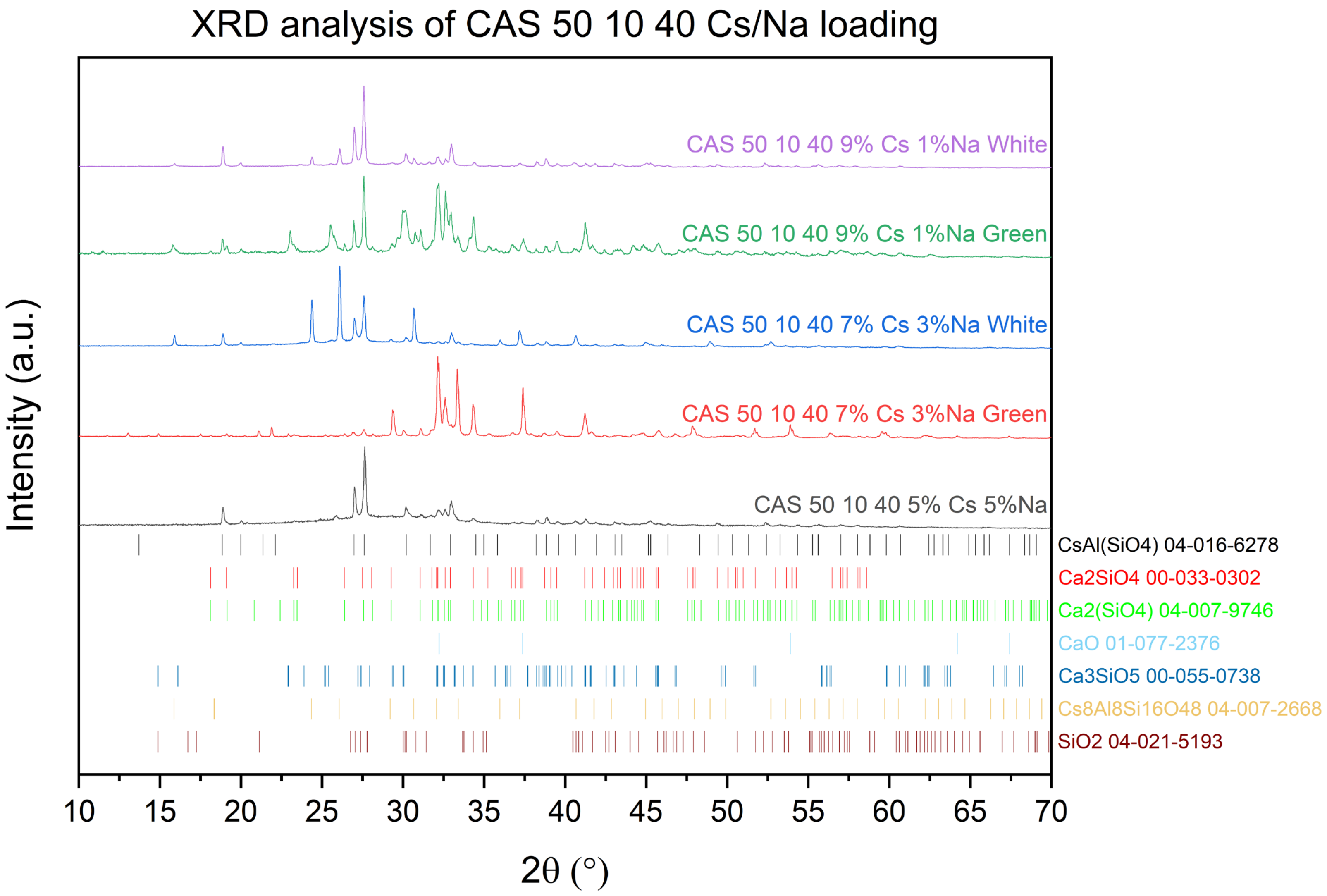




@ISL_Sheffield

# Raman of glasses

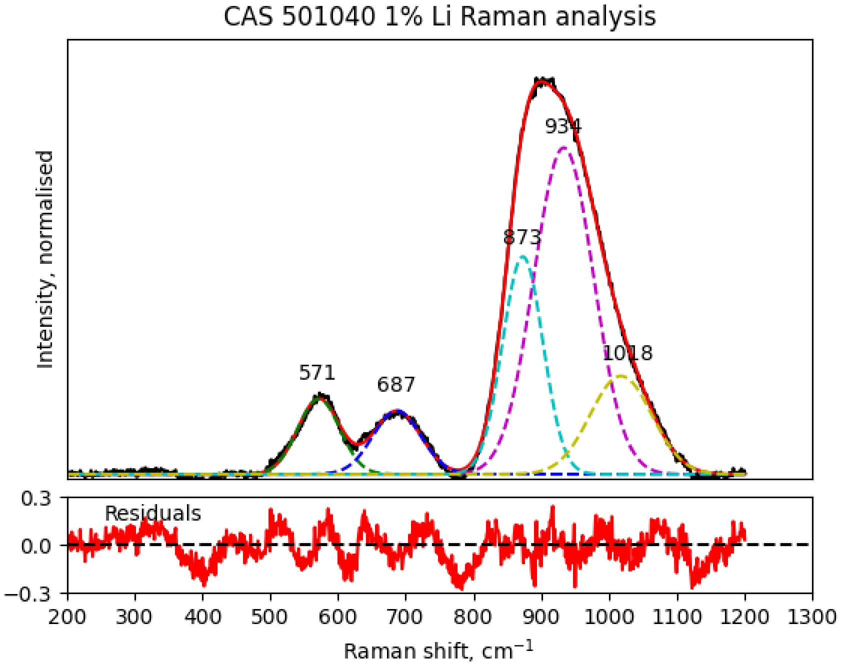


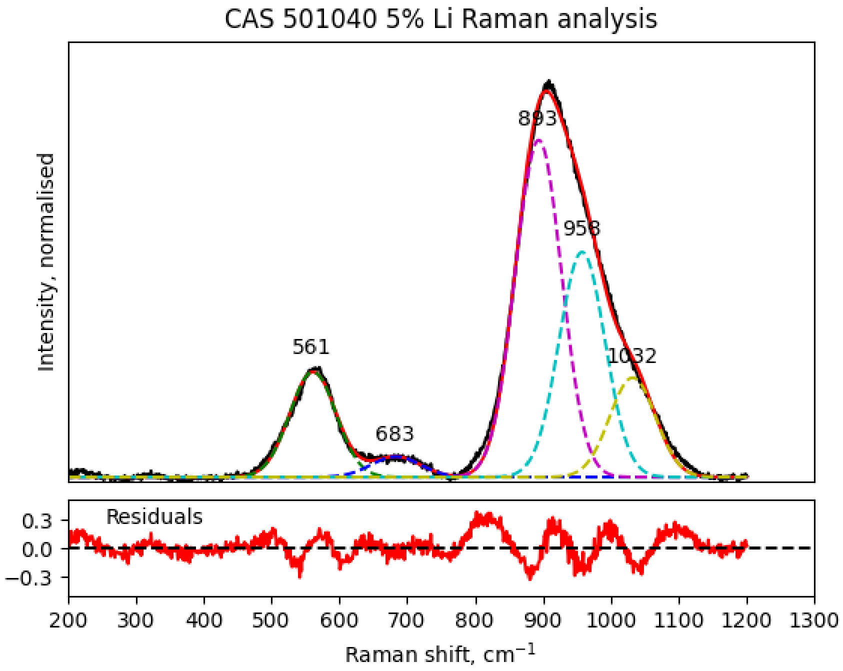


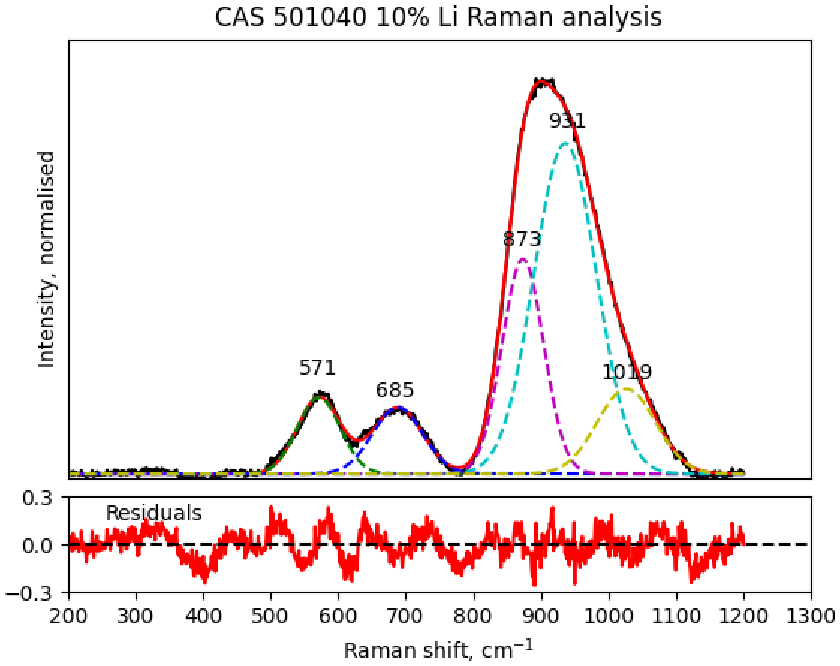


@ISL_Sheffield

The University Of Sheffield.

NucleUS
Immobilisation Science Laboratory

# Raman of glasses

CAS 501040 1% Na Raman analysis

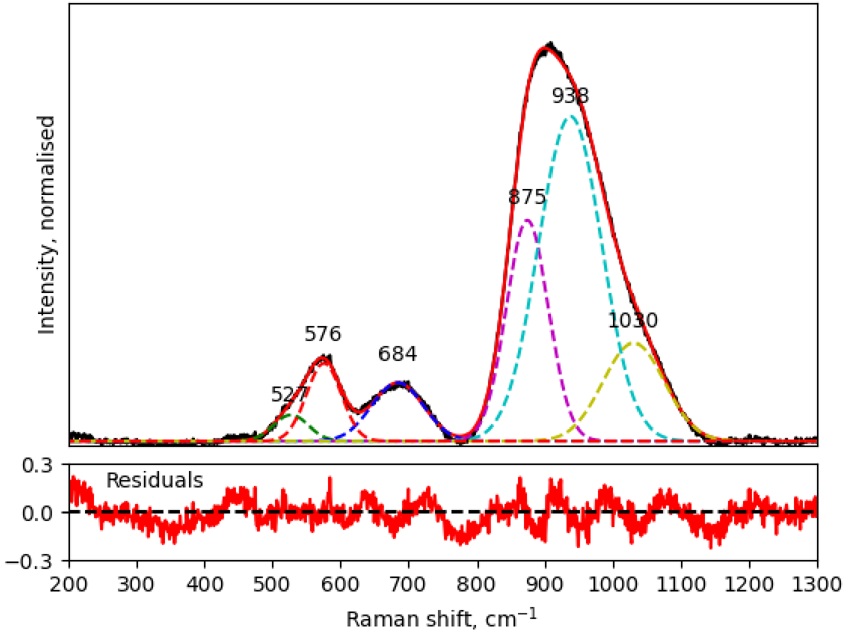


CAS 501040 5% Na Raman analysis

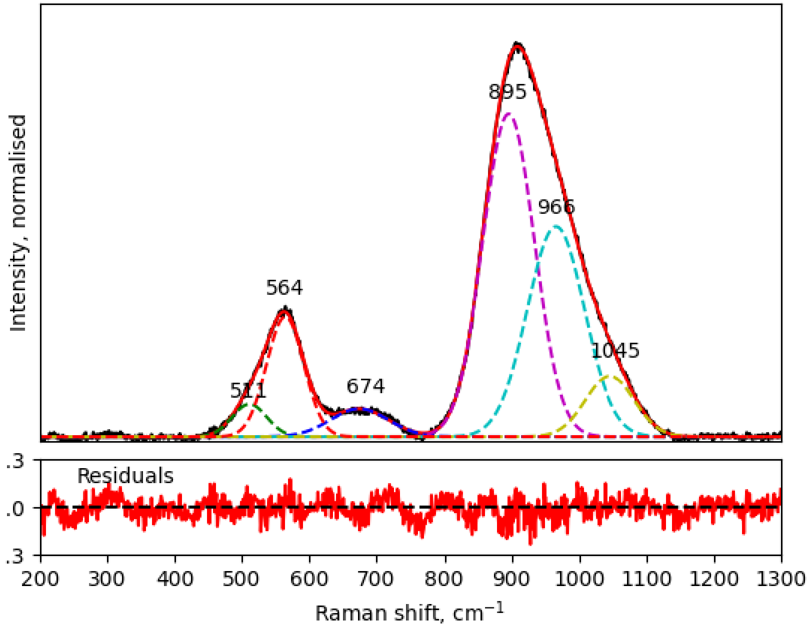


CAS 501040 10% Na Raman analysis

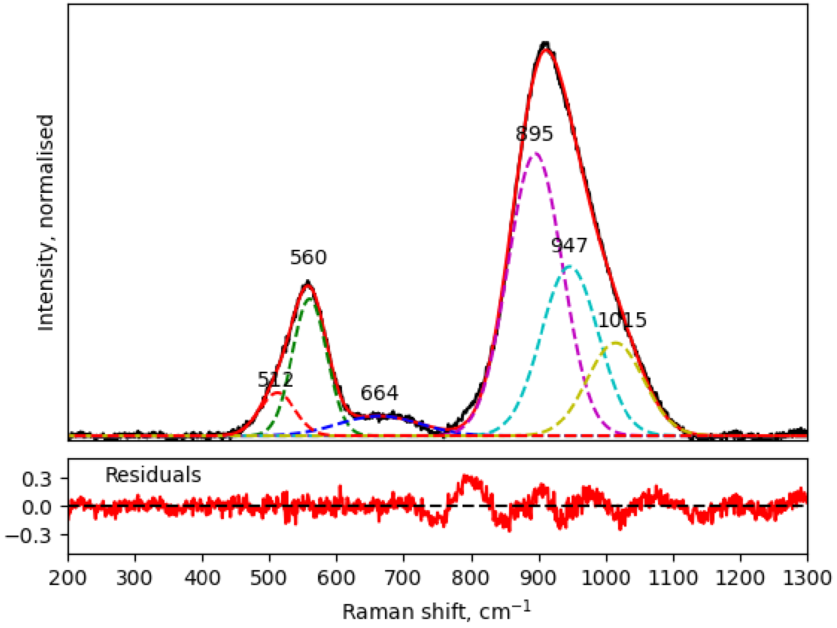


@ISL_Sheffield

# Raman of glasses

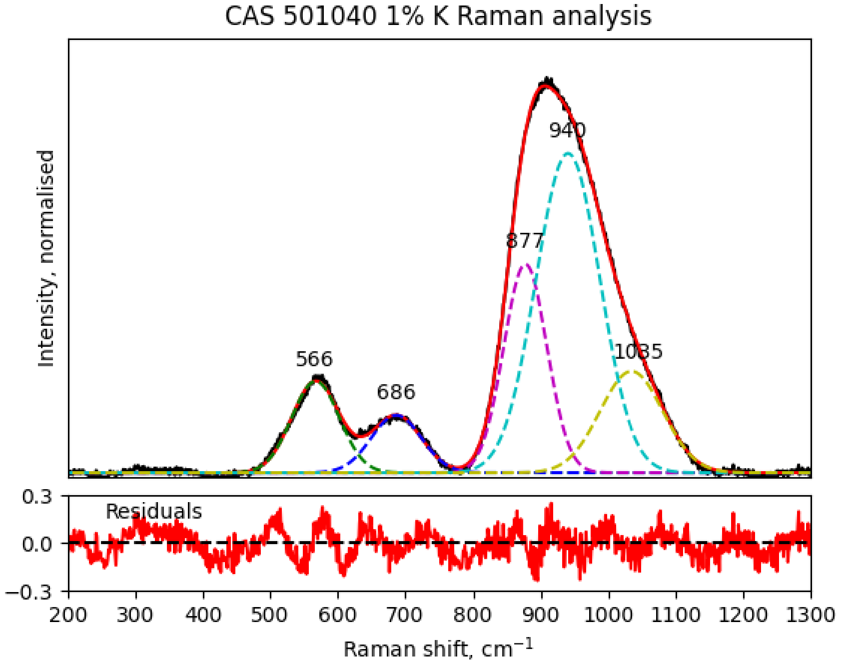


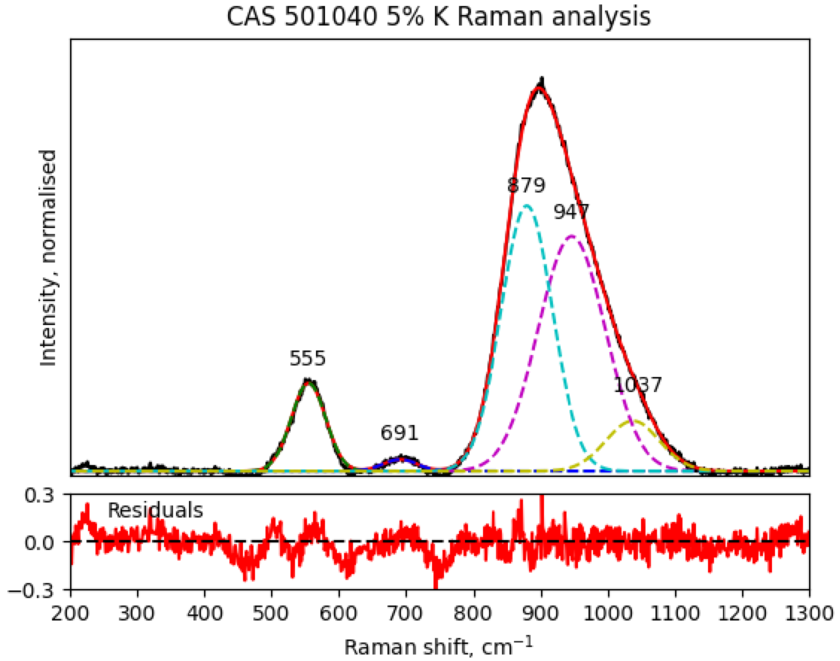


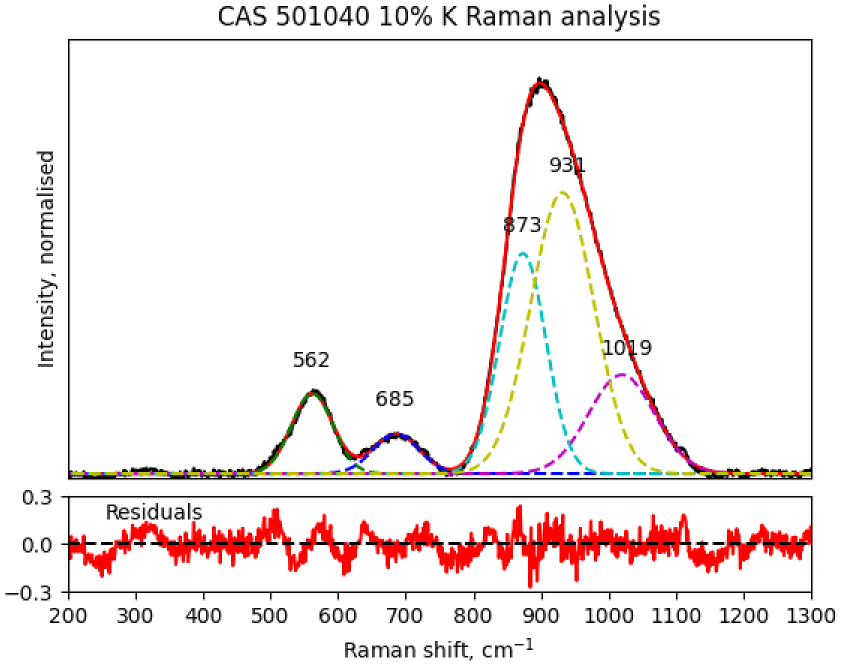


@ISL_Sheffield

# Raman of glasses

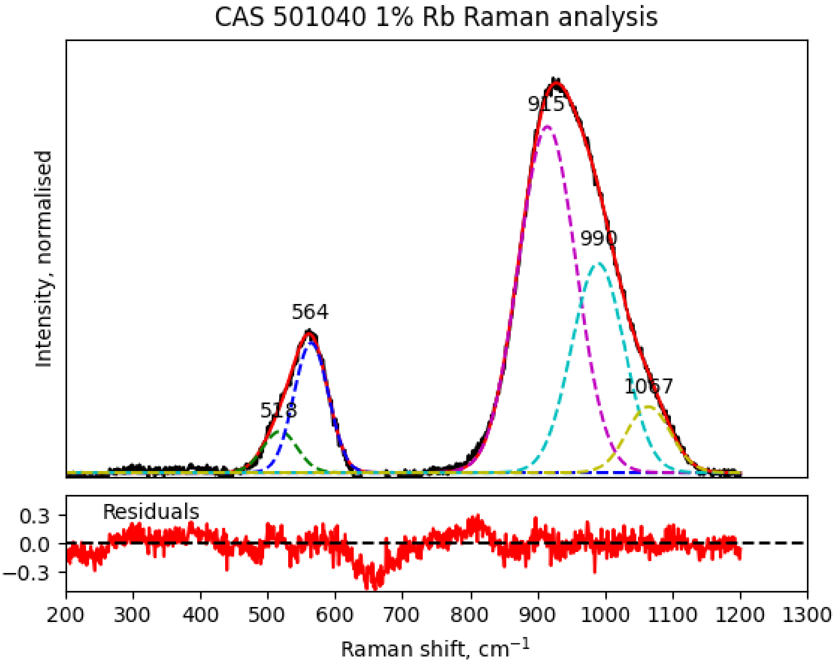


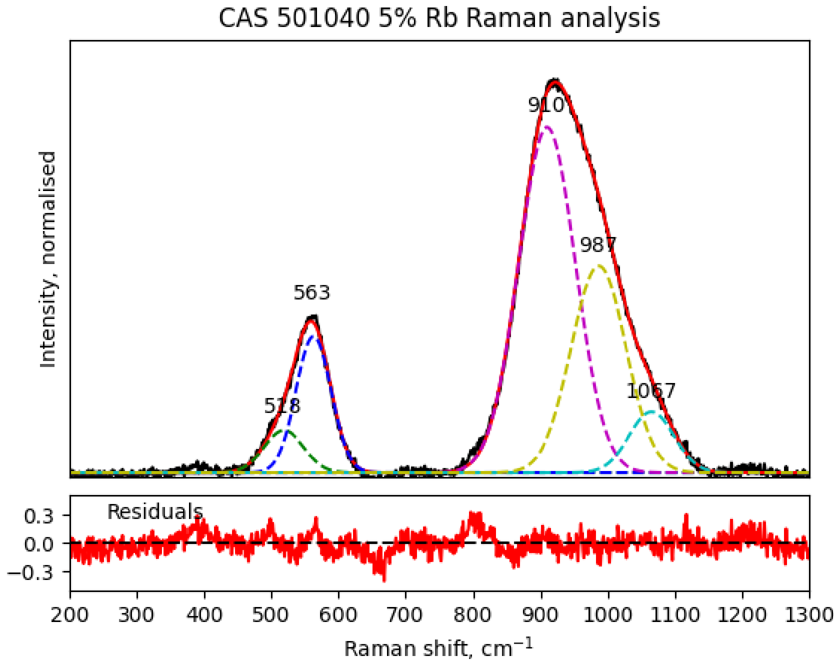


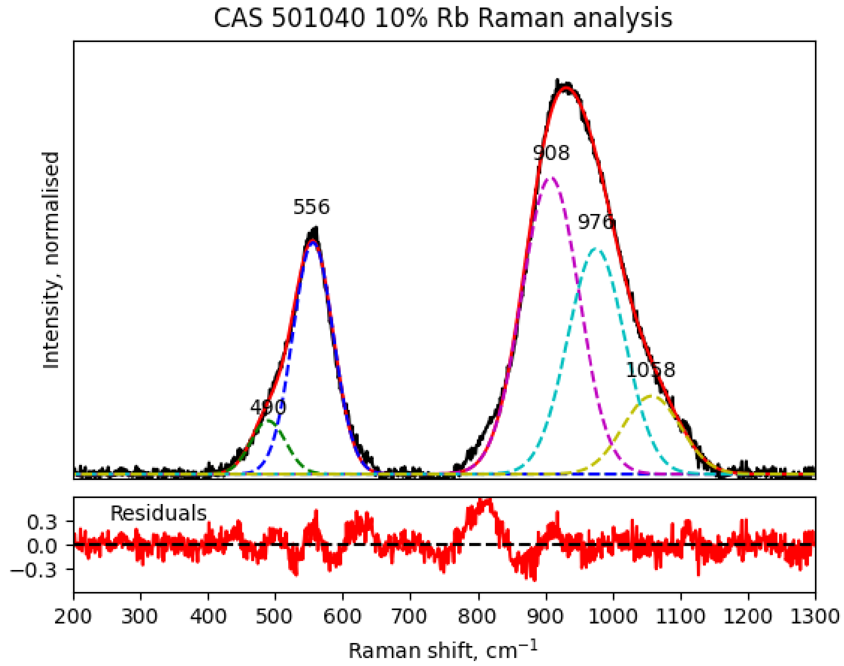


@ISL_Sheffield

## Raman of glasses

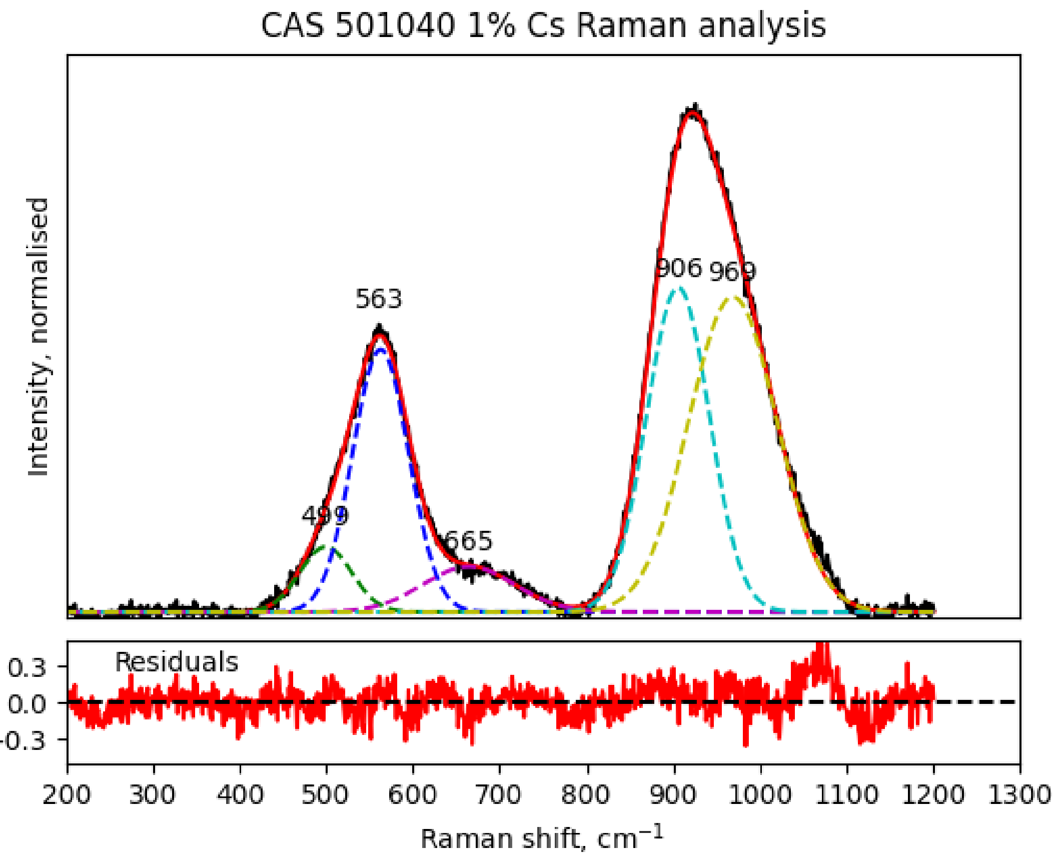


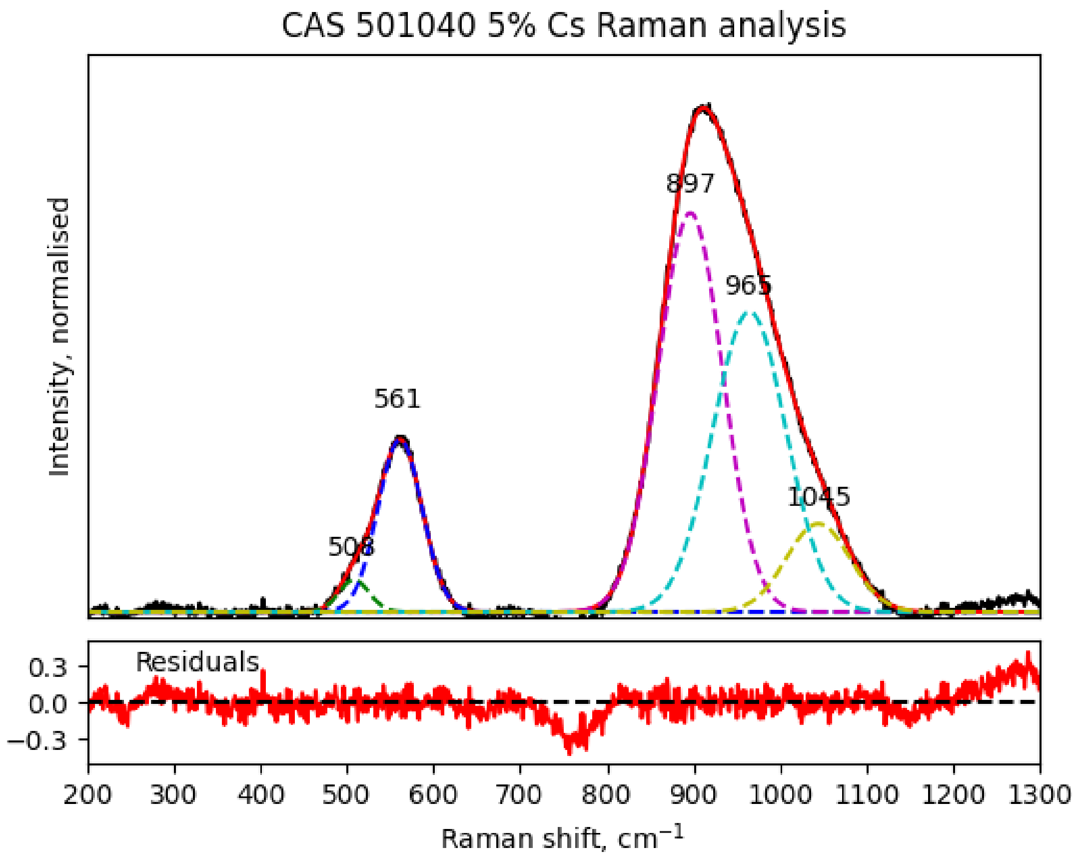




@ISL_Sheffield

# Raman of glasses

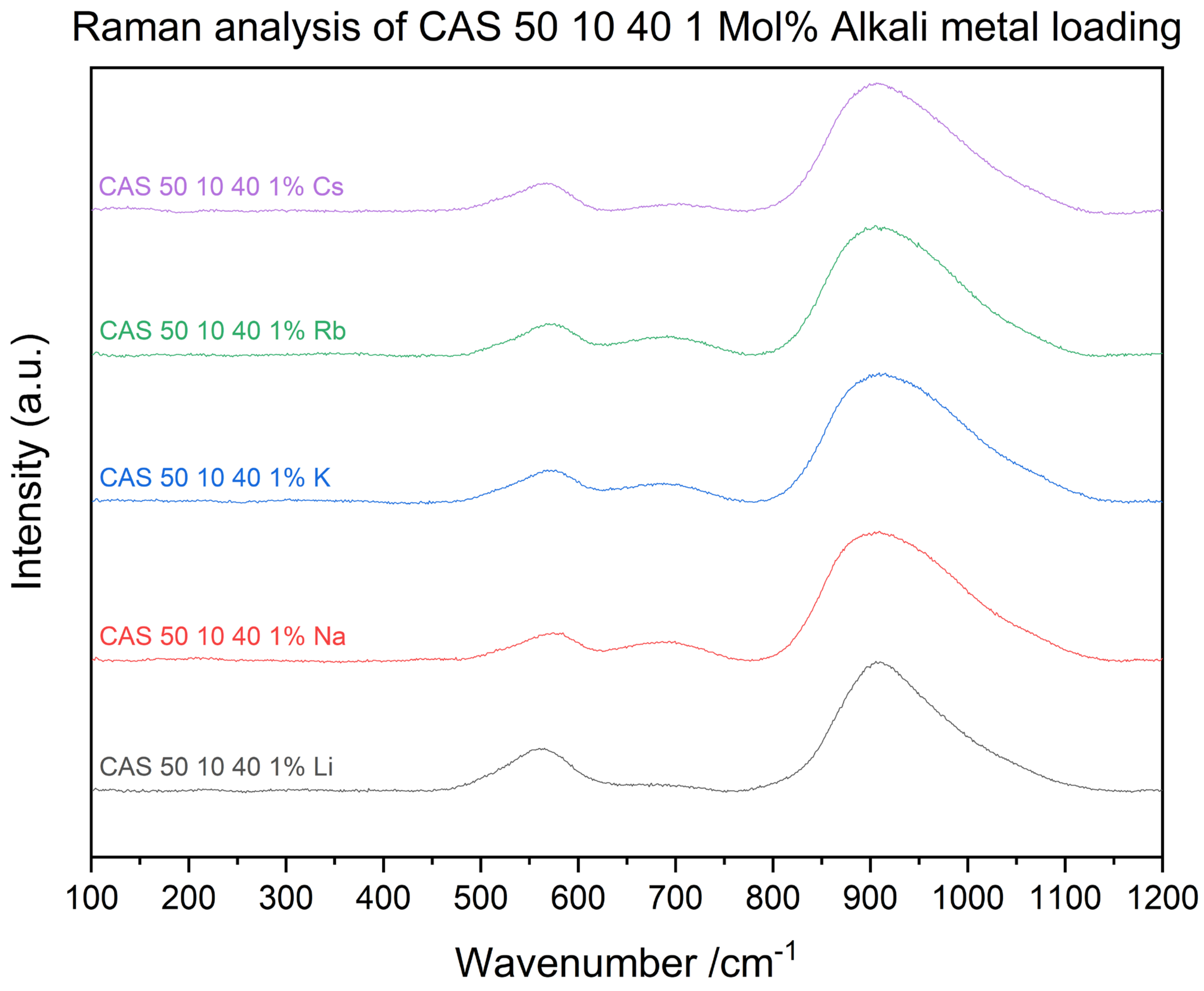


@ISL_Sheffield

# Raman of glasses

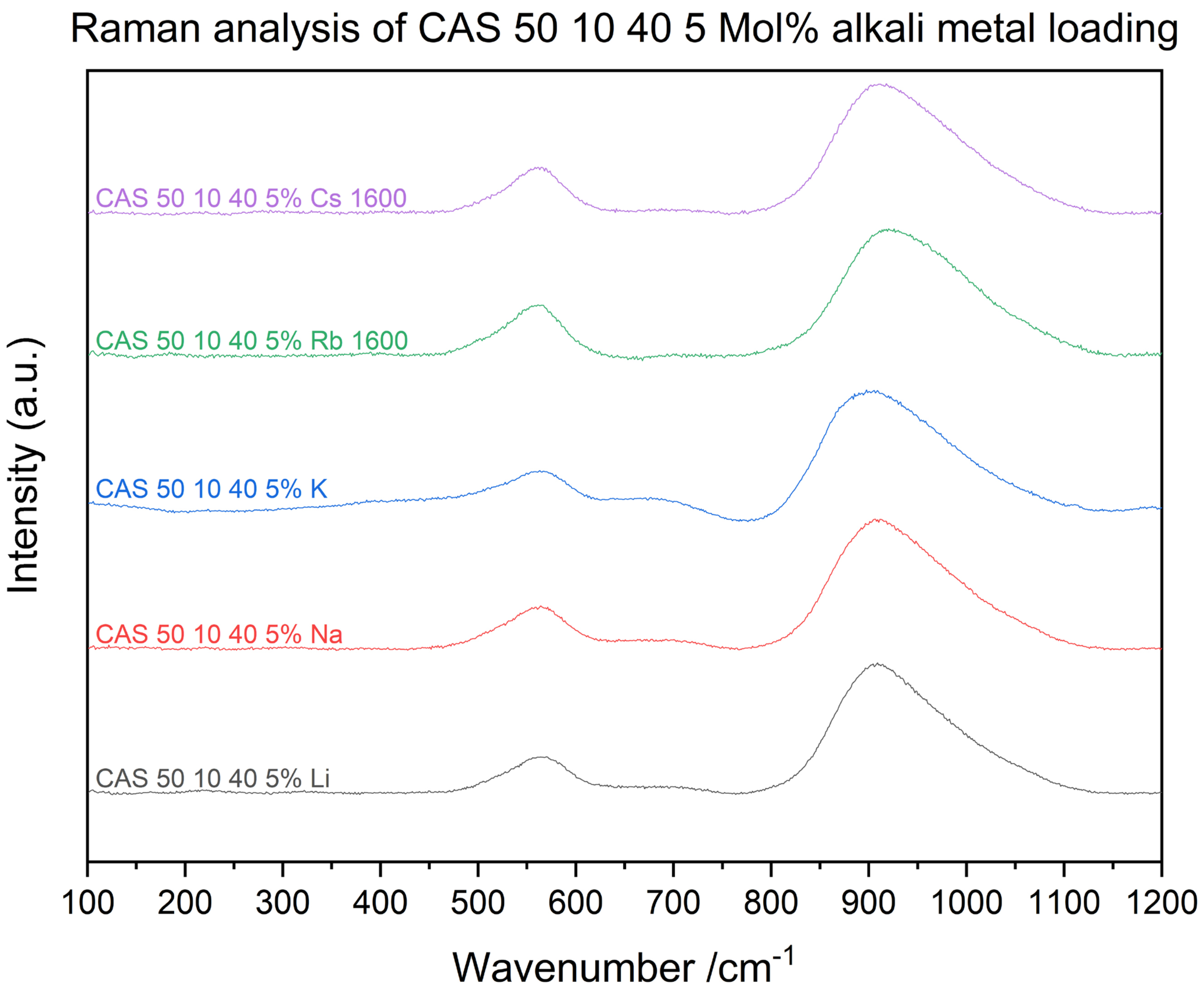


@ISL_Sheffield

# Raman of glasses

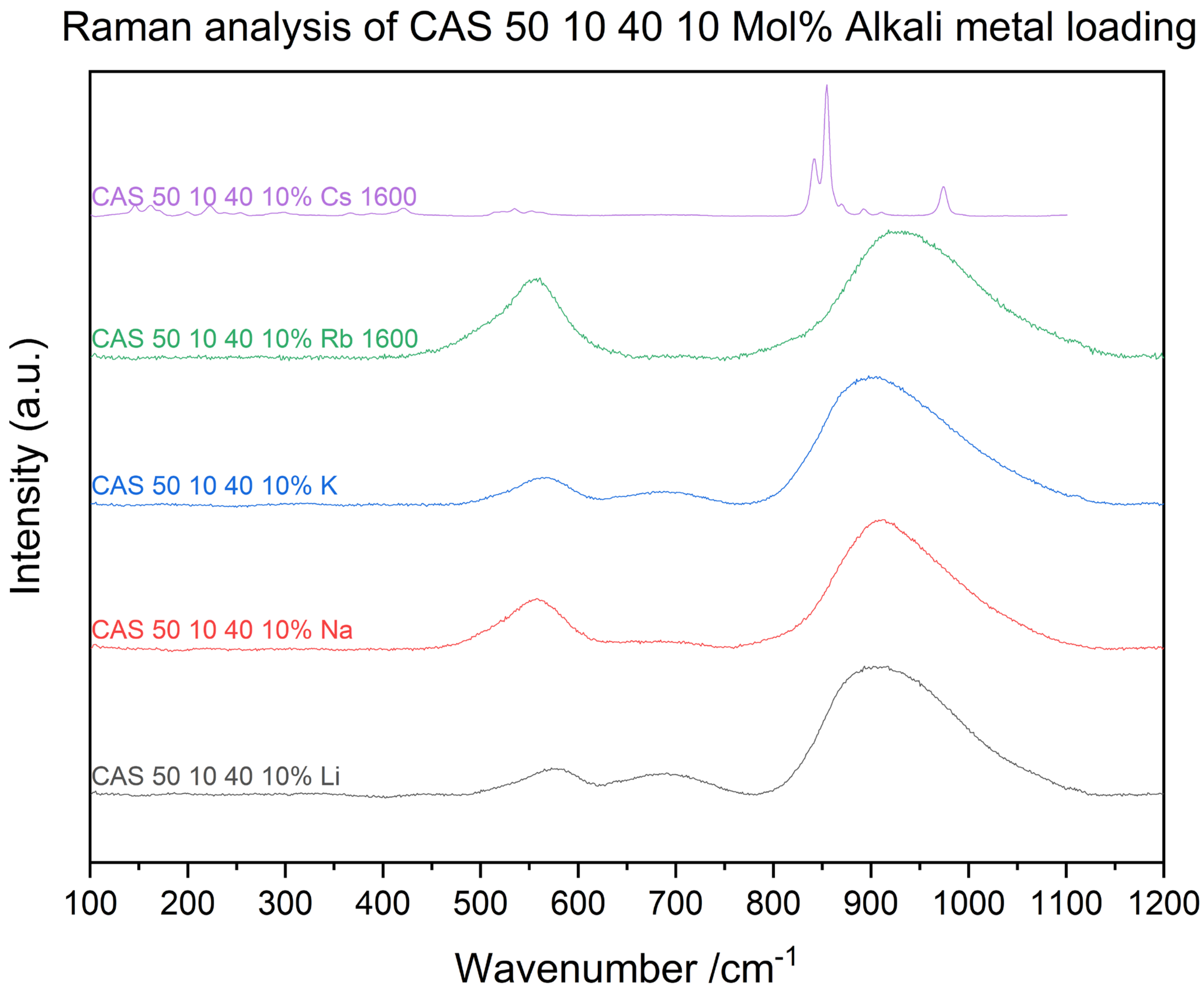


@ISL_Sheffield

# Further work

- Analyse XAS data
- Analyse NMR data (Si, Al and alkalis)
- Compositional data to see volatile retention
- Do melts of loaded Clino (time permitting)

@ISL_Sheffield

## Acknowledgements

This research utilised the HADES/ MIDAS facility at The University of Sheffield established with financial support from EPSRC and BEIS, under grant EP/T011424/1.

Special thanks to:

Russell Hand
Daniel Bailey
Lisa Hollands
Martin Stennett
ISL group members


@ISL_Sheffield



"This research utilised the HADES / MIDAS facility at The University of Sheffield established with financial support from EPSRC and BEIS, under grant EP/T011424/1."